NOVEL DIP-PEN NANOLITHOGRAPHY STRATEGIES FOR NANOPATTERNING

Chien-Ching Wu

Thesis committee members:

Prof. dr. K. J. Boller	University of Twente (Chairman)
Prof. dr. ir. D. N. Reinhoudt	University of Twente (Promotor)
Prof. dr. V. Subramaniam	University of Twente (Promotor)
Dr. A. H. Velders	University of Twente (Assistent Promotor)
Dr. C. Otto	University of Twente (Assistent Promotor)
Prof. dr. S. Speller	Radboud University Nijmegen
Prof. dr. H. Schönherr	University of Siegen
Prof. dr. ir. H. J. W. Zandvliet	University of Twente
Prof. dr. J. J. L. M. Cornelissen	University of Twente

NOVEL DIP-PEN NANOLITHOGRAPHY STRATEGIES FOR NANOPATTERNING

DISSERTATION

to obtain

the degree of doctor at the University of Twente,

on the authority of the rector magnificus,

Prof. dr. H. Brinksma,

on account of the decision of the graduation committee,

to be publicly defended

on Friday, June 18th 2010, at 13:15

by

Chien-Ching Wu

born on July 27th, 1981

in Kaohsiung City, Taiwan

This dissertation has been approved by:

Prof. dr. ir. David N. Reinhoudt (Promotor)

Prof. dr. Vinod Subramaniam (Promotor)

Dr. Aldrik H. Velders (Assistent Promotor)

Dr. Cees Otto (Assistent Promotor)

This thesis is dedicated to my family

給我摯愛的家人, 特別是阿公

Table of Contents

Chapter 1

General Introduction

Nanotechnology is a multidisciplinary research field aimed at manipulating matter at the nanometer scale, and even at an atomic or molecular level.[1] One rapidly emerging area of nanotechnology in the past decade is nanofabrication, which aims at building structures with nanometer-scale features. The fabricated nanostructures can be integrated into complex hierarchical systems that provide a variety of applications, such as integrated circuits for the memory and processors of computers, optical components for display units, miniaturized sensors for environmental and chemical monitoring, and biochips for clinical diagnosis.[2] Therefore, nanofabrication begins to exert dramatic influences on our daily life.

Nanofabrication methods can be roughly divided into two categories: (1) top-down approaches, such as traditional photolithography,[3] focused ion beam (FIB) lithography[4] and nanoimprint lithography (NIL)[5] that utilize irradiation or molding to reduce the lateral dimensions of a bulk substrate and to obtain a desired nanostructure,[6] and (2) bottom-up approaches, such as microcontact printing (μCP)[7] and scanning tunneling microscopy (STM) lithography,[8] that utilize self-assembly or manipulation of atoms or molecules to build up nanostructures.[6]

Dip-pen nanolithography (DPN) is an atomic force microscopy (AFM)-based lithography technique, which has the ability to fabricate patterns with a feature size down to ~ 15 nm using both top-down and bottom-up approaches.[9, 10] The serial nature of operation of DPN during its early development stages restricted the patterning efficiency. However, since the successful design and fabrication of AFM probe arrays, DPN has acquired the capacity to increase its throughput dramatically by generating patterns in parallel.[11] Therefore, DPN has become a popular tool for nanofabrication.

The research presented in this thesis focuses on two aspects: use of DPN to fabricate metal-ion and (bio)molecular patterns at micrometer or sub-micrometer scale, and development of AFM tip surface-modification methods for long-term DPN writing.

Chapter 2 is a literature review describing the development of the DPN technique in the past decade and the related chemical strategies that have been used to generate biomolecular architectures on solid surfaces with DPN. Some other AFM-based lithography techniques used for biopatterning are also briefly described at the end of the chapter.

Chapter 3 introduces a custom-built instrument, the atomic force fluorescence microscope (AFFM) implemented with a relative humidity (RH) control system, used for performing all the DPN experiments described in this thesis. AFFM allows one to write patterns and subsequently visualize *in situ* the written results in a sequential write-read mode. The controlled delivery of calcium metal ions with DPN on fluorescent sensitive monolayer-functionalized glass substrates is demonstrated by visualizing the modulation of the fluorescence intensity. The fabrication of metal ion patterns can be utilized to generate templates to immobilize biomolecules, and is described in detail in **Chapter 4**. Deposition of nickel ions onto nitrilotriacetic acid-terminated monolayer-functionalized glass substrates with DPN and μCP is demonstrated by immobilization of histidine-tagged visible fluorescent proteins *via* a specific metal-protein interaction. This approach also enabled us to characterize the dependence of transfer of nickel ions on fundamental parameters of DPN, such as writing speeds and tip-surface contact times.

Instead of using non-covalent interactions to generate patterns as presented in Chapter 3 and Chapter 4, *reactive* μCP and DPN are demonstrated in **Chapter 5**. Amine containing β-cyclodextrin (βCD-NH$_2$) and quantum dots (QD-NH$_2$) were microcontact printed and written onto *N,N*-carbonyldiimidazole-activated amino monolayer-functionalized glass slides *via* the covalent formation of urethane bonds. Additionally, orthogonal microcontact printing of βCD and QD-NH$_2$ is also demonstrated.

In **Chapter 6**, a simple method is presented to coat the surfaces of AFM tips with a thin layer of porous film by using Layer-by-Layer (LbL) techniques. This porous film can easily absorb biomolecules and act as a larger volume ink reservoir compared to a bare AFM tip. Fluorescent protein patterns were generated at micron and sub-micron length scales by using the porous tips. A further investigation of the morphology variations of porous films-coated AFM tips, prepared under various conditions, is described in **Chapter 7**. These porous tips, inked with two kinds of visible fluorescent proteins, are used to

study the ink reservoir properties of the porous films used to functionalize the DPN tips.

References

1. Bhushan, B., *Springer Handbook of Nanotechnology*. 2nd ed.; Springer Science+Business Media, Inc.: 2007.

2. Geissler, M.; Xia, Y. N. Patterning: Principles and Some New Developments. *Adv. Mater.* **2004,** *16*, 1249-1269.

3. Xia, Y. N.; Rogers, J. A.; Paul, K. E.; Whitesides, G. M. Unconventional Methods for Fabricating and Patterning Nanostructures. *Chem. Rev.* **1999,** *99*, 1823-1848.

4. Tseng, A. A. Recent Developments in Micromilling Using Focused Ion Beam Technology. *J. Micromech. Microeng.* **2004,** *14*, R15-R34.

5. Chou, S. Y.; Krauss, P. R.; Renstrom, P. J. Imprint Lithography with 25-Nanometer Resolution. *Science* **1996,** *272*, 85-87.

6. Whitesides, G. M.; Love, J. C. The Art of Building Small - Researchers Are Discovering Cheap, Efficient Ways to Make Structures Only a Few Billionths of a Meter Across. *Scientific American* **2001,** *285*, 38-47.

7. Xia, Y. N.; Whitesides, G. M. Soft Lithography. *Angew. Chem. Int. Ed.* **1998,** *37*, 551-575.

8. Tseng, A. A.; Notargiacomo, A.; Chen, T. P. Nanofabrication by Scanning Probe Microscope Lithography: A Review. *J. Vac. Sci. Technol., B* **2005,** *23*, 877-894.

9. Piner, R. D.; Zhu, J.; Xu, F.; Hong, S. H.; Mirkin, C. A. "Dip-Pen" Nanolithography. *Science* **1999,** *283*, 661-663.

10. Ginger, D. S.; Zhang, H.; Mirkin, C. A. The Evolution of Dip-Pen Nanolithography. *Angew. Chem., Int. Ed.* **2004,** *43*, 30-45.

11. Salaita, K.; Wang, Y. H.; Mirkin, C. A. Applications of Dip-Pen Nanolithography. *Nat. Nanotechnol.* **2007,** *2*, 145-155.

Chapter 2

Developments in Dip-Pen Nanolithography and Related Chemical Strategies for Patterning Biomolecules

Abstract

Dip-pen nanolithography (DPN) is a high-resolution atomic force microscopy (AFM)-based lithography technique. It utilizes the water meniscus formed between an AFM tip and a substrate to transfer ink molecules onto surfaces. This chapter reviews the development of this technique and its application to fabricate patterns of biomolecules at micrometer and nanometer scale.

2.1 Introduction

Controlled micro- and nano-patterning of biomolecules on solid surfaces while simultaneously maintaining the activity and structural integrity of the molecules has attracted a lot of attention in recent years because of its potential applications in biotechnology and medicine, including production and preparation of biochips and biosensors, drug discovery, and fundamental studies of biological processes.[1, 2] There are various techniques to fabricate architectures of small scale, such as traditional photolithography,[3, 4] microcontact/nanocontact printing (μCP/nCP),[5-7] nanoimprint lithography (NIL),[8, 9] electron-beam lithography,[10-12] and scanning probe-lithography (SPL).[13, 14] One scanning probe technique, atomic force microscopy (AFM), was invented in 1986 and uses Van der Waals interactions to study surface properties.[15] AFM has become a very popular technique to elucidate the nanometer scale topography of different materials including insulators, semiconductors, conductors, and biological molecules. Besides direct imaging, AFM has also been explored to manipulate atoms and molecules on surfaces. AFM-based lithography utilizes an AFM probe to create patterns chemically, mechanically or electrically. AFM-based lithography techniques such as dip-pen nanolithography (DPN), nanografting, nanoshaving, conductive AFM lithography and enzymatic lithography attract enormous interest due to the technical potential and relatively low cost. Among these techniques, DPN is a popular method for fabricating biomolecular patterns.

A comprehensive review of recent efforts in all directions mentioned above is beyond the scope of this chapter. Therefore, the focus in this chapter is on two aspects: the development of DPN and the use of DPN for generating biomolecular architectures on different solid surfaces. Finally, some other AFM-based lithography techniques used for the fabrication of bio-patterns will be briefly summarized.

2.2 Development of dip-pen nanolithography

Before dip-pen nanolithography (DPN) was officially introduced by the Mirkin group in 1999 for transferring 1-octadecanethiol (ODT) from an AFM tip to a gold surface,[14] Jaschke *et al.* had reported the deposition of aggregates of ODT onto high-energy surfaces of mica in 1995.[16] Although some of the conclusions of Jaschke *et al.* conflicted with the results reported by others, these disordered ODT deposits might be considered as the first

nanopatterns written with DPN.[16, 17] It is known that condensation of water results in a capillary force between a tip and a substrate when scanning force microscopy (SFM) is conducted in air. This has a significant influence on the contrast and resolution of AFM and lateral force microscopy (LFM) images.[18] In 1997, Piner *et al.* demonstrated how water was transported to and from polymeric and inorganic substrates by LFM *via* a narrow gap capillary.[19] They concluded that the phenomenon of water transport depended upon the relative humidity (RH), surface properties and dynamics of the tip motion. Although the main purpose of this work was to characterize the effects of water on LFM measurements, this research inspired the authors to explore the DPN technique further.

The basic idea of DPN is very similar to writing ink with a conventional quill pen. Figure 2.1 illustrates the general process of DPN.[20] A water meniscus is formed while an ink-coated AFM probe is brought into contact with a substrate in an ambient environment. The ink molecules are transferred to the surface *via* this water "bridge". Depending on the precise nature of the molecule-substrate interaction, which can be either (electro-)chemisorption or physisorption, the ink molecules may become immobilized.[14, 21, 22]
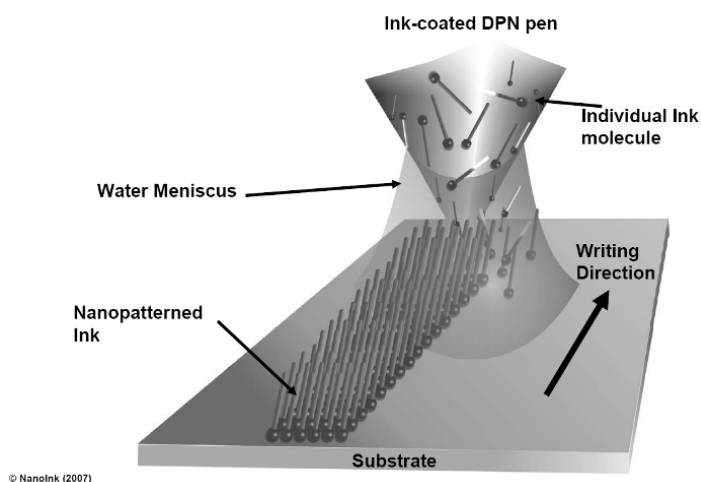

Figure 2.1. *Schematic representation of molecular transport in the dip-pen nanolithography (DPN) process. Reprinted with permission from Ref. [20]. Copyright (2005) Elsevier. .*

The precise mechanism of ink transportation is complicated and different from one system to another. Over the past years, several groups have reported factors which have an influence on the deposition processes, including the chemical properties of the ink molecules and the chemical nature of the tip and the substrate, as well as the probe geometry, the ambient environment (temperature and relative humidity), and writing speed.[14, 20-28] These conclusions are mostly based on studies of ODT or 16-mercaptohexadecanoic acid (MHA) deposited on gold surfaces. Haaheim *et al.* demonstrated that narrower MHA lines on gold surfaces were obtained by using sharper AFM tips or smoother surfaces.[20] Many inks including organic molecules or bio-molecules have been used to demonstrate that longer tip-surface contact times or slower writing speeds results in larger feature sizes.[14, 23-25, 29, 30] However, this was not observed in all cases. A negligible dependence of the writing speed while depositing ODT on a Au surface at ambient RH was reported by Sheehan *et al.*[26]

Since DPN utilizes the water meniscus to deliver ink molecules, the shape and size of the water meniscus is another crucial issue. Weeks *et al.* used environmental scanning electron microscopy (ESEM) to image the formation of the water meniscus between an AFM tip and a substrate.[31] The height of the meniscus is a function of RH as shown in Figure 2.2. There is no observation of meniscus formation while increasing RH until ~ 70% with an Au substrate and ~ 80% with a Si substrate. The height of the meniscus appears to increase exponentially with RH between 70% and 95% and is much larger than that calculated either using the Kelvin equation or Monte Carlo modeling. Because the resolution of ESEM is ~ 50 nm, these authors were not able to unequivocally visualize the formation of a meniscus at lower relative humidities.[31] These results suggested that the transport rate of MHA does not change much at RH between 0% and 50 %, but abruptly increases while the RH is larger than 50%.[32] Later, the same authors used ESEM to study the dynamic growth of the water meniscus. They found that the water meniscus took many minutes to reach an equilibrium state when the tip was brought into contact with the surface. This observation suggests that the meniscus growth may account for the DPN ink transport.[33] Rozhok *et al.* used ODT/MHA-Au systems to demonstrate how temperature and RH influence the growth rates of ODT and MHA. An increase of growth rate for both inks was observed with increasing temperature. However, only the growth rate of MHA rose with increasing RH. These results suggest that the nature of the ink influences ink transport. In this case, the authors deduced that differences in behavior between ODT and MHA could be explained in terms of their different solubilities in the water meniscus.[27]
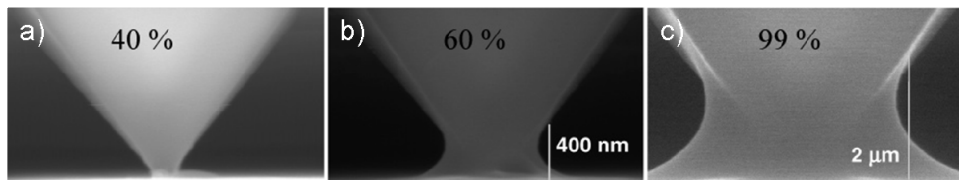
Figure 2.2. (a) - (c) ESEM images of water meniscus formed between an AFM tip and a substrate. Images collected at 5 ºC at relative humidities of 40%, 60% and 99%, respectively. Reprinted with permission from Ref. [31]. Copyright (2005), American Chemical Society.

According to the experimental DPN results, several models have been proposed to explain the ink transport. Jang *et al.* modeled the deposition of self-assembly molecules by DPN as a two-dimensional diffusion with a source.[34] They treated the flow of ink from an AFM tip as a constant flux of molecules. Later, Sheehan *et al.* suggested that the process of deposition could be modeled as two-dimensional diffusion from an annular source of constant concentration with a fixed surface diffusion coefficient independent of RH.[26] In addition, Weeks *et al.* brought up a model that takes the kinetics of ink dissolution as well as the effect of RH and meniscus growth into account.[31, 33] However, none of these models could be used to explain all conditions. Therefore, a thorough understanding of the interplay of all the mechanisms will enable the development of more optimized ink-substrate combinations and achieve a higher resolution.[21]

DPN enables the preparation and registration of patterns from the sub 100-nm to many micrometers length scale. The highest resolution achieved so far is with alkanethiol patterns fabricated on gold surfaces with a size of ~ 15 nm. Moreover, the flexibility of DPN allows the preparation of different patterns on substrates. Since its invention, DPN has been performed with a large variety of combinations of inks and substrates that are summarized in Table 2.1.

Table 2.1. *Overview of reported ink-substrate combinations which were used for DPN.*[35]

Ink molecules	Substrates
Various Alkanethiols	Au
Silane	SiO_x, Glass
Silazanes	SiO_x, GaAs
Alkynes	Si
Cystamine	Au
Sol-Gels (M_2O_n, M=Al, Si, Sn) or (Magnetic nanostructures, BaFe)	SiO_x
Nanoparticles (Q-Au); Gold Nanoclusters (thiol capped)	SiO_x, Electrodes
NanoParticles (Fe_3O_4, magnetic, quantum dots)	Si, SiO_x, Mica
Catalysts as sites for growing Polymer or GaN nanowires	SiO_x
Gold ($HAuCl_4$ Salt was used); Platinum (H_2PtCl_6 salt was used)	Si
Metal ions (Ca^{2+}, Ni^{2+})	silane modified SiO_x
DNA	Au, silane modified SiO_x
Proteins	Au, SiO_2, NiO_x, silane modified SiO_x
Collagen	Au
Peptide	Au, Ni, SiO_x
Biotin	SiO_x, silanized modified glass
poly(allylamine hydrochloride) (PAH)	SiO_x
poly (styrenesulfonate) (PSS)	SiO_x
Mercaptoimidazole	Gold
Conducting Polymers (PolyPyrrole & THF)	Gold electrodes
Solid inks (Octadecylphosphonic Acid)	Mica
Luminescent molecules (*e.g.* Rhodamine)	Glass
Polymer (Nanowires, poly(thiophene))	SiO_x
Dendrimers	SiO_x
Polylysine	Mica
phospholipid	Si, glass, evaporated metal films, polystyrene

The idea of DPN has been extended to several DPN-based techniques including nanopen reader and writer (NPRW),[36, 37] electrochemical DPN (E-DPN),[38] electro pen nanolithography (EPN)[39] and scanning probe contact printing (SP-CP).[40] The process of NPRW shown in Figure 2.3a is based on the combination of DPN and nanografting (Section 2.4).[36] A tip was inked with molecules different from the molecules of a self-assembled monolayer (SAM) on the substrate. Subsequently, the tip was brought into contact with the surface at higher load. The pre-functionalized SAM was removed mechanically, followed immediately by the deposition of molecules from the tip. The E-DPN and EPN approaches have in common that a bias voltage between a (semi)-conductive tip and a substrate is applied while patterning nanostructures. E-DPN utilizes the water meniscus as a tiny electrochemical cell where metal salts pre-coated on the tip, *e.g.* H_2PtCl_6, are dissolved and then reduced to metal that is deposited on the substrate.[38] For EPN (Figure 2.3b), a voltage-biased tip is moved over a methyl-terminated SAM-functionalized surface. By electro-oxidation, the methyl groups are converted to reactive carboxylic acid groups which can be used to attach ink molecules *in situ*.[39] SP-CP utilizes sharp or flat-topped DPN tips made of poly(dimethylsiloxane) (PDMS) to transfer ink onto a substrate.[40]
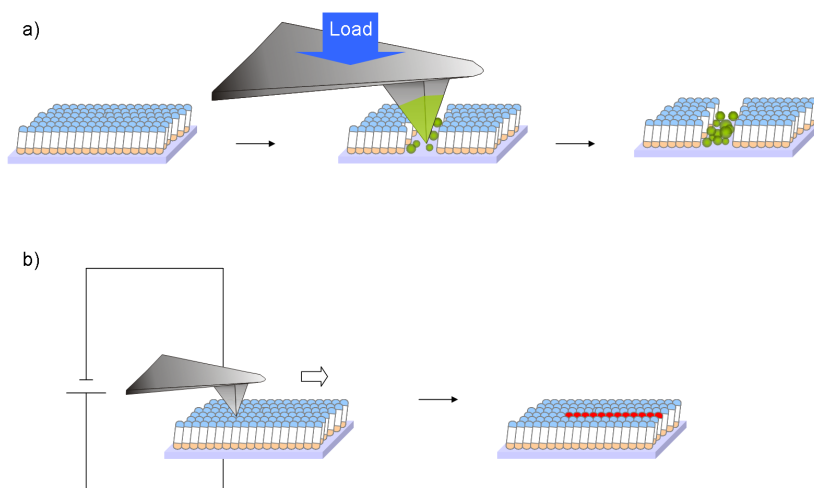

Figure 2.3. *The schematic processes of (a) nanopen reader and writer (NPRW) (b) electro pen nanolithography (EPN).*

Although DPN can be regarded as an effective tool for nanofabrication, initially a major drawback, like all other scanning probe lithography systems, was that it is inherently a serial process, which limits the throughput. In order to increase the efficiency of DPN, two different systems have been developed: one with passive "duplicating" tip arrays and the other with individually actuated active tips.[22]

The first and simplest passive probe array implemented for parallel DPN was described by Hong *et al.* in 2000.[41] The pens were brought simultaneously into contact with a slightly tilted substrate and scanned together. This produced the same number of patterns as the number of tips in the array at the same time. The results showed that the feature size of patterns had less than 10% standard deviation in line-width, implying that line-widths in DPN experiments are not strongly dependent on the tip-substrate contact force at least within certain ranges.[42] In designing passive probe arrays, the force constant has to be such that scratching of the substrate, oversensitivity to external noise, or difficulties in lifting the array due to large adhesive forces are prevented.[43, 44] Recently, passive probe arrays have been developed to write multiple arrays at one time and the number of probes of each array has dramatically increased to ~ 55,000 which allows users to obtain as many as 450,000,000 sophisticated features at sub-100nm scale within 30 minutes.[22, 45-47] Such an array has been used to pattern small molecules *e.g.* ODT and phospholipid membranes.[45, 48]

In order to write different patterns simultaneously, the development of active arrays in which each tip can be controlled separately is necessary. Zou *et al.* have developed a conductive-based contact sensing system for probe arrays in DPN.[49] This method uses the electrical resistance between the tip and the substrate as a sensitive indicator of physical contact and has the capability of switching each individual probe on/off independently based on electrical conduction.[49] Another way for controlling each tip is using thermal bimorph actuation (Figure 2.4a). Heating an embedded electrical heater causes differential expansion of components and therefore leads to bending of the cantilever close to/away from the substrate.[50-52] Since the distance between tips is fixed, it is possible to arrange the actions of tips spatially. Wang *et al*. used such a thermal bimorph actuator to develop an array consisting of different functional probes for nano-patterning and imaging shown in Figure 2.4b.[53] Advantages of this device are that the cross contamination is minimized, improving the efficiency of operation and increasing the registration accuracy. Recently, the electrostatic mechanism has also been utilized to actuate DPN probe arrays. This mechanism does not require probe heating, which is necessary for the thermal bimorph

actuation. In this way, the problem of cross talk between neighboring probes is reduced, which allows more closely spaced probe arrays.[54]
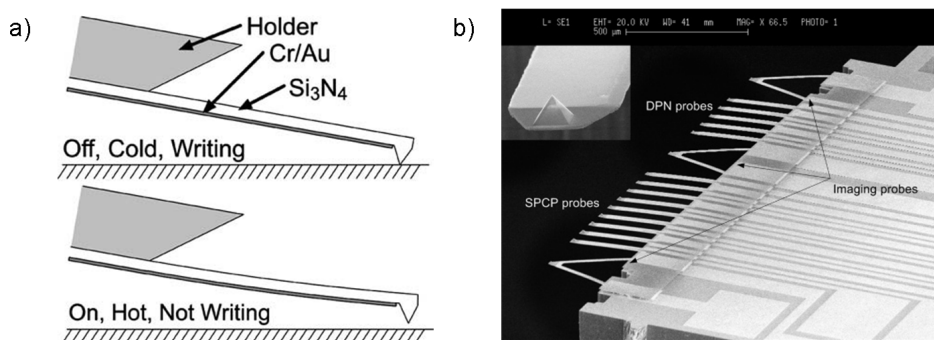
Figure 2.4. (a) The concept of operating an active DPN probe actuated by a thermal bimorph mechanism. Reprinted with permission from Ref. [50]. Copyright (2004) American Institute of Physics. (b) SEM image of a multifunctional probe array including five DPN Si_3N_4 probes, nine SP-CP PDMS probes and three imaging Si_3N_4 probes. The inset shows a Si_3N_4 tip with a curvature radius of 100 nm. Reprinted with permission from Ref. [53]. Copyright (2005) American Chemical Society.

All of these developments in DPN enable many applications in chemistry, materials sciences, and bio-sciences.[21, 22] Areas that are considered as unique applications of DPN include (1) fabricating biomolecular patterns as micro- and nano-arrays, (2) building chemical nanostructures as templates for the controlled orthogonal assembly of materials, and (3) generating hard features on surfaces such as etch-resist to obtain nanostructures with comparable feature sizes to those fabricated by e-beam lithography.[21, 22] In this chapter, the focus is on the first application, which will be described in detail in the next section.

2.3 Patterning biomolecules with dip-pen nanolithography

The range of biomolecules is very broad including cellulose, lipids, peptides, DNA, saccharides, and proteins. To focus the scope of this review, only proteins[23, 24, 30, 55-79], peptides[80-89], and DNA[29, 90-92] used for patterning by DPN are discussed.

Generally, two strategies can be discerned to pattern biomolecules with the DPN technique, namely an indirect method and a direct method (Figure 2.5). The indirect method (Section 2.3.1) places a suitable molecular functionality at a surface. For instance, first a layer of protein-adherent molecules is fabricated, followed by the immobilization of proteins from solution. The direct method (Section 2.3.2) comprises direct deposition of the biomolecule from an ink-coated tip onto a surface.[1, 2]

Functional immobilization of biomolecules, especially proteins, onto solid surfaces is very challenging since the interaction of proteins with a bare solid substrate frequently results in denaturation of proteins.[24] A variety of chemical strategies, sorted by non-covalent and covalent approaches, have been utilized in either indirect or direct DPN for patterning biomolecules, and are summarized in Table 2.2 and 2.3, respectively. In general, two main types of substrates, gold and silicon-based substrates have been used. Therefore, in each subsection, the chemical strategies utilized for patterning biomolecules are discussed based on the classification of the substrates used. In addition to the approaches summarized here, there are many other methods employed to fabricate biomolecular patterns onto a solid support using other lithography techniques, which have been described in several review articles and may also be applied to DPN in the near future.[93-96]
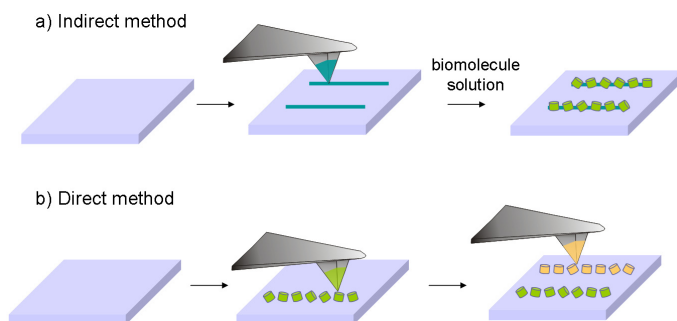
Figure 2.5. *Schematic representation of (a) indirect and (b) direct dip-pen nanolithography (DPN) method for patterning biomolecules.*

Table 2.2. *Overview of reported chemical strategies utilized for indirect DPN for patterning biomolecules on solid surface.*

Indirect DPN: non-covalent attachments
Mechanism	**Examples**	**Surfaces***
Electrostatic or hydrophobic interaction	➢ Immunoglobulin G (IgG)[60, 66, 69], lysozyme[60], retronectin[60], cytochrome c[57] and cowpea mosaic virus (CPMV) nanoparticles[55] on carboxylic acid-terminated surface. ➢ Membrane protein complexes[65] on protonated amino-terminated surface.	Au
	➢ Negatively charged DNA[90, 92] on poly(allylamine hydrochloride) (PAH)	Si-based
Biotin-streptavidin interaction	➢ Biotinylated bovine serum albumin (Biotin-BSA)[67] on streptavidin-terminated surface. ➢ Streptavidin[67, 75, 79] biotin-terminated surface.	Au
	➢ Neutravidin[68] and streptavidin[23, 75, 97] on biotin-terminated surface.	Si-based
Coordination chemistry	➢ Tobacco mosaic virus (TMV)[70] on Zn(II)-carboxylic acid rich-terminated surface. ➢ Histidine (His)-tagged ifnar2[79] on Ni-[BT]trisnickel(II)-nitrilotriacetic acid (NTA)-terminated surface.	Au
	➢ His-VFPs[63, 74, 75, 78] on Ni-NTA- terminated surface.	Si-based
ELP fusion	➢ ELP fusion proteins[87] on elastin-like polypeptides (ELP).	Au
Others (not specified)	➢ Antibodies[72], *e.g.* IgY, IgM on Zn(II)-carboxylic acid rich-terminated surface.	Au
Indirect DPN: covalent attachments
Thioether bond formation	➢ Cysteine mutant Cowpea mosaic virus (Cys-CPMV) nanoparticles[55, 76] on maleimide-terminated surface.	Au
	➢ Biotin-maleimide[23, 97] on thiol-terminated monolayer.	Si-based
Amide bond formation	➢ Amine-containing DNA[91] on carboxylic acid terminated monolayer ➢ protein A/G[71] and amine-containing biotin[67], peptide (ELPs)[87] on *N*-hydroxysuccinimidyl (NHS) ester-terminated monolayer.	Au
	➢ NHS functionalized biotin on polyethylenimine (PEI)-sputtered surface.[68]	Si-based
Oxyme formation	➢ Oxyamine-terminated linear peptide[83] on quinone-terminated surface.	Au
Ring opening polymerization (ROP)	➢ tryptophan-*N*-carboxyanhydride (Trp-NCA) on G4-NH$_2$ polyamidoamine (PAMAM) dendrimers deposited surface.[81]	Si-based

* *Si-based surfaces include silicon, silicon oxide and glass.*

Table 2.3. *Overview of reported chemical strategies utilized for direct DPN for patterning biomolecules on solid surface.*

Direct DPN: non-covalent attachments		
Mechanism	**Examples**	**Surfaces**
Electrostatic or hydrophobic interaction	➢ IgG[59] on negatively charged SiO_2 surface ➢ IgG[64] and His-VFPs[63] on amino-terminated surface.	Si-based
Crown ether to protonated amine interaction	➢ Angiogenin [56] and integrin $\alpha_v\beta_3$[56] on Prolinker[TM]-coated surface.	Au
coordination chemistry	➢ His-VFPs[63, 74, 75] on Ni-NTA-terminated surface. ➢ His-ubiquitin[58] and thioredoxin[58] on nickel oxide surface.	Si-based
Others (not specified)	➢ 3RGBP1 peptides[80] on Au surface.	Au
	➢ QBP1[80], QBP3[80] peptides and amphiphile (PA) nanofibers[86] on Si surface.	Si-based
	➢ Antibody[77] and streptavidin[77] on DNA.	biosurface
	➢ Biotin-collagen-binding peptides onto inner collagenous layer of Brunch's membrane (ICLBM)	
Direct DPN: covalent attachments		
Thioether bond formation	➢ TAT peptide with cysteine residues[85] on maleimide-terminated surface.	Si-based
Au-thiol interaction	➢ Thiol-containing collagen[62]; DNA[29], IgG[30], lysozyme[30] TAT peptide[88] and synthetic peptides (MH2)[84] on Au surface.	Au
Michael addition	➢ Acrylamide-containing DNA[29] and oligonucleotide[73] on thiol-terminated surface.	Si-based
Amide bond formation	➢ Amine-containing DNA[24] and IgG[24] on NHS ester-terminated surface.	Si-based
Imine bond formation	➢ Amine-containing IgG[59] on aldehyde-terminated monolayer	Si-based
Epoxy to amine reaction	➢ Amine-containing HCG[61] onto epoxy-terminated surface.	Si-based

* *Si-based surfaces include silicon, silicon oxide and glass.*

2.3.1 Indirect DPN Methods

2.3.1.1 Gold surfaces

The indirect method offers a very elegant and site-specific approach for biomolecule patterning. Several indirect DPN methods utilize 16-mercaptohexadecanoic acid (MHA) as ink molecules to generate dot or line patterns on gold surfaces. Subsequently, the non-patterned areas are passivated with ODT to prevent the non-specific adsorption of biomolecules. The carboxylic acid-terminated groups of MHA are subsequently used to immobilize biomolecules *via* electrostatic or hydrophobic interactions. Kwak *et al.* used this method to fabricate cytochrome c patterns on gold surfaces with a feature size of ~ 200nm.[57] Because of the electron transport properties of cytochrome c, these protein patterns have potential applications in biomolecular photodiode systems. Lee *et al.* generated lysozyme, Immunoglobulin G (IgG) and retronectin arrays with feature sizes of ~ 100-350 nm.[60] The areas surrounding MHA patterns were passivated with 11-mercaptoundecyl-tri(ethylene glycol) (EG$_3$-SH) instead of ODT. The biological activity of IgG arrays was retained as confirmed by binding anti-IgG to IgG. Patterns of retronectin, the cell adhesion recombinant fragment of fibronectin, were used to adhere to 3T3 Swiss fibroblast cells. This array was used for a study of cellular interactions with nanopatterned surfaces. The authors observed that the cells only attached to the printed region and were immobilized in a more flattened morphology.[60] Later, they extended this approach to fabrication of arrays of antibodies (anti-p24) with well-defined feature sizes of sub-100 nm. The bio-activity on Au surfaces in highly sensitive and selective immunoassays to detect human immunodeficiency virus type 1 p24 antigen (HIV-1 p24) was preserved (Figure 2.6). The HIV-1 p24 in plasma obtained from HIV-1-infected patients was hybridized with the antibody array. The bound protein was hybridized to a gold antibody-functionalized nanoparticle probe in order to amplify the detected signal. The nanoarray features in the three-component sandwich assay were confirmed by AFM. The authors demonstrated that such an immunoassay can exceed the detection limit of the conventional enzyme-linked ELISA based immunoassays by more than 1000-fold.[66] In these above mentioned cases, the biomolecular patterns were all fabricated on Au surfaces. Zhang *et al.* used the same concept to fabricate a single layer of Rabbit IgG dot patterns on MHA coated elevated Au nanostructures on SiO$_x$/Si substrates. The fluorophore-labeled anti rabbit IgG was used to confirm the bioactivity of proteins on solid supports.[69]
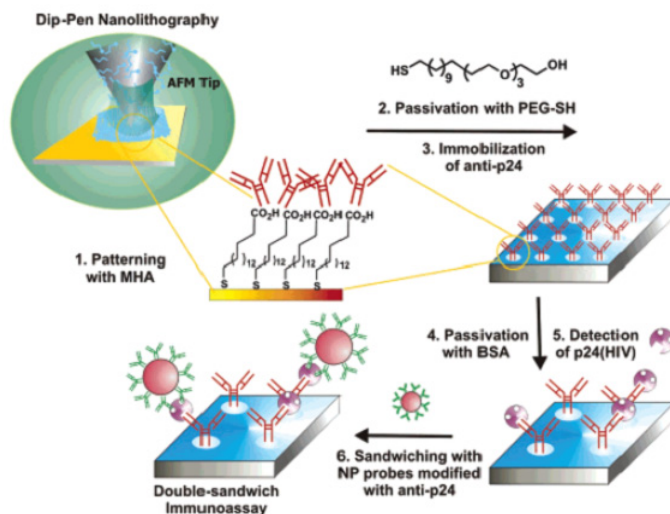
Figure 2.6. *Schematic representation of the fabrication of immunoassay for detecting HIV-1 p24 antigen with anti-p24 antibody. Reprinted with permission from Ref. [66]. Copyright (2004) American Chemical Society.*

Instead of utilizing electrostatic interactions, Demers *et al.* generated MHA patterns on Au surfaces to couple with alkylamine-modified DNA *via* formation of amide bonds.[91] The non-patterned area was passivated with ODT. The authors found that the MHA patterns could be fabricated again on the areas previously passivated with ODT during the initial writing procedure. Therefore, another sequence of alkylamine-modified DNA could be immobilized onto the newly-created MHA patterns. The formation of two DNA patterns was confirmed by coupling DNA with complementary predesigned oligonucleotide-modified particles of different sizes. Different heights of DNA dot patterns and some stray particles nonspecifically bound to the areas surrounding the oligonucleotide patterns were observed in the AFM topography images.[91]

Smith *et al.* reported two ways to fabricate cowpea mosaic virus (CPMV) particles onto solid surfaces: one is *via* electrostatic/hydrophobic interaction and the other is *via* covalent attachment.[55] In the non-covalent method, they immobilized CPMV particles onto DPN-generated MHA patterns with the rest of the area passivated with EG$_3$-SH. Since nonspecific adsorption of proteins often results in substantial denaturation and hence loss of biological activity, these authors developed a covalent method to immobilize

CPMV particles. They wrote mixed ink, including 11-mercaptoundecyl-penta(ethylene glycol) disulfide and a mixed disulfide substituted with one maleimide, onto gold surfaces. Subsequently, cysteine mutant CPMV (Cys-CPMV) particles were attached to the patterned area *via* a covalent reaction of cysteine and maleimide. In both cases, AFM topography measurements confirmed the formation of single layer CPMV particles patterns.[55] In the same year, Cheung *et al.* also demonstrated patterning Cys-CPMV particles with the same chemical reaction. They used DPN and nanografting to create amine-terminated alkanethiol molecules on gold surfaces. The amine groups were reacted subsequently with 3-maleimidopropionate N-hydroxysuccinimide ester (MPS) to form maleimide-terminated groups, to which Cys-CPMV particles were adhered.[76]

Membrane protein complexes attached to protonated amino-terminated SAMs created by DPN *via* electrostatic interactions have also been reported by Valiokas *et al.*.[65] The authors deposited $HS(CH_2)_{16}NH_2$ onto a Au surface with a resolution of ~ 300 nm and subsequently blocked the non-patterned region with $HS(CH2)_2CONH(CH_2CH_2O)_{\sim 15}CH_3$ for immobilization of the selective recruitment of membrane protein complexes from mutant *Rhodobacter sphaeroides*. These contain photosynthetic core complexes that form the reaction center of the light-harvesting complex one (LH1).[65]

Lee *et al.* demonstrated writing, with passive 26-probe arrays, of *N*-hydroxysuccinimide ester-terminated alkylthiols ($NHSC_{11}SH$) onto Au surfaces as a template for immobilizing protein A/G.[71] The NHS ester groups are frequently used to couple with the primary amino groups of biomolecules *via* the formation of amide bonds. Protein A/G has affinity to the Fc region of IgG. By utilizing this affinity binding, massively parallel nanoarrays with biologically active antibodies can be generated.[71] Hyun *et al.* also used NHS ester groups to fabricate biotin/streptavidin-terminated arrays. They first patterned MHA on Au surfaces with a feature size of ~ 200 nm. After obtaining the MHA patterns, they passivated the background with EG_3-SH and then activated carboxylic acid terminated groups of an MHA SAM with *N*-hydroxysuccinimide (NHS) and 1-ethyl-3-(dimethylamino)propyl carbodiimide (EDAC) to form NHS ester groups.[67] Biotinyl-3,6,9-trioxaundecanediamine (biotin-NH_2) was used to generate biotin-terminated patterns. Subsequently, streptavidin, a tetrameric protein with very high affinity to bind four biotins ($K_a \sim 10^{13}$ M^{-1}), was adhered to the patterned biotin area from solution. Therefore these protein arrays can be utilized to bind a variety of biotinylated molecules. The authors used biotinylated bovine serum albumin (Biotin-BSA) to demonstrate the retained functionality of this streptavidin-biotin system.[67] Later, Hyun *et*

al. extended their approach to immobilize amine-containing stimulus-responsive elastin-like polypeptide (ELP) onto patterned NHS ester-terminated regions.[87] The authors believe that ELP is end-grafted at the surface in a highly orientated manner because ELP only has two amino groups, one located at the N-terminus and the other on the side chain of the sole lysine residue. Such ELP patterns can be used as templates to capture an ELP fusion protein (Trx-ELP) above its lower critical solution temperature (LCST). The dissociation of Trx-ELP occurs when proteins become soluble in aqueous solution. This switch process is reversible which offers the potential application of building reusable protein nanoarrays.[87]

Rakickas *et al.* presented a platform to study protein-protein interactions and to form functional protein complexes at nanometer scale. For this purpose, multivalent chelator (MCh)-terminated templates were fabricated in a stepwise procedure combining dip-pen nanolithography and molecular recognition-directed assembly (Figure 2.7). The biotin-oligo(ethylene glycol) (OEG) disulfide molecules were first deposited on gold with line widths below 100 nm and then streptavidin was adhered to the biotin-terminated patterns from solution. Subsequently, the streptavidin groups were attached with tris-nitriloacetic acid biotin derivatives ([BT]trisNTA) to form MCh terminated templates for assembly of histidine-tagged (His-tagged) proteins. Histidine tags are generally engineered onto protein sequences to facilitate protein purification in analytical procedures. The [BT]trisNTA coordinated with Ni(II) area was used to immobilize His_{10}-ifnar2 proteins, whose functionality was confirmed by coupling INFα2 labeled with QD_{655}. This process was reversible by adding imidazole solution to remove His-tagged proteins.[79] This His-Ni(II)-NTA system is frequently used to immobilize biomolecules with orientation on solid surfaces.[93]

Hoover *et al.* presented an indirect approach to produce peptide arrays for immobilizing cells (3T3Swiss Albino mouse fibroblasts). They produced nanoarrays of hydroquinone terminated alkanethiol on glass substrates covered by a thin gold film. The non-patterned regions were passivated with tetra(ethylene glycol) terminated alkanethiol. By electrochemically oxidizing the nanopatterned hydroquinone, the corresponding quinone was obtained, which can react selectively with water soluble oxyamine-terminated linear Arg-Gly-Asp (RGD) peptide. These peptide patterns were used to study the polarity of adhered cells without the influences of cell-cell interactions. It was found that a cell was affected by its nano-environment to polarize toward the patterned higher density peptide region.[83]
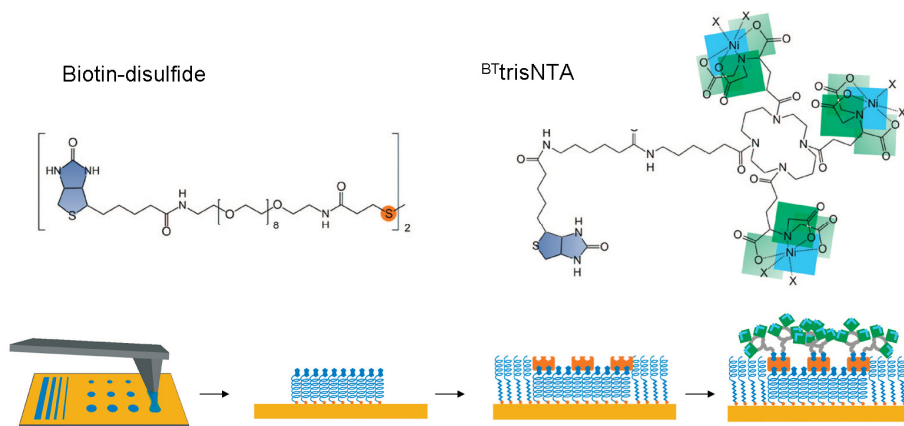
Figure 2.7. *Schematic representation of the fabrication of [BT]trisNTA-terminated nanoarrays by DPN used for studying protein-protein interactions. Reprinted with permission from Ref. [79]. Copyright (2008) American Chemical Society.*

Vega *et al.* relied on the ability of Zn(II) ions to bridge a surface patterned with MHA and the tobacco mosaic virus (TMV) with its carboxylate-rich surface. They demonstrated the possibility of isolating and controlling the orientation of TMV particles.[70] Later, they used the same approach to immobilize antibodies, such as IgY and IgM. Although they did not know the precise chemistry behind the reaction between the antibodies and Zn(II) ions, this approach enables the further adhesion of protein A, G, A/G or L with functionality.[72]

2.3.1.2 Silicon-based surfaces

The majority of DPN experiments use the thiol-on-gold couple, where the chemisorption of the thiol molecules onto gold surfaces is the driving force of ink transfer from tips. Patterning of biomolecules with indirect DPN on silicon-based surfaces is also reported.[23, 68, 74, 75, 78, 81, 90, 97]

Pena *et al.* reported one way to fabricate biotin-terminated arrays to immobilize fluorophore-labeled neutravidin on silicon based substrates.[68] They first sputtered polyethylenimine (PEI) onto SiO_2 surfaces, followed by depositing NHS functionalized biotin. Some nonspecific binding was observed, but the authors claimed that the signal to

noise ratio was sufficient. Nyamjav *et al.* fabricated poly(allylamine hydrochloride) (PAH), a polyelectrolyte, patterns on SiO$_x$ wafers, demonstrating that these well-defined positively charged regions can be used to guide the stretching of long DNA molecules.[90] Such stretched DNA adhered to patterned PAH areas and was subsequently used as a template to immobilize Fe$_3$O$_4$ nanoparticles by electrostatic interactions.[92]

Jung *et al.* demonstrated that it is possible to fabricate alkoxysilanes patterns on glass substrates. They used 3′-mercaptopropyltrimethoxysilane (MPTMS) as the ink molecules. The MPTPS patterns were verified by reaction with biotin-maleimide *via* the formation of thioether bonds to immobilize Cy3-labeled streptavidin.[97] Later, the authors extended this approach to fabricate (+)-biotinyl-3-maleimidopropionamidyl-3,6-dioxaoctanediamine (maleimide PEO$_2$-biotin) directly onto MPTPS-functionalized glass substrates.[23] However, the authors observed that obtaining consistent patterns of the maleimide-PEO$_2$-biotin was very difficult even when DPN experiments were performed with RH above 90%. Finally, they found that adding small amounts of the nonionic surfactant Tween-20 (polyoxyethylene sorbitan monolaurate) to the ink can activate the transfer of the biotin linker molecules from the tip to the MPTMS-coated substrates, enabling biotin patterning routinely with sub-100 nm resolution at a moderate relative humidity of 50-65% RH. Cy3-labeled streptavidin was again used to confirm the successful generation of maleimide PEO$_2$-biotin patterns.[23] The same chemical strategy has also been utilized by Kim *et al.*[74] They wrote maleimido-C$_3$-nitrilotriacetic acid (NTA) onto MPTMS-functionalized glass substrates for the effective immobilization of His-tagged enhanced green fluorescent proteins by utilizing coordination chemistry.[74] Sekula *et al.* demonstrated spatial patterned supported phospholipid membranes with biotin and nitrilotriacetic acid (NTA) head groups onto hydrophilic glass substrates as templates to immobilize Cy3-labeled streptavidin and His-tagged green fluorescent proteins (His-GFP) (Figure 2.8a), respectively. By using passive 26-probes arrays, integrated protein nanoarrays exploiting two different funtionalities were generated (Figure 2.8b). The authors also demonstrated that these biomimetic membrane patterns can be used as substrates for cell culture, by the selective adhesion and activation of T-cells.[75]

Zhou *et al.* reported an approach to fabricate nanopatterns of peptides of specific chain length. The preparation procedure started by depositing G4-NH$_2$ polyamidoamine (PAMAM) dendrimers onto Si/SiOx substrates with feature sizes of ∼ 180 nm *via* electrostatic interactions. The patterned dendrimer substrates were incubated in tryptophan-*N*-carboxyanhydride (Trp-NCA) solution for different times to initiate

ring-opening polymerization (ROP), a well known method to obtain oligopeptides with variable chain lengths.[81]
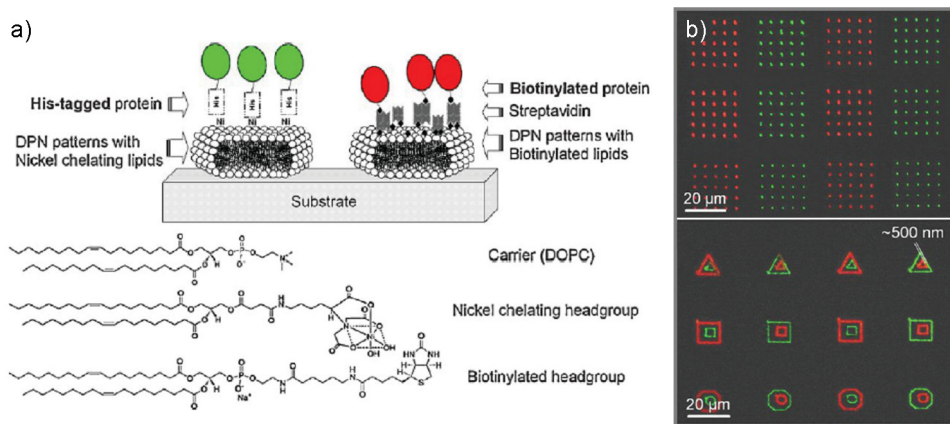
Figure 2.8. *(a) Schematic representation of the protein-coupling strategies by pattering lipids onto a substrate and the chemical structures of the used lipids. (b) Fluorescence image of Cy3-labeled streptavidin and His-GFP selectively immobilized on the pre-generated different lipid patterns written with a passive 26-probes array. Reproduced with permission from Ref. [75]. Copyright (2008) Wiley-VCH Verlag GmbH & Co. KGaA.*

2.3.2 Direct DPN Methods

Compared with indirect DPN, direct DPN is a simple and straightforward approach to fabricate protein patterns without non-specific binding.[2] However, it has several restrictions, such as, slow transportation of high molecular weight biomolecules from an AFM tip to a substrate, difficulties of preserving the biological functionalities of biomolecules on the tips surface during writing, and short operation time due to the limited ink volume.[64] To overcome these restrictions, chemical modification of AFM tip surfaces is a common strategy used to overcome the restrictions mentioned above. Therefore, in this section we separately address tips with and without surface functionalization.

2.3.2.1 With bare tips

2.3.2.1a Gold surfaces

Fabricating nanostructures with DPN is usually performed by operating AFM in contact mode. However, in the bio-related domain, the use of tapping-mode AFM for lithography and imaging may be more suitable, because of the sensitivity of biomolecules to the shear and friction forces required to control the surface in the contact mode. Two examples of utilizing tapping-mode AFM to deposit biomolecules were reported. The first was reported by Wilson *et al.* They delivered thiolated collagen and collagen-like peptides onto gold substrates with line widths as small as 30-50 nm and showed that collagen still preserved its native triple-helical structure and bioactivity.[62] Later, Agarwal *et al.* used DPN in tapping mode to deposit synthetic peptides (MH2) containing an active cysteine (Cys) residue onto a gold surface with a feature size as small as 70 nm.[84]

Cho *et al.* demonstrated that thiol-containing TAT peptides, derived from the TAT protein of the HIV-1, can be directly written onto Au substrates.[88] More recently, Wei *et al.* generated 3-repeat GBP1 peptide with biotin incorporated (biotin-3RGBP1) onto Au surfaces with the smallest feature size of ~ 80 nm. Alexa Fluor 594-labeled streptavidin was subsequently used to visualize the biotinylated peptide patterns.[80] Both Cho *et al.* and Wei *et al.* also demonstrated peptide patterns on Si-based surfaces, which are described in the next section.

2.3.2.1b Silicon-based surfaces

Noy *et al.* patterned lines of human chorionic gonadotropin (HCG) antibody tagged with tetramethylrhodamine (TMR) at sub-micrometer scale on a glass substrate pretreated with 3-glycidoxypropyltrimethoxysilane *via* the reaction of amines with epoxides. The epoxy-terminated monolayer facilitates the adhesion of proteins to surfaces. The resulting patterns were examined by an instrument that combines AFM and scanning confocal microscopy.[61] However, the biological activity of the resulting patterns was not demonstrated.

A ribosome display is a cell-free system for *in vitro* selection of proteins and peptides from large libraries that can produce protein-ribosome-mRNA fusion molecules by coupling individual proteins (phenotypes) to their corresponding mRNA (genotypes). Kim *et al.* demonstrated deposition of acrylamide-modified oligonucleotides mixed with deionized water and *N,N*-dimethylformamide (DMF) onto MPTMS-coated glass

substrates. The volume percentage of DMF used to facilitate the ink transport was very important for obtaining consistent patterns. The bioactivity of written oligonucleotide was confirmed *via* hybridization with fluorophore-labeled complementary oligonucleotide or protein-ribosome-mRNA fusion molecules. The authors demonstrated that this approach (Figure 2.9) can be used to fabricate protein arrays without prior protein purification.[73]
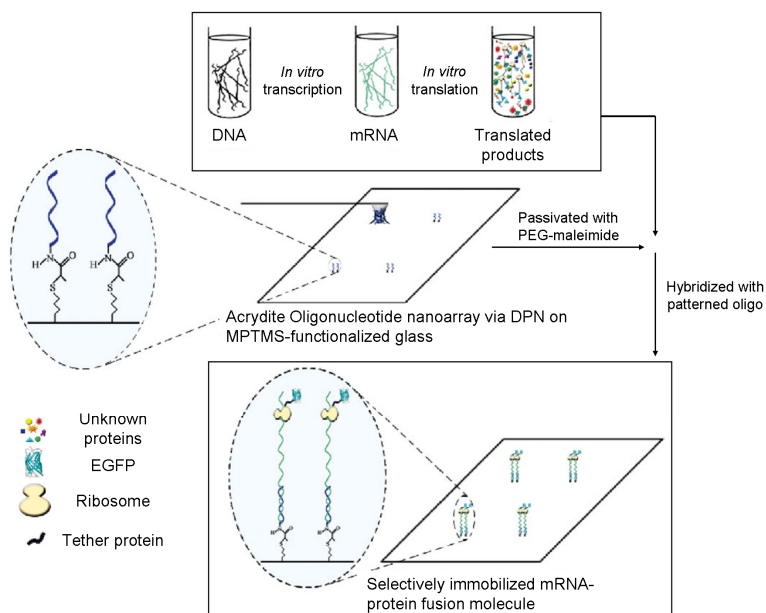
Figure 2.9. Schematic illustration of the ribosome display technique and the procedure of fabricating protein arrays by directly depositing oligonucleotide as templates. Reproduced with permission from Ref. [73]. Copyright (2008) Wiley-VCH Verlag GmbH & Co. KGaA.

Cho *et al.* not only demonstrated direct patterning of thiol-containing TAT peptides onto an Au surface but also onto Si substrates functionalized with a malemide-terminated monolayer.[85] For patterning TAT peptides on surface modified Si substrates, ~ 80% RH was required in order to obtain nanostructures. This was attributed to the high hydrophobicity of the malemide-terminated monolayer.[85] Besides fabricating biotin-3RGBP1 peptide patterns on Au surfaces, Wei *et al.* also deposited two kinds of

biotinylated peptide (biotin-QBP1 and biotin-QBP3) onto Si surfaces with the smallest feature size of ~ 80 nm and confirmed the formation of the peptide patterns with Alexa Fluor 594-labled streptavidin.[80] Sistiabudi *et al.* investigated how surface properties affected the direct writing of polyarginine and poly(glutamic acid) polypeptides. Three different surfaces were utilized including hydrophilic bare silicon oxide and 3-aminopropyltriethoxysilane (APTES)-functionalized Si substrate and hydrophobic trimethoxypropylsilane (TMPS)-functionalized Si substrate. Their results demonstrated that both polypeptides were not transferred onto hydrophobic TMPS-functionalized surface even when performing DPN experiments under high RH conditions. Besides, they found that the transport of polypeptides was facilitated by adding Tween-20 surfactant, because of the increased wettability of the collagenous surface. The deposition of ink was therefore able to be operated at lower contact force and RH.[89]

2.3.2.1c Other surfaces

Most DPN experiments have been performed by writing ink onto hard solid supports and it is a challenge to deliver molecules onto soft matter and therefore only few examples have been reported. Li *et al.* wrote Cy3-antibody and Cy3-streptavidin onto a stretched DNA, which was pre-deposited onto a 3-aminopropyltriethoxysilane (APTES)-functionalized mica surface. The smallest feature size achieved was ~ 40 nm.[77] Sistiabudi *et al.* not only deposited polyarginine and poly(glutamic acid) polypeptide onto Si-based substrates but also onto the inner collagenous layer of Brunch's membrane (ICLBM). More recently, they presented the deposition of biotin-collagen-binding peptide (CBP) molecules onto the ICLBM surface and verified their bioactivity through the binding of Cy3-labeled streptavidin.[82]

2.3.2.2. With functionalized tips

2.3.2.2a Gold surfaces

Lee *et al.* reported a method to functionalize Au-coated Si_3N_4 cantilevers, which was used to fabricate lysozyme (Lyz) and rabbit IgG arrays at the same time with the smallest feature size of ~ 45 nm in diameter without cross-contaminations.[30] The process started with growing a monolayer of symmetric 11-mercapto-undecylpenta(ethylene glycol)disulfide (PEG) on a cantilever, coating of an Au layer on the tip side *via* thermal

evaporation, and finally forming a carboxylic-terminated SAM on the tip surface. The PEG layer prevents the adsorption of protein on the backside of the cantilever and the hydrophilic carboxylic groups can facilitate the adsorption of proteins onto the tip surfaces. The Cys residues of rabbit IgG also provided a strong driving force to adhere proteins onto gold surfaces due to thiol-Au reaction. The bio-recognition properties of two component protein arrays were confirmed by the observation of anti-rabbit IgG binding to the rabbit IgG features only (Figure 2.10a).[30] The authors found that the optimum patterning results were obtained when performing DPN at a RH of ~ 80-90 % at room temperature.[30]

Another possibility to increase the hydrophilic property of the tip surface by functionalizing the tip with mercaptoundecanoic acid (MUDA) has been reported.[56] Angiogenin and integrin $\alpha_v\beta_3$ were written on a gold substrate coated with a layer of Prolinker™ with pattern sizes as small as 120 nm. The Prolinker™ contains crown ether moieties that act as a host cavity for protonated amino groups on protein surfaces.[56]

Demers *et al.* found that it was difficult to control patterned DNA sizes and shapes while using a bare Si_3N_4 tip. Therefore, they functionalized tip surfaces with 3'-aminopropyltrimethoxysilane (APTMS) to improve the adhesion of DNA to the tips.[29] Using these APTMS-functionalized tips, DNA bearing hexanethiol groups and oligonucleotides with 5'-terminal acrylamide groups were written onto gold at sub-100 nm scale.[29]

2.3.2.2b Silicon-based surfaces

Demers *et al.* again used APTMS-functionalized AFM tips to write oligonucleotides containing 5'-terminal acrylamide groups onto MPTPS-modified SiO_2 substrates at sub-100 nm scale.[29] The authors demonstrated the possibility of generating two-component DNA arrays on SiO_2 surfaces while retaining their biological activities, which was confirmed by hybridization with complementary fluorophore-labeled DNA (Figure 2.10b).[29]

Lim *et al.* modified an AFM tip with 2-[methoxypoly(ethyleneoxy)-propyl] trimethoxysilane (Si-PEG) to write (Anti-)rabbit IgG onto a negatively charged, aldehyde-terminated SiO_2 surface *via* respectively electrostatic interaction and covalent bonding down to a length scale of ~ 50 nm.[59] Si-PEG can facilitate the transfer of proteins from tip to surfaces and also prevent the denaturation of proteins on the tip surface.[59]

Jiang *et al.* demonstrated direct patterning of two kinds of amphiphile (PA) peptide nanofibers onto Si substrates at micrometer scale by using AFM tips coated with poly(ethylene glycol) (PEG), which avoids the self-assembly of nanofibers on the tip surfaces.[86]
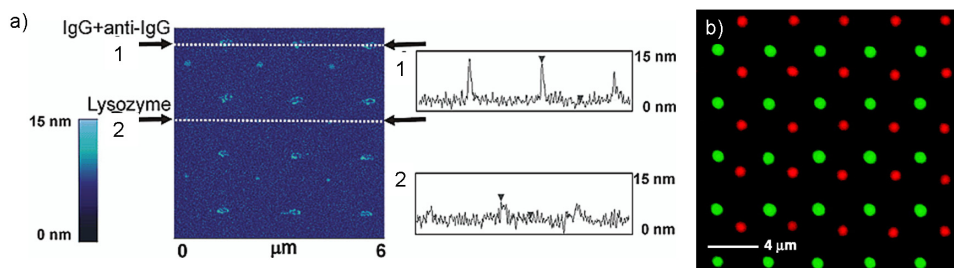
Figure 2.10. (a) AFM topography image of two-components protein nanoarrays after reacting with anti-IgG. The height increase was only observed on the the IgG features indicating that the bio-recognition properties of IgG were preserved. Reprinted with permission from Ref. [30]. Copyright (2003) American Chemical Society. (b) Combined red-green epifluorescence image of two-components DNA nanoarrays after simultaneously hybridizing with two different complementary fluorophore-labeled DNA. Reprinted with permission from Ref. [29]. Copyright (2003) AAAS.

Apart from microfluidic approaches, porous matrix materials have been developed to functionalize the AFM tip surfaces to increase the total amount of coated ink molecules. A few methods have been reported. Choi *et al.* fabricated hydrophilic nanoporous polyoxazoline-coated Si AFM tips by functionalizing the bare surface with 11-iodoundecyltrichlorosilane as an initiator and performing the polymerization of 2-methyl-2-oxazoline monomers on the pre-treated surface.[64] Human IgG and prostate specific antigen (PSA) protein arrays were generated onto *N*-2-amino-ethyl-11-aminoundecyltrimethoxysilane (AUMS)-functionalized Si substrate with feature sizes as small as ~ 250 nm and ~ 85 nm in diameter, respectively. The authors demonstrated that it is at least five times faster to generate protein nanoarrays with the nanoporous polyoxazoline-coated tip than with a conventional Si tip.[64] By using agarose as a "universal" carrier to generate biomolecular patterns, Senesi *et al.* presented another way

(Figure 2.11a and b) to encapsulate proteins (IgG) and oligonucleotides onto AFM tip surfaces. They wrote the smallest feature size of ~ 50 nm on *N*-hydroxysuccinimide-ester activated glass substrates. By reacting with fluorophore-labeled anti-IgG and complementary oligonucleotides, respectively, the biorecognition properties of IgG and oligonucleotides were confirmed. Combined with passive probe arrays, Cy3-labeled oligonucleotide arrays were fabricated in a parallel manner (Figure 2.11c). The authors reported that the process of agarose-assisted DPN for patterning biomolecules is very fast and can be systematically adjusted by controlling the concentrations of accelerating agents, *e.g.* tricine buffer, used in agarose matrix.[24]
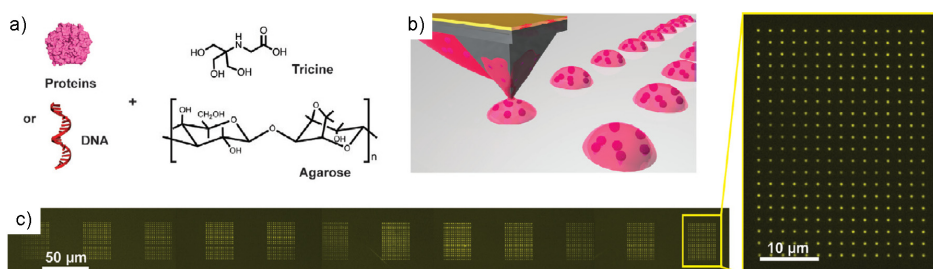
Figure 2.11. *(a) Schematic representation of ink and matrix components; (b) an illustration showing the process of agarose-assisted DPN; (c) epifluorescent microscope image of a 15 × 20 array of 500 nm Cy3 labeled oligonucleotide features generated in parallel from a 12-tip cantilever array. Reprinted with permission from Ref. [24]. Copyright (2009) American Chemical Society.*

2.3.2.2c Other surfaces

Most direct DPN experiments have been performed by writing ink onto either Au or Si-based substrates. There is one example of using other surfaces reported by Nam *et al.*. They described a way to facilitate the wetting and transport of His-tagged ubiquitin or thioredoxin by coating a thin layer of ~ 5 nm nickel onto a Si_3N_4 AFM tip. These proteins were deposited onto nickel oxide surfaces with a feature size down to ~ 85 nm.[58]

2.4 Other AFM-based lithography techniques for patterning biomolecules

Besides DPN, there are a few other AFM-based lithography techniques for generating biomolecule patterns including nanoshaving/nanografting, enzymatic lithography, bias-AFM lithography, and fountain pen lithography.[13]

Figure 2.12a illustrates the operation procedures for indirect and direct nanografting. The concept is to shave SAM molecules by force with an AFM tip and then refill from solution the gaps with desired molecules that have higher affinity to the surface than the removed molecules.[98] In indirect nanografting, it was reported that carboxylic acid-terminated SAMs or aldhyde-terminated SAMs were nanografted onto methyl-terminated SAMs on Au surfaces for immobilizing Lysozyme and IgG onto the patterned region with a feature size as small as 10 nm, either *via* electrostatic interaction or formation of imine bonds, respectively.[99, 100] By using 1-ethyl-3-(3-dimethylaminopropyl)-carbodiimide (EDC), IgG was also bound to carboxylic acid groups *via* the formation of amide bonds.[101] Cheung *et al.* used indirect DPN to pattern Cys-CPMV onto maleimide-terminated monolayers.[76] A few years later, they demonstrated nanografting of Ni-NTA alkanethiol molecules onto PEG-terminated alkanethiol for immobilizing His-tagged CPMV with a line width equal to the virus diameter (~ 28 nm).[102] Lee *et al.* demonstrated nanografting of octyldimethylmonochlorosilane (C_8DMS) with aminosilane on a silicon oxide surface. The aminosilane area created was subsequently used to immobilize negatively charged DNA *via* electrostatic interactions.[103]

Direct nanografting is in most of the cases based on immobilizing DNA[104] and proteins[105, 106] containing thiol groups onto Au surfaces *via* the well-known Au-thiol interaction. An extended approach of nanografting called native protein nanolithography was reported by Tinazli *et al.* to assemble proteins or multiprotein complexes at nanometer scale under native conditions. Their concept (Figure 2.12b) uses the contact oscillation mode of AFM to detach one kind of His-tagged proteins and replace them by another kind on a Ni-NTA-terminated monolayer. Functional protein complexes, with uniform orientation at dimensions down to 50 nm, were obtained (Figure 2.12c).[107] The disadvantage of nanografting is that the type of surface is limited to Au. However, this technique enables generating high resolution nanostructures with a feature size as small as 10 nm.[100]
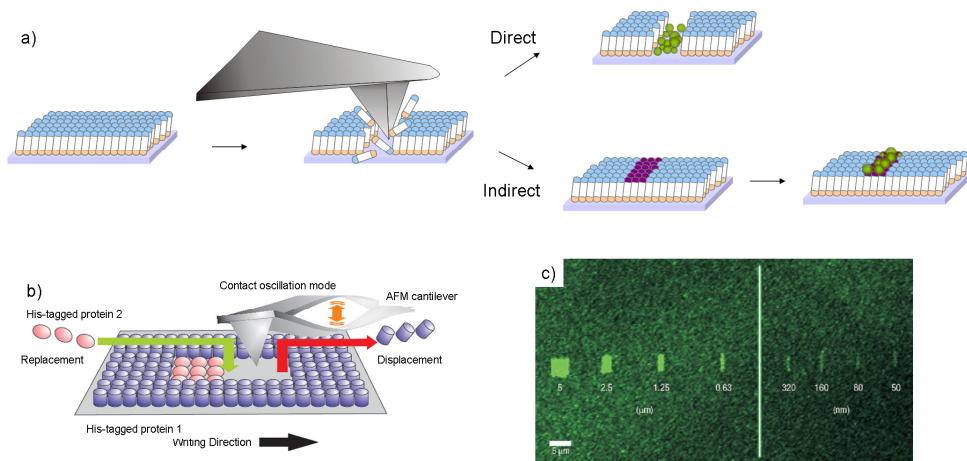
Figure 2.12. *Schematic representation of (a) direct and indirect nanografting technique for patterning biomolecules, (b) native protein lithography. (c)Fluorescent image of protein patterns generated by local exchange of affinity-captured proteasome complexes (αN-His$_6$)with Oregon Green-labeled MBP-His$_{10}$. Reprinted by permission from Macmillan Publishers Ltd: [Nature Nanotechnology, Ref. 107], copyright (2007).*

The idea of enzymatic lithography is to bring an enzyme-coated tip to touch a surface and then induce an enzymatic reaction. Takeda *et al.* first demonstrated this technique by using a *Staphylococcal* serine V8 protease-coated AFM tip to digest peptide functionalized mica on a μm scale surface in a buffered solution.[108] Later, the authors utilized resonance energy transfer (FRET) peptides to confirm the reaction of enzymatic lithography. A quencher residue was released from the peptide when *Staphylococcal* serine V8 protease digested the reporter peptide. This resulted in the enhancement of fluorescence intensity.[109] Hyun *et al.* proposed another approach by scanning oligonucleotide-functionalized Au surfaces with a DNase I-coated tip. The DNase I was activated by adding Mg(II) ions in the solution and then the local digestion of oligonucleotides was carried out to form nanotrenches on surfaces.[110]

Tang *et al.* presented another approach to deliver proteins with nanoscale precision by functionalizing tip surfaces with a streptavidin-terminated photocleavable cross linker. By irradiating with UV light, the streptavidin molecules were released from the tip surface and bound well to the biotin-terminated monolayer.[111]

Several groups demonstrated that applying a bias between tip and substrate locally modifies the surface properties[112-115] for adhering biomolecules or facilitating the transport of biomolecules.[116] Pavlovic *et al.* converted a thiol-terminated monolayer to a thiolsulfinates/thiolsulfonates-terminated monolayer by applying a voltage. Thiol-containing proteins were immobilized onto the oxidized area *via* the formation of disulfide bonds. The advantage of this approach is that the bonding can be reversed by adding dithiothreithol (DTT) to break the disulfide bonds.[115] Gu *et al.* applied a voltage on oligo(ethylene glycol) (OEG)-terminated substrates to generate dot patterns with a diameter of ~ 90nm. Their results suggested that the bias-applied hydroxyl groups could be converted to carboxylic groups by adding succinic anhydride. Subsequently, avidin was attached to the patterned region in the presence of 1-ethyl-3-(3-dimethylaminopropyl)carbodiimide (EDAC) and biotinylated-BSA was used to confirm the success of the reaction.[114] Recently, the same group demonstrated that the resolution of feature size can be scaled down to sub-10 nm.[117]

The disadvantages of DPN for patterning biomolecules are the short operation times due to the limited ink volume and difficulties of maintaining biological activity on dry tip surfaces. Therefore, cantilevers connected to an ink reservoir were developed to overcome these restrictions. Taha *et al.* used cantilevered nanopipette fountain pens to deliver protein G and GFP onto super-aldehyde surfaces and BSA-coated substrates respectively. The smallest feature size was ~ 200 nm.[118] Xu *et al.* developed quill-type surface patterning chips including both single and multiple cantilevers which were used to generate Cy3-streptavidin arrays with routine spot sizes of 2-3 μm onto dithiobis(succinimidyl) undecanoate monolayer-functionalized Au substrates.[119] Moldovan *et al.* designed so called nanofountain pen (NFP) arrays[120-122] with the ability of carrying multiple inks (Figure 2.13a and 2.13b). Several other examples of generating biomolecular features with these nanofountain pen arrays were reported by Espinosa's group.[122-124] For example, Kim *et al.* utilized NFP to deposit alkanethiol-modified oligonucleotides onto Au surfaces with smallest feature sizes of ~ 200 nm and subsequently passivated the unpatterned area with hexanethiol to avoid unspecific binding. The formation of oligonucleotide patterns was confirmed by hybridization of the linker and probe DNA strands (Figure 2.13c).[122]
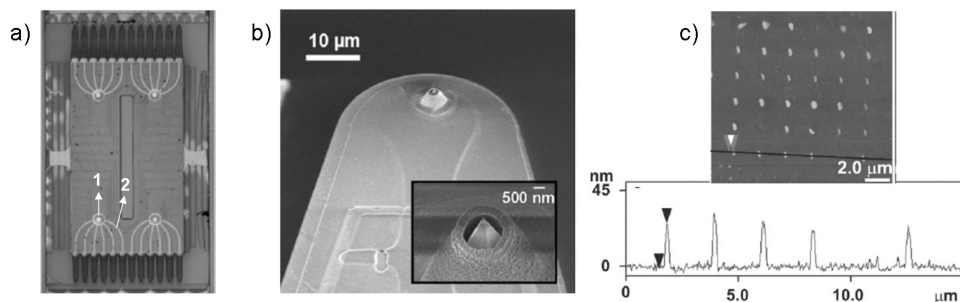
Figure 2.13. *(a) Optical image of the second generation nanofountain pen (NFP) chip. 1 and 2 indicate on-chip reservoir and microchannel, respectively. (b) SEM image of a cantilever integrated with a volcano tip at the end; in the inset a close-up of the volcano tip is shown. (c) AFM tapping-mode topography image of an array of dots generated with three different tip-surface contact times of 2, 1, and 0.5 s, for each alternating row of the array. The height profile of the same array indicated by the black line is shown below of the AFM image. Reproduced with permission from Ref. [122]. Copyright (2008) Wiley-VCH Verlag GmbH & Co. KGaA..*

2.5 Conclusions

In summary, in the first part of this chapter, recent developments of dip-pen nanolithography (DPN), which is a relatively inexpensive and high-resolution AFM-based lithography technique, are reviewed. Although the patterning efficiency of DPN was low during the early stages of development of the technique, the successful design and fabrication of active and passive probe arrays during the past few years has dramatically improved the patterning efficiency. These probe arrays allow users to deposit different ink molecules simultaneously and in a massively parallel manner at sub-micrometer scale.

In the second part of this chapter, different chemical strategies used to fabricate biomolecular nanostructures on solid supports with either direct or indirect DPN are reviewed. It can be concluded that gold and Si-based materials are the most commonly used solid substrates for DPN. Also, chemical modification of AFM tip surfaces is a frequently utilized strategy for direct DPN to facilitate the deposition of biomolecules onto surfaces. In addition to DPN, a selection of AFM-based lithography techniques used for bio-patterning was briefly described.

Besides the strategies reviewed in this chapter, an indirect DPN approach (see also Chapter 4) and a direct DPN approach (see also Chapter 6) are presented in this thesis to fabricate protein patterns. Chapter 4 describes how Ni(II) ions can be written onto NTA-terminated monolayer-functionalized glass substrates as templates to immobilize His-tagged visible fluorescent proteins (His-VFPs) *via* a specific metal-protein interaction. This approach not only enables the generation of protein patterns but also the characterization of the dependence of Ni(II) ions transfer on fundamental parameters of DPN, such as writing speeds and tip-surface contact times. In Chapter 6, direct depositions of His-VFPs onto Ni(II)-NTA monolayers will be described. In order to absorb larger amount of biomolecules onto tip surfaces, a method is developed to coat the surfaces of AFM tips with a thin layer of porous film by using Layer-by-Layer (LbL) techniques. Compared to a bare AFM tip, this porous film can act as a larger volume ink reservoir for long-term DPN writing.

The combination of nanofabrication and biomolecules enables the study of fundamental interactions between cells and nano-structured surfaces, and the development of high-density bio-nanoarrays with potential for several applications including fast screening of routine diagnostic tests.

2.6 References

1. Mendes, P. M.; Yeung, C. L.; Preece, J. A. Bio-Nanopatterning of Surfaces. *Nanoscale Res. Lett.* **2007,** *2*, 373-384.

2. Christman, K. L.; Enriquez-Rios, V. D.; Maynard, H. D. Nanopatterning Proteins and Peptides. *Soft Matter* **2006,** *2*, 928-939.

3. Lom, B.; Healy, K. E.; Hockberger, P. E. A Versatile Technique for Patterning Biomolecules onto Glass Coverslips. *J. Neurosci. Meth.* **1993,** *50*, 385-397.

4. Schwarz, A.; Rossier, J. S.; Roulet, E.; Mermod, N.; Roberts, M. A.; Girault, H. H. Micropatterning of Biomolecules on Polymer Substrates. *Langmuir* **1998,** *14*, 5526-5531.

5. Rozkiewicz, D. I.; Gierlich, J.; Burley, G. A.; Gutsmiedl, K.; Carell, T.; Ravoo, B. J.; Reinhoudt, D. N. Transfer Printing of DNA by "Click" Chemistry. *Chembiochem* **2007,** *8*, 1997-2002.

6. Rozkiewicz, D. I.; Brugman, W.; Kerkhoven, R. M.; Ravoo, B. J.; Reinhoudt, D. N. Dendrimer-Mediated Transfer Printing of DNA and Rna Microarrays. *J. Am. Chem. Soc.* **2007,** *129*, 11593-11599.

7. Li, H. W.; Muir, B. V. O.; Fichet, G.; Huck, W. T. S. Nanocontact Printing: A Route to Sub-50-Nm-Scale Chemical and Biological Patterning. *Langmuir* **2003,** *19*, 1963-1965.

8. Escalante, M.; Zhao, Y. P.; Ludden, M. J. W.; Vermeij, R.; Olsen, J. D.; Berenschot, E.; Hunter, C. N.; Huskens, J.; Subramaniam, V.; Otto, C. Nanometer Arrays of Functional Light Harvesting Antenna

Complexes by Nanoimprint Lithography and Host-Guest Interactions. *J. Am. Chem. Soc.* **2008,** *130*, 8892-8893.

9. Escalante, M.; Maury, P.; Bruinink, C. M.; van der Werf, K.; Olsen, J. D.; Timney, J. A.; Huskens, J.; Hunter, C. N.; Subramaniam, V.; Otto, C. Directed Assembly of Functional Light Harvesting Antenna Complexes onto Chemically Patterned Surfaces. *Nanotechnology* **2008,** *19*, -025101.

10. Rundqvist, J.; Hoh, J. H.; Haviland, D. B. Directed Immobilization of Protein-Coated Nanospheres to Nanometer-Scale Patterns Fabricated by Electron Beam Lithography of Poly(Ethylene Glycol) Self-Assembled Monolayers. *Langmuir* **2006,** *22*, 5100-5107.

11. Rundqvist, J.; Mendoza, B.; Werbin, J. L.; Heinz, W. F.; Lemmon, C.; Romer, L. H.; Haviland, D. B.; Hoh, J. H. High Fidelity Functional Patterns of an Extracellular Matrix Protein by Electron Beam-Based Inactivation. *J. Am. Chem. Soc.* **2007,** *129*, 59-67.

12. Glezos, N.; Misiakos, K.; Kakabakos, S.; Petrou, P.; Terzoudi, G. Electron Beam Patterning of Biomolecules. *Biosens. Bioelectron.* **2002,** *17*, 279-282.

13. Ngunjiri, J.; Garno, J. C. Afm-Based Lithography for Nanoscale Protein Assays. *Anal. Chem.* **2008,** *80*, 1361-1369.

14. Piner, R. D.; Zhu, J.; Xu, F.; Hong, S. H.; Mirkin, C. A. "Dip-Pen" Nanolithography. *Science* **1999,** *283*, 661-663.

15. Binnig, G.; Gerber, C.; Stoll, E.; Albrecht, T. R.; Quate, C. F. Atomic Resolution with Atomic Force Microscope. *Europhys. Lett.* **1987,** *3*, 1281-1286.

16. Jaschke, M.; Butt, H. J. Deposition of Organic Material by the Tip of a Scanning Force Microscope. *Langmuir* **1995,** *11*, 1061-1064.

17. Kramer, S.; Fuierer, R. R.; Gorman, C. B. Scanning Probe Lithography Using Self-Assembled Monolayers. *Chem. Rev.* **2003,** *103*, 4367-4418.

18. Thundat, T.; Zheng, X. Y.; Chen, G. Y.; Warmack, R. J. Role of Relative-Humidity in Atomic-Force Microscopy Imaging. *Surf. Sci.* **1993,** *294*, L939-L943.

19. Piner, R. D.; Mirkin, C. A. Effect of Water on Lateral Force Microscopy in Air. *Langmuir* **1997,** *13*, 6864-6868.

20. Haaheim, J.; Eby, R.; Nelson, M.; Fragala, J.; Rosner, B.; Zhang, H.; Athas, G. Dip Pen Nanolithography (Dpn): Process and Instrument Performance with Nanoink's Nscriptor System. *Ultramicroscopy* **2005,** *103*, 117-132.

21. Ginger, D. S.; Zhang, H.; Mirkin, C. A. The Evolution of Dip-Pen Nanolithography. *Angew. Chem., Int. Ed.* **2004,** *43*, 30-45.

22. Salaita, K.; Wang, Y. H.; Mirkin, C. A. Applications of Dip-Pen Nanolithography. *Nat. Nanotechnol.* **2007,** *2*, 145-155.

23. Jung, H.; Dalal, C. K.; Kuntz, S.; Shah, R.; Collier, C. P. Surfactant Activated Dip-Pen Nanolithography. *Nano Lett.* **2004,** *4*, 2171-2177.

24. Senesi, A. J.; Rozkiewicz, D. I.; Reinhoudt, D. N.; Mirkin, C. A. Agarose-Assisted Dip-Pen Nanolithography of Oligonucleotides and Proteins. *Acs Nano* **2009,** *3*, 2394-2402.

25. Giam, L. R.; Wang, Y. H.; Mirkin, C. A. Nanoscale Molecular Transport: The Case of Dip-Pen Nanolithography. *J. Phys. Chem. A* **2009,** *113*, 3779-3782.

26. Sheehan, P. E.; Whitman, L. J. Thiol Diffusion and the Role of Humidity in "Dip Pen Nanolithography". *Phys. Rev. Lett.* **2002,** *88*, -.

27.   Rozhok, S.; Piner, R.; Mirkin, C. A. Dip-Pen Nanolithography: What Controls Ink Transport? *J. Phys. Chem. B* **2003,** *107*, 751-757.

28.   Schwartz, P. V. Molecular Transport from an Atomic Force Microscope Tip: A Comparative Study of Dip-Pen Nanolithography. *Langmuir* **2002,** *18*, 4041-4046.

29.   Demers, L. M.; Ginger, D. S.; Park, S. J.; Li, Z.; Chung, S. W.; Mirkin, C. A. Direct Patterning of Modified Oligonucleotides on Metals and Insulators by Dip-Pen Nanolithography. *Science* **2002,** *296*, 1836-1838.

30.   Lee, K. B.; Lim, J. H.; Mirkin, C. A. Protein Nanostructures Formed Via Direct-Write Dip-Pen Nanolithography. *J. Am. Chem. Soc.* **2003,** *125*, 5588-5589.

31.   Weeks, B. L.; Vaughn, M. W.; DeYoreo, J. J. Direct Imaging of Meniscus Formation in Atomic Force Microscopy Using Environmental Scanning Electron Microscopy. *Langmuir* **2005,** *21*, 8096-8098.

32.   Peterson, E. J.; Weeks, B. L.; De Yoreo, J. J.; Schwartz, P. V. Effect of Environmental Conditions on Dip Pen Nanolithography of Mercaptohexadecanoic Acid. *J. Phys. Chem. B* **2004,** *108*, 15206-15210.

33.   Weeks, B. L.; DeYoreo, J. J. Dynamic Meniscus Growth at a Scanning Probe Tip in Contact with a Gold Substrate. *J. Phys. Chem. B* **2006,** *110*, 10231-10233.

34.   Jang, J. Y.; Schatz, G. C.; Ratner, M. A. Liquid Meniscus Condensation in Dip-Pen Nanolithography. *J. Chem. Phys.* **2002,** *116*, 3875-3886.

35.   http://www.nanoink.net/TheChemistry.htm, NanoInk.

36.   Amro, N. A.; Xu, S.; Liu, G. Y. Patterning Surfaces Using Tip-Directed Displacement and Self-Assembly. *Langmuir* **2000,** *16*, 3006-3009.

37.   Garno, J. C.; Yang, Y. Y.; Amro, N. A.; Cruchon-Dupeyrat, S.; Chen, S. W.; Liu, G. Y. Precise Positioning of Nanoparticles on Surfaces Using Scanning Probe Lithography. *Nano Lett.* **2003,** *3*, 389-395.

38.   Li, Y.; Maynor, B. W.; Liu, J. Electrochemical Afm "Dip-Pen" Nanolithography. *J. Am. Chem. Soc.* **2001,** *123*, 2105-2106.

39.   Cai, Y. G.; Ocko, B. M. Electro Pen Nanolithography. *J. Am. Chem. Soc.* **2005,** *127*, 16287-16291.

40.   Wang, X. F.; Ryu, K. S.; Bullen, D. A.; Zou, J.; Zhang, H.; Mirkin, C. A.; Liu, C. Scanning Probe Contact Printing. *Langmuir* **2003,** *19*, 8951-8955.

41.   Hong, S. H.; Mirkin, C. A. A Nanoplotter with Both Parallel and Serial Writing Capabilities. *Science* **2000,** *288*, 1808-1811.

42.   Mirkin, C. A.; Hong, S. H.; Demers, L. Dip-Pen Nanolithography: Controlling Surface Architecture on the Sub-100 Nanometer Length Scale. *Chemphyschem* **2001,** *2*, 37-39.

43.   Zhang, M.; Bullen, D.; Chung, S. W.; Hong, S.; Ryu, K. S.; Fan, Z. F.; Mirkin, C. A.; Liu, C. A Mems Nanoplotter with High-Density Parallel Dip-Pen Manolithography Probe Arrays. *Nanotechnology* **2002,** *13*, 212-217.

44.   Liu, C. Parallel Scanning Probe Arrays: Their Applications. *Mater. Today* **2008,** *11*, 22-29.

45.   Salaita, K.; Wang, Y. H.; Fragala, J.; Vega, R. A.; Liu, C.; Mirkin, C. A. Massively Parallel Dip-Pen Nanolithography with 55000-Pen Two-Dimensional Arrays. *Angew. Chem., Int. Ed.* **2006,** *45*, 7220-7223.

46.   Haaheim, J.; Nafday, O. A. Dip Pen Nanolithography (R): A "Desktop Nanofab (Tm)" Approach Using High-Throughput Flexible Nanopatterning. *Scanning* **2008,** *30*, 137-150.

47. Salaita, K.; Lee, S. W.; Wang, X. F.; Huang, L.; Dellinger, T. M.; Liu, C.; Mirkin, C. A. Sub-100 Nm, Centimeter-Scale, Parallel Dip-Pen Nanolithography. *Small* **2005,** *1*, 940-945.

48. Lenhert, S.; Sun, P.; Wang, Y. H.; Fuchs, H.; Mirkin, C. A. Massively Parallel Dip-Pen Nanolithography of Heterogeneous Supported Phospholipid Multilayer Patterns. *Small* **2007,** *3*, 71-75.

49. Zou, J.; Bullen, D.; Wang, X. F.; Liu, C.; Mirkin, C. A. Conductivity-Based Contact Sensing for Probe Arrays in Dip-Pen Nanolithography. *Appl. Phys. Lett.* **2003,** *83*, 581-583.

50. Bullen, D.; Chung, S. W.; Wang, X. F.; Zou, J.; Mirkin, C. A.; Liu, C. Parallel Dip-Pen Nanolithography with Arrays of Individually Addressable Cantilevers. *Appl. Phys. Lett.* **2004,** *84*, 789-791.

51. Wang, X. F.; Bullen, D. A.; Zou, J.; Liu, C.; Mirkin, C. A. Thermally Actuated Probe Array for Parallel Dip-Pen Nanolithography. *J. Vac. Sci. Technol., B* **2004,** *22*, 2563-2567.

52. Bullen, D.; Wang, X. F.; Zou, J.; Chung, S. W.; Mirkin, C. A.; Liu, C. Design, Fabrication, and Characterization of Thermally Actuated Probe Arrays for Dip Pen Nanolithography. *J. Microelctromec. Sys.* **2004,** *13*, 594-602.

53. Wang, X. F.; Liu, C. Multifunctional Probe Array for Nano Patterning and Imaging. *Nano Lett.* **2005,** *5*, 1867-1872.

54. Bullen, D.; Liu, C. Electrostatically Actuated Dip Pen Nanolithography Probe Arrays. *Sensors and Actuators a-Physical* **2006,** *125*, 504-511.

55. Smith, J. C.; Lee, K. B.; Wang, Q.; Finn, M. G.; Johnson, J. E.; Mrksich, M.; Mirkin, C. A. Nanopatterning the Chemospecific Immobilization of Cowpea Mosaic Virus Capsid. *Nano Letters* **2003,** *3*, 883-886.

56. Lee, M.; Kang, D. K.; Yang, H. K.; Park, K. H.; Choe, S. Y.; Kang, C.; Chang, S. I.; Han, M. H.; Kang, I. C. Protein Nanoarray on Prolinker (Tm) Surface Constructed by Atomic Force Microscopy Dip-Pen Nanolithography for Analysis of Protein Interaction. *Proteomics* **2006,** *6*, 1094-1103.

57. Kwak, S. K.; Lee, G. S.; Ahn, D. J.; Choi, J. W. Pattern Formation of Cytochrome C by Microcontact Printing and Dip-Pen Nanolithography. *Mater. Sci. Eng., C* **2004,** *24*, 151-155.

58. Nam, J. M.; Han, S. W.; Lee, K. B.; Liu, X. G.; Ratner, M. A.; Mirkin, C. A. Bioactive Protein Nanoarrays on Nickel Oxide Surfaces Formed by Dip-Pen Nanolithography. *Angew. Chem., Int. Ed.* **2004,** *43*, 1246-1249.

59. Lim, J. H.; Ginger, D. S.; Lee, K. B.; Heo, J.; Nam, J. M.; Mirkin, C. A. Direct-Write Dip-Pen Nanolithography of Proteins on Modified Silicon Oxide Surfaces. *Angew. Chem., Int. Ed.* **2003,** *42*, 2309-2312.

60. Lee, K. B.; Park, S. J.; Mirkin, C. A.; Smith, J. C.; Mrksich, M. Protein Nanoarrays Generated by Dip-Pen Nanolithography. *Science* **2002,** *295*, 1702-1705.

61. Noy, A.; Miller, A. E.; Klare, J. E.; Weeks, B. L.; Woods, B. W.; DeYoreo, J. J. Fabrication of Luminescent Nanostructures and Polymer Nanowires Using Dip-Pen Nanolithography. *Nano Lett.* **2002,** *2*, 109-112.

62. Wilson, D. L.; Martin, R.; Hong, S.; Cronin-Golomb, M.; Mirkin, C. A.; Kaplan, D. L. Surface Organization and Nanopatterning of Collagen by Dip-Pen Nanolithography. *PNAS* **2001,** *98*, 13660-13664.

63. Wu, C. C.; Xu, H. P.; Otto, C.; Reinhoudt, D. N.; Lammertink, R. G. H.; Huskens, J.; Subramaniam, V.; Velders, A. H. Porous Multilayer-Coated Afm Tips for Dip-Pen Nanolithography of Proteins. *J. Am. Chem. Soc.* **2009,** *131*, 7526-7527.

64.   Choi, D. S.; Yun, S. H.; An, Y. C.; Lee, M. J.; Kang, D. G.; Chang, S. I.; Kim, H. K.; Kim, K. M.; Lim, J. H. Nanopatterning Proteins with a Stamp Tip for Dip-Pen Nanolithography. *Biochip J.* **2007,** *1*, 200-203.

65.   Valiokas, R.; Vaitekonis, A.; Klenkar, G.; Trinkunas, G.; Liedberg, B. Selective Recruitment of Membrane Protein Complexes onto Gold Substrates Patterned by Dip-Pen Nanolithography. *Langmuir* **2006,** *22*, 3456-3460.

66.   Lee, K. B.; Kim, E. Y.; Mirkin, C. A.; Wolinsky, S. M. The Use of Nanoarrays for Highly Sensitive and Selective Detection of Human Immunodeficiency Virus Type 1 in Plasma. *Nano Lett.* **2004,** *4*, 1869-1872.

67.   Hyun, J.; Ahn, S. J.; Lee, W. K.; Chilkoti, A.; Zauscher, S. Molecular Recognition-Mediated Fabrication of Protein Nanostructures by Dip-Pen Lithography. *Nano Lett.* **2002,** *2*, 1203-1207.

68.   Pena, D. J.; Raphael, M. P.; Byers, J. M. "Dip-Pen" Nanolithography in Registry with Photolithography for Biosensor Development. *Langmuir* **2003,** *19*, 9028-9032.

69.   Zhang, H.; Lee, K. B.; Li, Z.; Mirkin, C. A. Biofunctionalized Nanoarrays of Inorganic Structures Prepared by Dip-Pen Nanolithography. *Nanotechnology* **2003,** *14*, 1113-1117.

70.   Vega, R. A.; Maspoch, D.; Salaita, K.; Mirkin, C. A. Nanoarrays of Single Virus Particles. *Angew. Chem., Int. Ed.* **2005,** *44*, 6013-6015.

71.   Lee, S. W.; Oh, B. K.; Sanedrin, R. G.; Salaita, K.; Fujigaya, T.; Mirkin, C. A. Biologically Active Protein Nanoarrays Generated Using Parallel Dip-Pen Nanolithography. *Adv. Mater.* **2006,** *18*, 1133-1136.

72.   Vega, R. A.; Maspoch, D.; Shen, C. K. F.; Kakkassery, J. J.; Chen, B. J.; Lamb, R. A.; Mirkin, C. A. Functional Antibody Arrays through Metal Ion-Affinity Templates. *Chembiochem* **2006,** *7*, 1653-1657.

73.   Kim, J. D.; Ahn, D. G.; Oh, J. W.; Park, W. J.; Jung, H. I. Ribosome Display and Dip-Pen Nanolithography for the Fabrication of Protein Nanoarrays. *Adv. Mater.* **2008,** *20*, 3349-3353.

74.   Kim, K. H.; Kim, J. D.; Kim, Y. J.; Kong, S. H.; Jung, S. Y.; Jung, H. Protein Immobilization without Purification Via Dip-Pen Nanolithography. *Small* **2008,** *4*, 1089-1094.

75.   Sekula, S.; Fuchs, J.; Weg-Remers, S.; Nagel, P.; Schuppler, S.; Fragala, J.; Theilacker, N.; Franueb, M.; Wingren, C.; Ellmark, P*., et al.* Multiplexed Lipid Dip-Pen Nanolithography on Subcellular Scales for the Templating of Functional Proteins and Cell Culture. *Small* **2008,** *4*, 1785-1793.

76.   Cheung, C. L.; Camarero, J. A.; Woods, B. W.; Lin, T. W.; Johnson, J. E.; De Yoreo, J. J. Fabrication of Assembled Virus Nanostructures on Templates of Chemoselective Linkers Formed by Scanning Probe Nanolithography. *J. Am. Chem. Soc.* **2003,** *125*, 6848-6849.

77.   Li, B.; Zhang, Y.; Hu, J.; Li, M. Q. Fabricating Protein Nanopatterns on a Single DNA Molecule with Dip-Pen Nanolithography. *Ultramicroscopy* **2005,** *105*, 312-315.

78.   Wu, C. C.; Reinhoudt, D. N.; Otto, C.; Velders, A. H.; Subramaniam, V. Protein Immobilization on Ni(Ii) Ion Patterns Prepared by Microcontact Printing and Dip-Pen Nanolithography. *Acs Nano* **2010,** *in press*.

79.   Rakickas, T.; Gavutis, M.; Reichel, A.; Piehler, J.; Liedberg, B.; Valiokas, R. Protein-Protein Interactions in Reversibly Assembled Nanopatterns. *Nano Lett.* **2008,** *8*, 3369-3375.

80.   Wei, J. H.; Kacar, T.; Tamerler, C.; Sarikaya, M.; Ginger, D. S. Nanopatterning Peptides as Bifunctional Inks for Templated Assembly. *Small* **2009,** *5*, 689-693.

81.   Zhou, X. Z.; Chen, Y. H.; Li, B.; Lu, G.; Boey, F. Y. C.; Ma, J.; Zhang, H. Controlled Growth of Peptide Nanoarrays on Si/Siox Substrates. *Small* **2008,** *4*, 1324-1328.

82. Sistiabudi, R.; Ivanisevic, A. Dip-Pen Nanolithography of Bioactive Peptides on Collagen-Terminated Retinal Membrane. *Adv. Mater.* **2008,** *20*, 3678-3681.

83. Hoover, D. K.; Chan, E. W. L.; Yousaf, M. N. Asymmetric Peptide Nanoarray Surfaces for Studies of Single Cell Polarization. *J. Am. Chem. Soc.* **2008,** *130*, 3280-3281.

84. Agarwal, G.; Sowards, L. A.; Naik, R. R.; Stone, M. O. Dip-Pen Nanolithography in Tapping Mode. *J. Am. Chem. Soc.* **2003,** *125*, 580-583.

85. Cho, Y.; Ivanisevic, A. Siox Surfaces with Lithographic Features Composed of a Tat Peptide. *J. Phys. Chem. B* **2004,** *108*, 15223-15228.

86. Jiang, H. Z.; Stupp, S. I. Dip-Pen Patterning and Surface Assembly of Peptide Amphiphiles. *Langmuir* **2005,** *21*, 5242-5246.

87. Hyun, J.; Lee, W. K.; Nath, N.; Chilkoti, A.; Zauscher, S. Capture and Release of Proteins on the Nanoscale by Stimuli-Responsive Elastin-Like Polypeptide "Switches". *J. Am. Chem. Soc.* **2004,** *126*, 7330-7335.

88. Cho, Y.; Ivanisevic, A. Tat Peptide Immobilization on Gold Surfaces: A Comparison Study with a Thiolated Peptide and Alkylthiols Using Afm, Xps, and Ft-Irras. *J. Phys. Chem. B* **2005,** *109*, 6225-6232.

89. Sistiabudi, R.; Ivanisevic, A. Patterning of Polypeptides on a Collagen-Terminated Tissue Surface. *J. Phys. Chem. C* **2007,** *111*, 11676-11681.

90. Nyamjav, D.; Ivanisevic, A. Alignment of Long DNA Molecules on Templates Generated Via Dip-Pen Nanolithography. *Adv. Mater.* **2003,** *15*, 1805-1809.

91. Demers, L. M.; Park, S. J.; Taton, T. A.; Li, Z.; Mirkin, C. A. Orthogonal Assembly of Nanoparticle Building Blocks on Dip-Pen Nanolithographically Generated Templates of DNA. *Angew. Chem., Int. Ed.* **2001,** *40*, 3071-3073.

92. Nyamjav, D.; Ivanisevic, A. Templates for DNA-Templated Fe3o4 Nanoparticles. *Biomaterials* **2005,** *26*, 2749-2757.

93. Jonkheijm, P.; Weinrich, D.; Schroder, H.; Niemeyer, C. M.; Waldmann, H. Chemical Strategies for Generating Protein Biochips. *Angew. Chem., Int. Ed.* **2008,** *47*, 9618-9647.

94. Rozkiewicz, D. I. Covalent Microcontact Printing of Biomolecules. University of Twente, Enschede, 2007.

95. You, C.; Bhagawati, M.; Brecht, A.; Piehler, J. Affinity Capturing for Targeting Proteins into Micro and Nanostructures. *Anal. Bioanal. Chem.* **2009,** *393*, 1563-1570.

96. Ariga, K.; Nakanishi, T.; Michinobu, T. Immobilization of Biomaterials to Nano-Assembled Films (Self-Assembled Monolayers, Langmuir-Blodgett Films, and Layer-by-Layer Assemblies) and Their Related Functions. *J. Nanosci. Nanotechnol.* **2006,** *6*, 2278-2301.

97. Jung, H.; Kulkarni, R.; Collier, C. P. Dip-Pen Nanolithography of Reactive Alkoxysilanes on Glass. *J. Am. Chem. Soc.* **2003,** *125*, 12096-12097.

98. Liu, M.; Amro, N. A.; Liu, G. Y. Nanografting for Surface Physical Chemistry. *Annu. Rev. Phys. Chem.* **2008,** *59*, 367-386.

99. Wadu-Mesthrige, K.; Amro, N. A.; Garno, J. C.; Xu, S.; Liu, G. Y. Fabrication of Nanometer-Sized Protein Patterns Using Atomic Force Microscopy and Selective Immobilization. *Biophys. J.* **2001,** *80*, 1891-1899.

100. Wadu-Mesthrige, K.; Xu, S.; Amro, N. A.; Liu, G. Y. Fabrication and Imaging of Nanometer-Sized Protein Patterns. *Langmuir* **1999,** *15*, 8580-8583.

101.   Kenseth, J. R.; Harnisch, J. A.; Jones, V. W.; Porter, M. D. Investigation of Approaches for the Fabrication of Protein Patterns by Scanning Probe Lithography. *Langmuir* **2001,** *17*, 4105-4112.

102.   Cheung, C. L.; Chung, S. W.; Chatterji, A.; Lin, T. W.; Johnson, J. E.; Hok, S.; Perkins, J.; De Yoreo, J. J. Physical Controls on Directed Virus Assembly at Nanoscale Chemical Templates. *J. Am. Chem. Soc.* **2006,** *128*, 10801-10807.

103.   Lee, M. V.; Nelson, K. A.; Hutchins, L.; Becerril, H. A.; Cosby, S. T.; Blood, J. C.; Wheeler, D. R.; Davis, R. C.; Woolley, A. T.; Harb, J. N*., et al.* Nanografting of Silanes on Silicon Dioxide with Applications to DNA Localization and Copper Electroless Deposition. *Chem. Mater.* **2007,** *19*, 5052-5054.

104.   Liu, M. Z.; Amro, N. A.; Chow, C. S.; Liu, G. Y. Production of Nanostructures of DNA on Surfaces. *Nano Lett.* **2002,** *2*, 863-867.

105.   Hu, Y.; Das, A.; Hecht, M. H.; Scoles, G. Nanografting De Novo Proteins onto Gold Surfaces. *Langmuir* **2005,** *21*, 9103-9109.

106.   Case, M. A.; McLendon, G. L.; Hu, Y.; Vanderlick, T. K.; Scoles, G. Using Nanografting to Achieve Directed Assembly of De Novo Designed Metalloproteins on Gold. *Nano Lett.* **2003,** *3*, 425-429.

107.   Tinazli, A.; Piehler, J.; Beuttler, M.; Guckenberger, R.; Tampe, R. Native Protein Nanolithography That Can Write, Read and Erase. *Nat. Nanotechnol.* **2007,** *2*, 220-225.

108.   Takeda, S.; Nakamura, C.; Miyamoto, C.; Nakamura, N.; Kageshima, M.; Tokumoto, H.; Miyake, J. Lithographing of Biomolecules on a Substrate Surface Using an Enzyme-Immobilized Afm Tip. *Nano Lett.* **2003,** *3*, 1471-1474.

109.   Nakamura, C.; Miyamoto, C.; Obataya, I.; Takeda, S.; Yabuta, M.; Miyake, J. Enzymatic Nanolithography of Fret Peptide Layer Using V8 Protease-Immobilized Afm Probe. *Biosens. Bioelectron.* **2007,** *22*, 2308-2314.

110.   Hyun, J.; Kim, J.; Craig, S. L.; Chilkoti, A. Enzymatic Nanolithography of a Self-Assembled Oligonucleotide Monolayer on Gold. *J. Am. Chem. Soc.* **2004,** *126*, 4770-4771.

111.   Tang, Q. L.; Zhang, Y. X.; Chen, L. H.; Yan, F. N.; Wang, R. Protein Delivery with Nanoscale Precision. *Nanotechnology* **2005,** *16*, 1062-1068.

112.   Naujoks, N.; Stemmer, A. Using Local Surface Charges for the Fabrication of Protein Patterns. *Colloids Surf., A* **2004,** *249*, 69-72.

113.   Sarveswaran, K.; Hu, W. C.; Huber, P. W.; Bernstein, G. H.; Lieberman, M. Deposition of DNA Rafts on Cationic Sams on Silicon [100]. *Langmuir* **2006,** *22*, 11279-11283.

114.   Gu, J. H.; Yam, C. M.; Li, S.; Cai, C. Z. Nanometric Protein Arrays on Protein-Resistant Monolayers on Silicon Surfaces. *J. Am. Chem. Soc.* **2004,** *126*, 8098-8099.

115.   Pavlovic, E.; Oscarsson, S.; Quist, A. P. Nanoscale Site-Specific Immobilization of Proteins through Electroactivated Disulfide Exchange. *Nano Lett.* **2003,** *3*, 779-781.

116.   Agarwal, G.; Naik, R. R.; Stone, M. O. Immobilization of Histidine-Tagged Proteins on Nickel by Electrochemical Dip Pen Nanolithography. *J. Am. Chem. Soc.* **2003,** *125*, 7408-7412.

117.   Qin, G. T.; Cai, C. Z. Sub-10-Nm Patterning of Oligo(Ethylene Glycol) Monolayers on Silicon Surfaces Via Local Oxidation Using a Conductive Atomic Force Microscope. *Nanotechnology* **2009,** *20*, -355306.

118.   Taha, H.; Marks, R. S.; Gheber, L. A.; Rousso, I.; Newman, J.; Sukenik, C.; Lewis, A. Protein Printing with an Atomic Force Sensing Nanofountainpen. *Appl. Phys. Lett.* **2003,** *83*, 1041-1043.

119. Xu, J. T.; Lynch, M.; Huff, J. L.; Mosher, C.; Vengasandra, S.; Ding, G. F.; Henderson, E. Microfabricated Quill-Type Surface Patterning Tools for the Creation of Biological Micro/Nano Arrays. *Biomed. Microdevices* **2004,** *6*, 117-123.

120. Moldovan, N.; Kim, K. H.; Espinosa, H. D. Design and Fabrication of a Novel Microfluidic Nanoprobe. *J. Microelctromec. S.* **2006,** *15*, 204-213.

121. Moldovan, N.; Kim, K. H.; Espinosa, H. D. A Multi-Ink Linear Array of Nanofountain Probes. *J. Micromech. Microeng.* **2006,** *16*, 1935-1942.

122. Kim, K. H.; Sanedrin, R. G.; Ho, A. M.; Lee, S. W.; Moldovan, N.; Mirkin, C. A.; Espinosa, H. D. Direct Delivery and Submicrometer Patterning of DNA by a Nanofountain Probe. *Adv. Mater.* **2008,** *20*, 330-334.

123. Loh, O.; Lam, R.; Chen, M.; Moldovan, N.; Huang, H. J.; Ho, D.; Espinosa, H. D. Nanofountain-Probe-Based High-Resolution Patterning and Single-Cell Injection of Functionalized Nanodiamonds. *Small* **2009,** *5*, 1667-1674.

124. Loh, O. Y.; Ho, A. M.; Rim, J. E.; Kohli, P.; Patankar, N. A.; Espinosa, H. D. Electric Field-Induced Direct Delivery of Proteins by a Nanofountain Probe. *PNAS* **2008,** *105*, 16438-16443.

Chapter 3

Fabrication and Visualization of Metal-ion Patterns on Glass by Dip-Pen Nanolithography[*]

Abstract

Fluorescent monolayers sensitive to metal ions were used as dip-pen nanolithography (DPN) substrates for the fabrication of patterns of Ca(II) ions. The driving force for the transfer of these ions from an atomic force microscope (AFM) tip to the surface is their complexation to the organic ligands on the monolayer. Using the fluorescent surfaces, the patterns could be visualized using a fluorescence microscope. A custom-built atomic force fluorescence microscope (AFFM), a combination of an atomic force microscope and a confocal fluorescence microscope, was used to deposit the metal ions onto the sensitive monolayers by DPN and to subsequently visualize the modulations of fluorescence intensity in a sequential write-read mode.


3.1 Introduction

Chemical sensing of ions and small organic molecules is significant for various fields including environmental science, medical diagnostics, and the food industry.[1] High sensitivity and easy operation are two essential requirements for such sensors; fluorescence based approaches are among the most suitable candidates for chemical sensing because of the sensitivity and specificity of fluorescence, and the relative simplicity of the assays.[1] The traditional design of a fluorescent indicator comprises a receptor and a fluorophore, which are responsible for recognizing the analyte and signaling the recognition event, respectively. These fluorescent indicators have to be incorporated into a solid support to function as a chemosensor. The most common approaches of incorporation reported to date are physical entrapment or covalent attachment of sensitive probes to a polymeric matrix, and confining the fluorophore indicators in space. Among these methods, surface-confinement of the chemical sensing system provides some advantages, *e.g.* avoiding problems of leaking, fast response times, easy and reproducible synthesis, and the introduction of additional chelating effects from the pre-organized surface platform.[1, 2]

The sensitive monolayers previously developed in our group offer a simple and efficient method for detecting metal ions by observing the modulation of fluorescence intensity.[3-5] This methodology is comprised of randomly functionalizing monolayers with different fluorophores and ligand molecules onto amino-terminated monolayers on glass substrates, as shown in Scheme 3.1. By taking advantage of the interaction of organic ligands with metal ions, these monolayer-functionalized glass slides become metal-ion sensing platforms. Modulation of the fluorescence properties, *i.e.* different degrees of fluorescence enhancement or quenching, occurs upon complexation of different kinds of metal ions by the organic monolayers on top of the glass slide. It has also been demonstrated previously that the metal-ion patterns at micrometer (μm) scale can be fabricated on the sensitive monolayer-functionalized glass slides with microcontact printing (μCP)[2, 4] and dip-pen nanolithography (DPN)[2] techniques, where the sensing properties of the fluorescent substrates allow the visualization of the patterns by confocal fluorescence microscopy. It is well-known that patterns with sub-μm feature sizes can be achieved easily with DPN.[6-8] However, due to the intrinsic difficulty of finding the written pattern after transferring the sample from an atomic force microscope (AFM) to a confocal fluorescence microscope, only patterns with larger feature sizes (20 μm or larger) have been reported.[2]
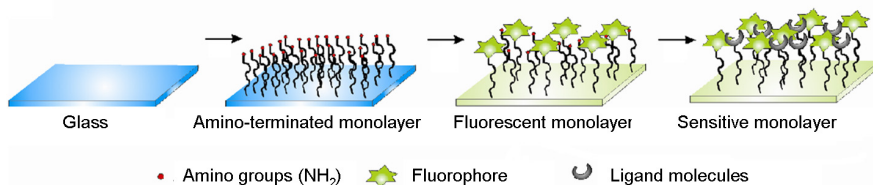
Scheme 3.1. *General schematic of the fabrication procedure of the metal-ion-sensitive monolayer-functionalized glass substrates.*

In this chapter, a modification of the protocol for preparing sensitive monolayers is described. The metal ion sensing property of the modified monolayers was confirmed by μCP. μCP is a soft lithographic approach using an elastomeric stamp with relief features prepared from a solid master to transfer ink molecules onto the target hard surface, as shown in Scheme 3.2. Poly(dimethylsiloxane) (PDMS) is typically used to prepare soft stamps. The generation of patterns relies on the conformal contact between the stamp and the substrate.[9] Subsequently, the controlled delivery of metal ions in well-defined μm and sub-μm patterns on discrete areas of the monolayer-functionalized glass by DPN with a custom-built instrument, the atomic force fluorescence microscope (AFFM), is presented. AFFM enables us to write metal ions and subsequent visualize *in situ* the written results in a sequential write-read mode.
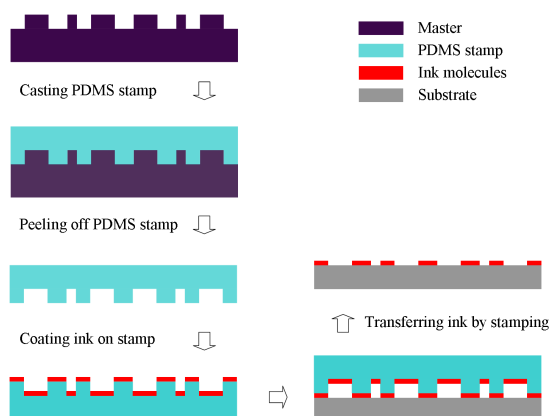

Scheme 3.2. *Schematic representation of preparing PDMS stamp and the microcontact printing (μCP) technique.*

3.2 Results and Discussion

3.2.1 The Atomic force fluorescence microscope (AFFM)

Scheme 3.3a shows the layout of the AFFM, which is an analysis tool combining an AFM and a confocal fluorescence microscope. A detailed description of AFFM has been reported by Kassies *et al.*[10, 11] AFFM enables the possibility to do DPN experiments and to immediately observe patterning results *in situ*, thereby facilitating the scaling down of feature sizes of the metal-ion patterns to sub-μm range without facing the difficulty of finding the written patterns back after moving samples from an AFM to a confocal fluorescence microscope. Scheme 3.3b depicts how the writing and visualization can be performed *in situ*. An AFM tip has to be brought into contact with a substrate right above the focus point of the objective lens while writing.
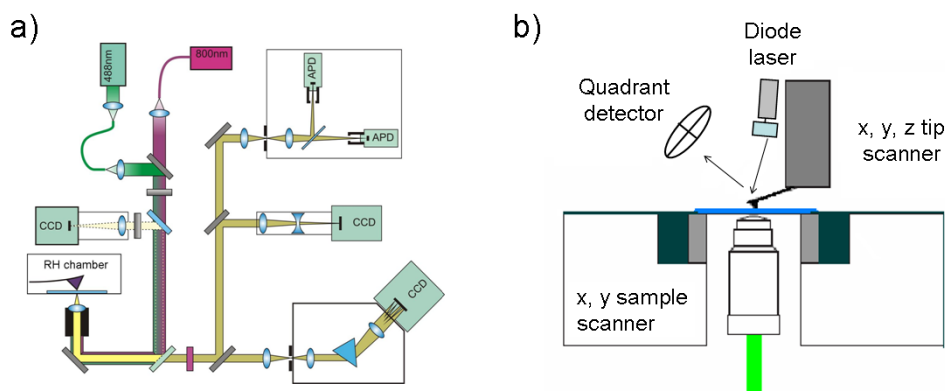
Scheme 3.3. *(a) Schematic layout of the atomic force fluorescence microscope (AFFM) shows two excitation wavelengths of lasers, 488 nm and 800 nm and two different detection paths for photon accounting (APD) available. Spectral discrimination can be obtained by a prism-based spectrograph. (b) Schematic of DPN and in situ fluorescence visualization by AFFM.*

Over the past years, several groups have presented their DPN experimental results mostly based on the studies of depositing mercaptohexadecanoic acid (MHA) or 1-octadecanethiol (ODT) on gold substrates and concluded that relative humidity (RH) is one of the important factors affecting the transportation of ink molecules from the tip

surface to the substrate.[12-17] In the original AFFM setup, there was no equipment for controlling relative humidity while writing ink molecules. Therefore, building a chamber with a relative humidity generator on the AFFM set-up has been necessary in order to have better control of DPN experiments.

The specific manner in which to build a humidity chamber on an AFM strongly depends on the original design of the instrument. Several requirements have to be considered including sealing, small volume, and avoiding exposing electronic components and optics to high humidity and temperature. Some approaches to building custom humidity chambers on an AFM have been reported. For example, Maxwell *et al.* used a small Perspex chamber to enclose the whole AFM scanner head and sample stage, or the lower portion of the AFM scanner tube.[18] This approach is very straightforward but it takes a long time to reach a desired RH value due to the large volume of the chamber. Stukalov *et al.* presented another method to control RH near an AFM probe by only enclosing the sample and the cantilever holder.[19] This kind of chamber is more suitable to adapt on the AFFM because the volume is small and enables one to quickly reach a desired RH value. Besides, not too many modifications to the AFFM have to be made. Photographs of the designed RH chamber and AFM head are shown in Figure 3.1a and b. The diameter and height of the chamber are ~ 5 cm and ~ 1 cm, respectively. A commercial sensor (SHT75, Sensirion, Switzerland) was placed into the chamber for monitoring relative humidity (RH) and temperature while performing DPN experiments. It can be seen in Figure 3.1b that the chamber is not fully sealed because of the open access for the AFM nose and therefore there is a leakage of the flowing humid air. Nevertheless, the RH still can reach a desired value with $\pm$ 3% deviation within 20 minutes in the chamber. Moist air with different RH near the AFM tip was created by mixing dry and wet nitrogen (N_2) with varying ratios. (Figure 3.1c) The wet N_2 was generated by flowing dry N_2 through two bottles of milliQ water followed by a bottle containing 5 mm diameter glass beads.[18] This home-built RH chamber combined with the simple humidity generator is not suitable for performing DPN experiments under the condition of high RH because the electronic components of AFM exposed to moist air may be damaged. This humidity control system was only used to raise the RH to approximately 50 % when the environmental humidity was too low.
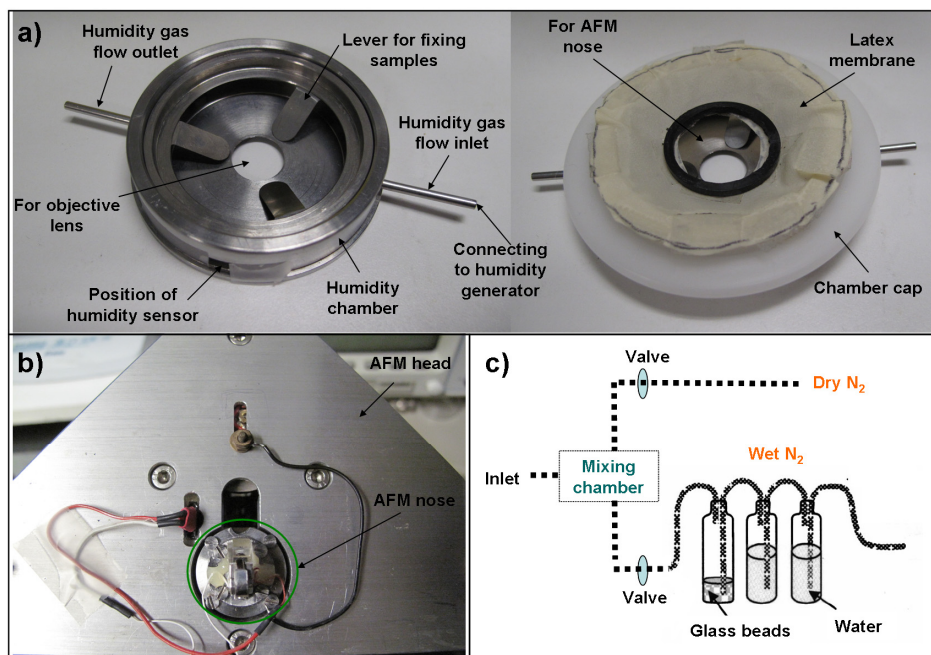
Figure 3.1. *(a) Photographs of the home-built relative humidity chamber with (top left) and without (top right) the chamber cap. (b) Photographs of the AFM head. The AFM nose can access the substrate via the open area of chamber cap shown in (a). (c) Schematic illustration of the generator of moist air.*

3.2.2 Sensitive monolayers

The monolayer functionalized-substrate chosen for DPN experiments was selected from a library of sensitive monolayers, presented by Basabe-Desmonts *et al.* previously, based on its high sensitivity for calcium ions.[20] The synthesis of the sensitive monolayer is depicted in Scheme 3.4. A three-step procedure was followed. An amino-terminated monolayer was first formed by silylation of the glass substrates with (N-[3-(trimethoxysilyl)propyl]-ethylenediamine) (TPEDA). Subsequently the TPEDA monolayer was converted into a fluorescent monolayer by reacting amino groups with the fluorophore 5-(and-6)-carboxytetramethylrhodamine succinimidyl ester (TAMRA). The sensitive monolayer was obtained in the end by covalently attaching the ligand molecules, hexanoyl chloride, to the remaining amino groups.
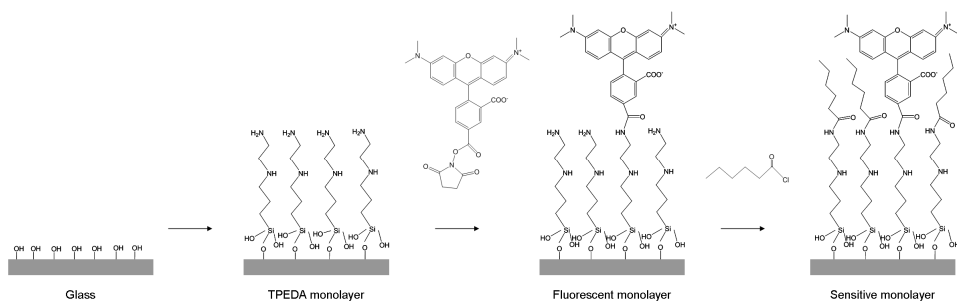
Scheme 3.4. *Illustration of the preparation procedure of a sensitive monolayer on glass.*

When beginning with DPN experiments, an experimental problem with the fluorescent monolayers prepared by following the original protocol came to light. It was found that the emission of fluorescence could be enhanced simply by scanning with 488 nm Argon laser light. We conjectured that the anomalous fluorescence enhancement might result from the dequenching of closely-packed fluorophore molecules on the top of the fluorescent monolayer. By scanning with the laser light, some self-quenchers were likely removed by photobleaching and consequently resulted in fluorescence enhancement.

To avoid any influence on the analyses of DPN results, modifying the original protocol for preparing fluorescent monolayers was necessary. The fluorescent monolayers prepared with different concentrations of TAMRA were examined by scanning laser light for two minutes. The corresponding fluorescence images are displayed in Figure 3.2. The effect of initial enhancement of fluorescence intensity was not visible only in the monolayers prepared in TAMRA solution of 0.01 mM.

Further, the fluorescent monolayers prepared with 0.07 mM and 0.01 mM TAMRA solutions were microcontact printed with metal ions to inspect if they still retained the ability to sense metal ions. The freshly prepared PDMS stamps were oxidized with UV/ozone cleaner to increase the wettability and then inked with 0.1 M ethanol solutions of the perchlorate salts of Ca(II) ions. After μCP process, the fluorescent monolayers were imaged with a fluorescence microscope. Figure 3.3a and 3.3b show the fluorescence images of fluorescent monolayers-functionalized substrates after printing with Ca(II) ions. The enhancement of fluorescence by the printed Ca(II) ions corresponds to the result

published before.[4, 20] The µCP results show that the modified monolayers are capable of sensing metal ions and there is no conspicuous difference between the monolayer prepared from different concentrations of used fluorophore solutions. In accordance with these test experiments, fluorescent monolayers prepared at 0.01 mM were chosen for DPN experiments.
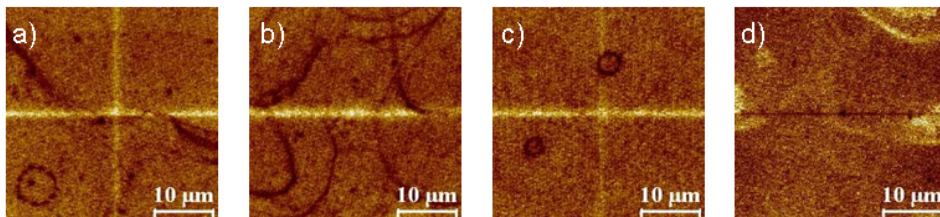

Figure 3.2. *Fluorescence images of fluorescent monolayers prepared in (a) 0.07 mM, (b) 0.05 mM, (c) 0.03 mM, (d) 0.01 mM TAMRA solutions were obtained by AFFM after continuous illumination with 488 nm laser light for two minutes during an intro-scanning routine.*
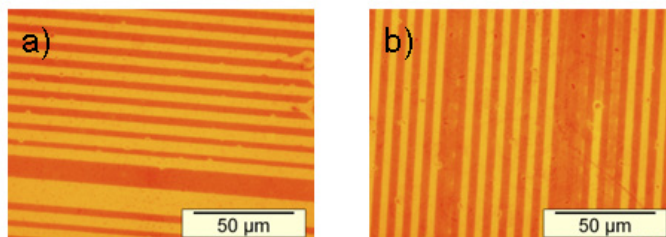

Figure 3.3. *Fluorescence images of fluorescent monolayers prepared from (a) 0.07 mM and (b) 0.01 mM TAMRA solution acquired after microcontact printing with calcium metal ions.*

3.2.3 Fabrication and visualization of metal-ion patterns

3.2.3.1 Writing metal ions at micron scale

Commercial Si_3N_4 AFM tips incubated in 0.1 M ethanol solutions of the perchlorate salts of Ca(II) ions were used to generate metal-ion patterns on the sensitive monolayer-functionalized substrate. Sequential AFFM write-read experiments confirm an increase in the fluorescence upon complexation of Ca(II) ions to the sensitive monolayers. Figure 3.4 shows a 15 x 15 μm² square written with Ca(II) ions. The bright square in the fluorescence image indicates the transfer of the metal ions onto the written area. The vertical edges and the central part of the square are brighter, suggesting that larger amounts of metal ions were transferred from the tip onto the sensitive monolayer at these specific locations. This is in agreement with the fact that the tip is in contact with the substrate for longer time in these areas. The center part corresponds to the intro-scanned process, which was performed before writing the whole square pattern in order to adjust the electronic offset signal to the tilt of the substrate. During this adjustment the Ca(II) ions-loaded tip scans the same line several times. The tip was also longer in contact with the substrate at the vertical edges of the square due to the change of direction between trace and retrace at the end of each scan line. The darker cross lines shown in Figure 3.4 resulted from the photobleaching of the substrate when scanning with the 488 nm Argon laser light before performing DPN.

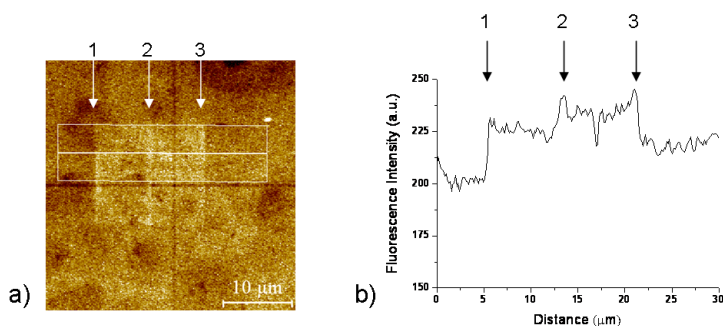***Figure 3.4.*** *(a) Fluorescence image of a sensitive monolayer-funstionalized substrate obtained by AFFM. A square pattern (15 x 15 μm²) was generated by dip-pen nanolithography using an AFM tip inked with Ca (II) ions. (b) Average fluorescence intensity profile of the area defined by the white lines. The arrows indicate the lines with higher fluorescence intensity.*

3.2.3.2 Writing metal ions at sub-micron scale

The fabrication and visualization of sub-μ scale metal-ion patterns have also been explored. Single lines of Ca(II) ions were deposited onto the substrates, and therefore bright lines with sub-micrometer widths were expected in the fluorescence images. During the experiments, we varied the scan speed between ∼ 18 and ∼ 1.8 μm/s to observe the relation between the tip-substrate contact time and the level of modulation of fluorescence. It was expected that a slower speed (longer contact time between the tip and the substrate on a certain area) would result in a higher amount of ink molecules transferred to the substrate and therefore it would induce higher enhancement of fluorescence. Figures 3.5a and 3.5c show that the widths of lines written on a sensitive monolayer-functionalized substrate are ∼ 0.8 μm and ∼ 0.6 μm respectively. In Figure 3.5a, six horizontal lines of 18μm in length were generated with six different scan speeds without retracting the tip during the whole DPN process. Each line was scanned 15 times and the fluorescence image was recorded immediately after completion of DPN of all six lines. As expected, slight differences in the brightness of the lines can be observed in Figure 3.5a. Lines written at a lower scan rate show higher fluorescence intensity, which is in agreement with a larger amount of transferred Ca(II) ions. Close inspection of the fluorescence intensity profile shown in Figure 3.5b exhibits a gradual increase of signal with the lower scan rates. However, the trend is reversed in the last two lines. This effect may be attributed to depletion of ink from the tip. Figure 3.5c shows two lines written with a scan rate of ∼ 1.8 μm/s for 5 and 10 minutes. In spite of the fact that one line was written for a longer time, the amplitude of the fluorescence emission from both lines was similar. We postulate that after scanning for a few minutes, the surface was saturated with Ca(II) ions leading to the observation of the maximum possible emission intensity. Some variations of line width between different experiments, such as those presented in Figure 3.5, have been observed. These differences might result from a different RH in the environment of the cantilever, or manufacturing differences of the tip. These effects have been already reported in literature.[7, 21, 22]
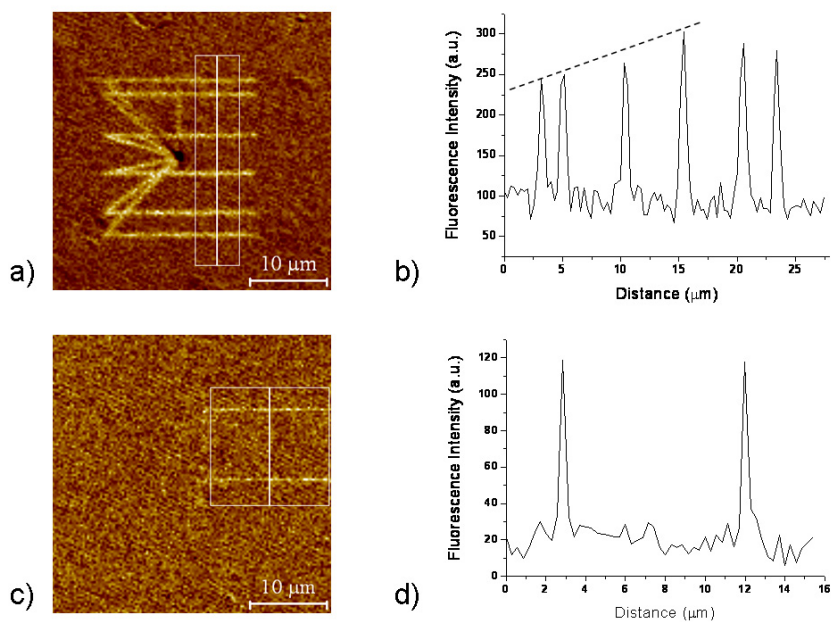
Figure 3.5. *(a) Fluorescence image of a sensitive monolayer-functionalized substrate acquired immediately after DPN with the AFFM. Six horizontal lines (18 μm in length) were successively generated by using an AFM tip inked with Ca (II) ions using scanning speeds of 17.7, 14.1, 10.6, 7.1, 3.5 and 1.8 μm/s, from top to bottom. (b) The average fluorescence intensity profile of the area inside the rectangle indicated in (a) The peaks from left to right correspond to the written lines from top to bottom. The dashed line indicates the increasing enhancement of fluorescence trend corresponding to a lower scanning speed (c) Fluorescent image of a sensitive monolayer-functionalized substrate acquired with the AFFM. Two horizontal lines (18 μm long) were generated by DPN using an AFM tip inked with Ca(II) ions for 5 (top) and 10 (bottom) minutes, respectively. The upper line was written first. (d) Average fluorescence intensity profile of the area defined by the white lines. The left peak corresponds to the upper written line. In both images a) and c) the background, which is the fluorescence image before DPN, was subtracted.*

3.3 Conclusions

In summary, the AFFM instrument used in this thesis work has been briefly described. A custom-built humidity chamber was designed for the AFFM for performing DPN experiments while controlling the relative humidity. Then it has been demonstrated that it is possible to fabricate Ca(II)-ion patterns, at micrometer and sub-micrometer scale, on the modified non-conductive sensitive monolayer-functionalized glass substrates with DPN. The driving force for the transfer of ink from the AFM tip to the substrate is the formation of Ca(II) ion complexes on the organic monolayer on the glass substrates. Such transfer of metal ions was revealed by an enhancement of the fluorescence response. The sensitive monolayer coated glass substrates used for the deposition offer a number of advantages, allowing optical visualization of the pattern even in cases in which the concentration of metal ions on the surface is so low that the AFM images do not exhibit any feature. Moreover, the combination of the topographic resolution of the AFM and the confocal fluorescence microscope in the AFFM enhances the possibilities of this approach by allowing immediate fluorescence imaging of the fabricated patterns in a sequential write-read mode *in situ*. Additionally, the fabrication of metal ion patterns by DPN can be used for the production of protein nanopatterns, which is described in detail in Chapter 4.

3.4 Experimental

General procedures.

All glassware used to prepare the monolayers was cleaned by sonicating for 60 minutes in a 2% v/v Hellmanex II solution in high purity water (MilliQ, 18.2 MΩcm), and then rinsed thoroughly with MilliQ water, and dried in an ambient environment. Microscope glass slide substrates and Si_3N_4 AFM cantilevers (NP, Veeco) were cleaned in piranha solution for 20 minutes and 1 minute, respectively, (concentrated H_2SO_4 and 33% aqueous H_2O_2 in a 3:1 ratio). [**Warning**: Piranha solution should be handled with caution: it has been reported to detonate unexpectedly.] The glass slides and cantilevers were then rinsed several times with Milli-Q water, and dried gently under a nitrogen stream before forming the monolayer.

Monolayer preparation.

Preparation of the amino terminated monolayer (TPEDA). Formation of the *N*-[3-(trimethoxysilyl)propyl]-ethylenediamine monolayer (TPEDA) was achieved in a glovebox under an atmosphere of dry nitrogen. The freshly cleaned substrates were immersed in a 5 mM solution of *N*-[3-(trimethoxysilyl)propyl]-ethylenediamine in freshly distilled toluene for 3.5 hours.

After the substrates were taken from the solution, they were rinsed twice with toluene (under nitrogen atmosphere) to remove excess silane and avoid polymerization. The substrates were then removed from the glovebox and rinsed with ethanol and dichloromethane to remove physisorbed material. The following protocol was repeated twice: shaking of the slide in a beaker filled with EtOH, then rinsing with a stream of EtOH, followed by stirring in CH_2Cl_2, then rinsing with a stream of CH_2Cl_2. The slides were then dried under an air stream.

Preparation of sensitive monolayer. For the synthesis of the sensitive monolayers, the fluorescent monolayers have to be prepared first by attaching the fluorophores to the TPEDA monolayers. This step was achieved by immersing the TPEDA monolayers-functionalized slides into the acetonitrile solutions of different concentrations of the fluorophore, (5-(and-6)-carboxytetramethylrhodamine, succinimidyl ester (5(6)-TAMRA, SE) *mixed isomers)) (TAMRA) for 4 hours. Then the substrates were taken out from the solution and rinsed with CH_3CN, EtOH, and CH_2Cl_2 to remove physisorbed material. The slides were then dried under an air stream. The fluorescent monolayers-functionalized slides were subsequently immersed in the 50 mM acetonitrile solution of hexanoyl chloride with 100 μL Et_3N to yield sensitive monolayers. The reaction was carried out under an atmosphere of dry N_2 for 16 hours. After the substrates were taken out from the solution, they were rinsed sequentially with CH_3CN, EtOH, and CH_2Cl_2 to remove physisorbed material. The slides were then dried under an air stream. All monolayer-functionalized glass slides were then sonicated for 1 minute in a beaker filled with CH_2Cl_2, then rinsed again with CH_2Cl_2 and dried under an air stream, to assure clean sensitive monolayers. The formation of monolayers on the glass slides was characterized by ellipsometry, water contact angle goniometry, fluorescent spectroscopy and XPS as reported elsewhere.[20]

Microcontact printing (μCP) with Ca(II) ions on sensitive monolayers.

A 10:1 (v/v) mixture of poly(dimethylsiloxane) (PDMS) and curing agent (Sylgard 184, Dow Corning) was cast against patterned silicon master and cured at 60 °C overnight. The PDMS stamps were obtained after carefully peeling them off from the silicon master after curing. Prior to inking process, all the freshly prepared PDMS stamps were oxidized by exposure to UV/ozone cleaner for 30 minutes to increase the wettability of stamps' surfaces. The oxidized stamps were immediately incubated into the 10^{-1} M ethanol solutions of the perchlorate salts of Ca(II) ions for at least 20 minutes. After inking, the stamps were dried under a stream of N_2 to blow the excess ink away. The inked stamps were brought into conformal contact with sensitive monolayers-functionalized substrates for 3 minutes without the use of external pressure. The sensitive monolayers-functionalized substrates printed with Ca(II) ions were examined with a fluorescence microscope.

Dip-pen nanolithography (DPN) with Ca(II) ions on sensitive monolayers.

Commercial Si_3N_4 AFM cantilevers with nominal spring constant of 0.05 N/m were used. Immediately before a DPN experiment, cantilevers were rinsed rigorously with ethanol and dried under a N_2 stream very gently. After cleaning, the cantilevers were exposed to UV light for 30 minutes to break down contaminants and make the cantilever surface more hydrophilic. Cleaned cantilevers were then immersed into 0.1 M ethanol solutions of the perchlorate salts of Ca(II) ions for 5 minutes and then dried in air. The Ca(II)-coated cantilever was immediately mounted on the AFM head to carry out DPN experiments on sensitive monolayers in contact mode with or without humid control at a temperature between 20 and 23 °C. The trace of the scanned cantilever was consistent with the re-trace.

The 15 x 15μm^2 square-shaped patterns were written twice with a scan rate of 28 μm/s. Furthermore, 18 μm long fluorescent lines were fabricated with defined number of scans (15 scans) or controlled scan rate (1.8 μm/s). During the writing period, the fluorescence excitation light was switched off to prevent the samples from photobleaching. Immediately after DPN, the patterned substrate was excited with 488 nm Argon laser light and the emission of the fluorescence was recorded by an avalanche photodiode (APD) (SPCM-AQR-14, Perkin Elmer Optoelectronics). The acquired fluorescent images were analyzed by the commercial software SPIP (Image Metrology, Version 4.4.3.0).

3.5 Acknowledgements

3.6 References

1. Basabe-Desmonts, L.; Reinhoudt, D. N.; Crego-Calama, M. Design of Fluorescent Materials for Chemical Sensing. *Chem. Soc. Rev.* **2007,** *36*, 993-1017.

2. Lourdes, B.-D. Fluorescent Self-Assembled Monolayers as New Sensing Materials. University of Twente, 2005.

3. Zimmerman, R.; Basabe-Desmonts, L.; van der Baan, F.; Reinhoudt, D. N.; Crego-Calama, M. A Combinatorial Approach to Surface-Confined Cation Sensors in Water. *J. Mater. Chem.* **2005,** *15*, 2772-2777.

4. Basabe-Desmonts, L.; Reinhoudt, D. N.; Crego-Calama, M. Combinatorial Fabrication of Fluorescent Patterns with Metal Ions Using Soft Lithography. *Adv. Mater.* **2006,** *18*, 1028-1032.

5. Crego-Calama, M.; Reinhoudt, D. N. New Materials for Metal Ion Sensing by Self-Assembled Monolayers on Glass. *Adv. Mater.* **2001,** *13*, 1171-1174.

6.   Piner, R. D.; Zhu, J.; Xu, F.; Hong, S. H.; Mirkin, C. A. "Dip-Pen" Nanolithography. *Science* **1999,** *283*, 661-663.

7.   Ginger, D. S.; Zhang, H.; Mirkin, C. A. The Evolution of Dip-Pen Nanolithography. *Angew. Chem., Int. Ed.* **2004,** *43*, 30-45.

8.   Salaita, K.; Wang, Y. H.; Mirkin, C. A. Applications of Dip-Pen Nanolithography. *Nat. Nanotechnol.* **2007,** *2*, 145-155.

9.   Kumar, A.; Whitesides, G. M. Features of Gold Having Micrometer to Centimeter Dimensions Can Be Formed through a Combination of Stamping with an Elastomeric Stamp and an Alkanethiol Ink Followed by Chemical Etching. *Appl. Phys. Lett.* **1993,** *63*, 2002-2004.

10.   Kassies, R.; Van der Werf, K. O.; Lenferink, A.; Hunter, C. N.; Olsen, J. D.; Subramaniam, V.; Otto, C. Combined Afm and Confocal Fluorescence Microscope for Applications in Bio-Nanotechnology. *J. Microsc* **2005,** *217*, 109-116.

11.   Kassies, R. Atomic Force Fluorescence Microscopy. University of Twente, 2005.

12.   Weeks, B. L.; Noy, A.; Miller, A. E.; De Yoreo, J. J. Effect of Dissolution Kinetics on Feature Size in Dip-Pen Nanolithography. *Phys. Rev. Lett.* **2002,** *88*, 255505.

13.   Jang, J. Y.; Schatz, G. C.; Ratner, M. A. Liquid Meniscus Condensation in Dip-Pen Nanolithography. *J. Chem. Phys.* **2002,** *116*, 3875-3886.

14.   Peterson, E. J.; Weeks, B. L.; De Yoreo, J. J.; Schwartz, P. V. Effect of Environmental Conditions on Dip Pen Nanolithography of Mercaptohexadecanoic Acid. *J. Phys. Chem. B* **2004,** *108*, 15206-15210.

15.   Weeks, B. L.; Vaughn, M. W.; DeYoreo, J. J. Direct Imaging of Meniscus Formation in Atomic Force Microscopy Using Environmental Scanning Electron Microscopy. *Langmuir* **2005,** *21*, 8096-8098.

16.   Nafday, O. A.; Weeks, B. L. Relative Humidity Effects in Dip-Pen Nanolithography of Alkanethiol Mixtures. *Langmuir* **2006,** *22*, 10912-10914.

17.   Wang, W. C. M.; Stoltenberg, R. M.; Liu, S. H.; Bao, Z. N. Direct Patterning of Gold Nanoparticles Using Dip-Pen Nanolithography. *Acs Nano* **2008,** *2*, 2135-2142.

18.   Maxwell, J. M.; Huson, M. G. Using the Scanning Probe Microscope to Measure the Effect of Relative Humidity on Sample Stiffness. *Rev. Sci. Instrum.* **2002,** *73*, 3520-3524.

19.   Stukalov, O.; Murray, C. A.; Jacina, A.; Dutcher, J. R. Relative Humidity Control for Atomic Force Microscopes. *Rev. Sci. Instrum.* **2006,** *77*, 033704.

20.   Basabe-Desmonts, L.; Beld, J.; Zimmerman, R. S.; Hernando, J.; Mela, P.; Parajo, M. F. G.; van Hulst, N. F.; van den Berg, A.; Reinhoudt, D. N.; Crego-Calama, M. A Simple Approach to Sensor Discovery and Fabrication on Self-Assembled Monolayers on Glass. *J. Am. Chem. Soc.* **2004,** *126*, 7293-7299.

21.   Su, M.; Pan, Z. X.; Dravid, V. P.; Thundat, T. Locally Enhanced Relative Humidity for Scanning Probe Nanolithography. *Langmuir* **2005,** *21*, 10902-10906.

22.   Haaheim, J.; Eby, R.; Nelson, M.; Fragala, J.; Rosner, B.; Zhang, H.; Athas, G. Dip Pen Nanolithography (Dpn): Process and Instrument Performance with Nanoink's Nscriptor System. *Ultramicroscopy* **2005,** *103*, 117-132.

Chapter 4

Protein Immobilization on Ni(II) Ion Patterns Prepared by Microcontact Printing and Dip-Pen Nanolithography[*]

Abstract

An indirect method of protein patterning by using Ni(II) ion templates for immobilization *via* a specific metal-protein interaction is described. A nitrilotriacetic acid (NTA)-terminated monolayer allows oriented binding of histidine-tagged proteins *via* complexation with late first-row transition metal ions, such as Ni(II). Patterns of nickel(II) ions were prepared on NTA-terminated monolayer-functionalized glass slides by microcontact printing (μCP) and dip-pen nanolithography (DPN) to obtain micrometer and submicrometer scale patterns. Consecutive dipping of the slides in His$_6$-protein solutions resulted in the formation of protein patterns, as was subsequently proven by AFM and confocal fluorescence microscopy. This indirect method prevents denaturation of fragile biomolecules caused by direct printing or writing of proteins. Moreover, it yields well-defined patterned monolayers of proteins and, in principle, is well suited for biomolecules with a high molecular weight. This approach also enabled us to characterize the dependence of transfer of Ni(II) ions on fundamental parameters of DPN, such as writing speeds and tip-surface contact times.

4.1 Introduction

Micro- and nanopatterning of biomolecules on surfaces attracts growing attention due to the potential applications in medicine and biotechnology.[1] Applications include production and preparation of biochips and biosensors for diagnostics, drug discovery, and fundamental studies of biological processes.[1, 2] Different techniques have been developed to accomplish biopatterning at the micro- and nanoscale, such as soft lithography,[3-5] scanning probe lithography,[6-11] nanoimprint lithography,[12-14] and electron beam lithography.[15-17]

In Chapter 3, it had been demonstrated that metal ions can be transferred onto fluorescent monolayers using microcontact printing (μCP) and dip-pen nanolithography (DPN) with micrometer and sub-micrometer precision.[18] Subsequent modulations of fluorescent signals were visualized *in situ* by using a hybrid atomic force fluorescence microscope (AFFM).[18, 19] A potential application of metal-ion patterns is their use as a template for selective and controlled immobilization of biomolecules *via* a specific metal-protein interaction.[20, 21]

Nickel(II)-nitrilotriacetic acid (Ni-NTA) was originally developed in immobilized metal affinity chromatography (IMAC) for purifying proteins labeled with a short sequence of histidines (His-tagged proteins).[22] NTA is a tetradentate ligand which can form a hexagonal complex with Ni(II) ions (or other divalent metal ions such as Cu(II) or Co(II). This way, four of six binding sites are occupied by the metal ion and the other two binding positions are available for histidines. The affinity of the hexahistidine (His$_6$) to Ni-NTA is high ($K_d \approx 10^{-13}$ M),[23] but the complexation of His$_6$ to Ni-NTA can also be reversed by adding imidazole or EDTA.[12, 24] These characteristics make the Ni-NTA system a popular choice for fabricating oriented and reversible His-tagged biomolecule patterns on surfaces.[8, 11, 12, 24] The Ni-NTA-His-tag system is thus a suitable candidate to prove our concept of using metal-ion patterns as templates for the immobilization of biomolecules.

In this chapter, the use of microcontact printing (μCP) to fabricate μm scale Ni(II) ion patterns onto NTA-terminated monolayer-functionalized glass slides is first described because of the simplicity and high-throughput production of the μCP technique.[3] The metal-ion patterned substrates were incubated immediately with His-tagged protein solutions to anchor the proteins onto the printed areas. Subsequently, the AFFM was utilized to perform DPN to scale down the size of Ni(II) ion patterns to the sub-μm scale, accompanied by direct visualization of the results by atomic force microscopy (AFM) and

confocal fluorescence microscopy. The procedure of fabricating protein patterns is illustrated in Scheme 4.1.
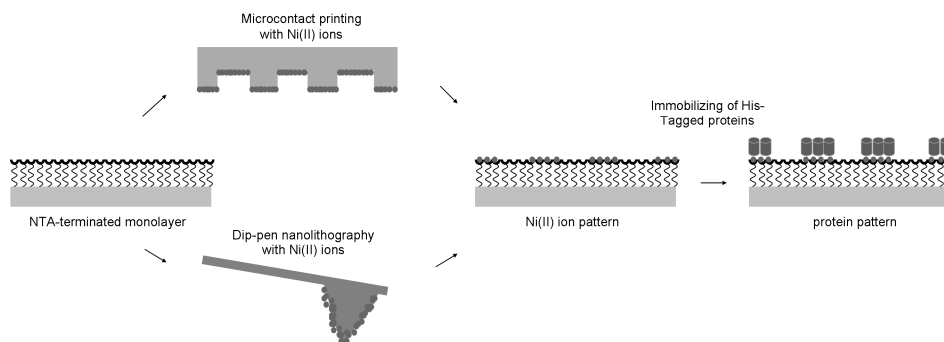
Scheme 4.1. *Fabrication of Ni(II)-ion patterns onto NTA monolayer with microcontact printing (µCP) and dip-pen nanolithography (DPN) to immobilize His-tagged proteins.*

Using metal ion patterns as a template is an indirect approach to fabricate protein patterns, with the advantage that denaturation of fragile biomolecules readily observed when printing or writing proteins directly is avoided.[25] Enhanced green fluorescent protein incorporating a His$_6$-tag (His-EGFP) was used as a model protein. EGFP is intrinsically fluorescent when properly folded and thus can be directly used for optical recognition. The intrinsic fluorescence is also a marker of the structural integrity of the protein; misfolded or otherwise structurally damaged proteins do not fluoresce. The AFFM enables both fabrication of Ni(II) ion patterns and *in situ* observation of the fluorescence and AFM topography of the protein patterns. AFM measurements provide a better determination of the actual size of protein patterns as they surpass the resolution limitation of confocal fluorescence microscopy. Despite the difference in sizes of the proteins and the intermediate metal ions, fluorescence and topographic images of the protein patterns enabled us to quantitatively characterize the transfer and diffusion on the surface of Ni(II) ions as a function of fundamental parameters of DPN, such as writing speeds and tip-surface contact times. In a further demonstration of the general applicability of this method, a higher molecular weight histidine-tagged protein, the tetrameric reef coral fluorescent protein (His-DsRed), has also been used for patterning.

4.2 Results and Discussion

4.2.1 Ni-NTA system

The Ni-NTA monolayers were prepared following the procedures reported by Paik *et al.*[26] The approach starts with the formation of epoxy-terminated monolayers of 3-glycidyloxypropyl trimethoxysilane on cleaned microscope glass slides. The epoxy groups were subsequently reacted with *N,N*-bis(carboxymethyl)-L-lysine to form NTA-terminated monolayers. Ni-NTA monolayers were obtained by immersing NTA-functionalized substrates into NiCl$_2$ solution for the complexation of metal ions. The process of Ni-NTA monolayer preparation is depicted in Scheme 4.2. The formation of the monolayers was examined by water contact-angle goniometry and ellipsometry. The results are consistent with the values reported in literature.[12, 27]
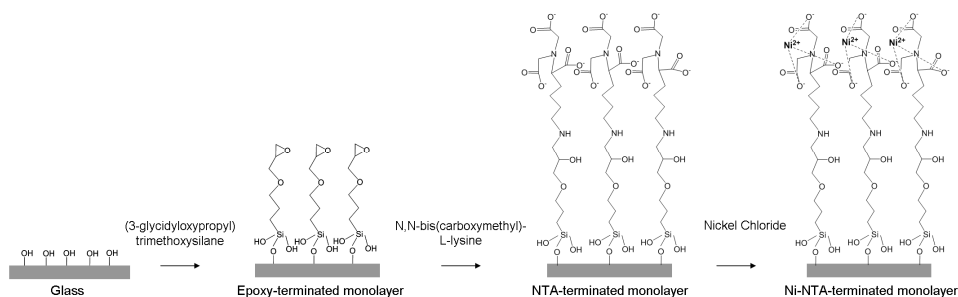
Scheme 4.2. *Illustration of the preparation procedure for Ni-NTA-terminated monolayers.*

In order to confirm that there is sufficient fluorescence contrast for further μCP and DPN experiments, ~ 20 μl of 100 nM His-EGFP solution was placed onto NTA and Ni-NTA-functionalized surfaces for 30 minutes, which then were rinsed with 10 mM Tris-HCl buffer (pH 8.0) and Milli-Q water before drying with N$_2$. The background-subtracted fluorescence images on NTA and Ni-NTA-functionalized surfaces obtained by AFFM are shown in Figure 4.1a and 4.1b, respectively. Non-specific binding of His-EGFP on the NTA-terminated monolayer was observed. The average fluorescence intensity values (a.u.) of Figure 4.1a and 4.1b, plotted in Figure 4.1c, are 1.26 and 14.02, respectively, yielding a ratio of average fluorescence intensity of the specifically-bound protein to the unspecifically bound protein of ~ 11:1, which is a sufficiently large fluorescence contrast to perform μCP and DPN experiments.
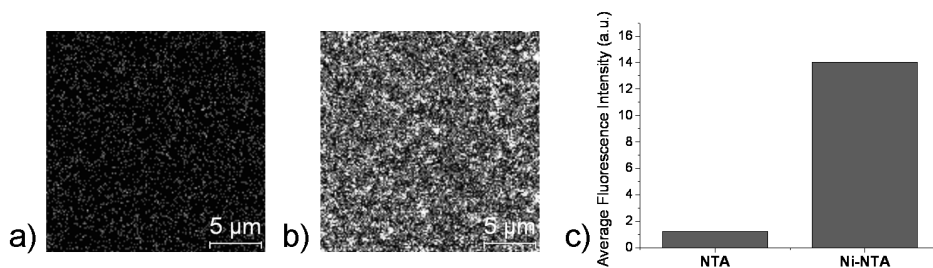
Figure 4.1. *Fluorescence image of His-EGFP attached on (a) NTA- and (b) Ni-NTA-terminated monolayer-functionalized surface. The exposure time of the images is 0.25 ms per pixel. (c) The bars in the graph indicate the average fluorescence intensity of (a) and (b).*

4.2.2 Fabrication of His-EGFP patterns by microcontact printing (µCP)

Microcontact printing (µCP) is an easy and fast approach to prove that Ni(II) ion patterns on NTA-terminated monolayer-functionalized surfaces can be used as templates for the immobilization of His-tagged proteins at µm scale. A PDMS stamp with 5 µm line features with a spacing of 3 µm was coated with Ni(II) ions and brought into conformal contact with the NTA-modified surface for 3 minutes before incubating the latter in a 100 nM His-EGFP solution. In Figure 4.2a, the fluorescence image of a patterned surface shows His-EGFP functionalized areas with the expected feature size of the microcontact printed Ni(II) ion pattern, illustrating that His-EGFP patterns can be readily obtained by this indirect method of using Ni(II) ions as templates. It has been previously reported that His-tagged proteins complexed on Ni(II)-NTA-terminated monolayers can be easily removed by an EDTA solution for reusing the functionalized substrates.[12] To demonstrate that our functionalized surfaces are reusable, a substrate with a His-EGFP pattern was incubated in a 0.1 M EDTA solution overnight and then rinsed with water and 10 mM Tris-HCl buffer (pH 8). Figure 4.2b shows that there are no apparent fluorescent features on the substrate after treatment with EDTA solution. A PDMS stamp with a different feature size (10 µm line features, separated by 5 µm) was used for a second microcontact printing step of Ni(II) ions on the regenerated slide. Figure 4.2c shows that His-EGFP was successfully immobilized on these surfaces, confirming that the NTA-functionalized surface is robust and can be reutilized. The slight difference in fluorescence intensities

between panels a and c of Figures 4.2 may result from the difference in the amount of Ni(II) ions adsorbed onto the surfaces of the different PDMS stamps used.
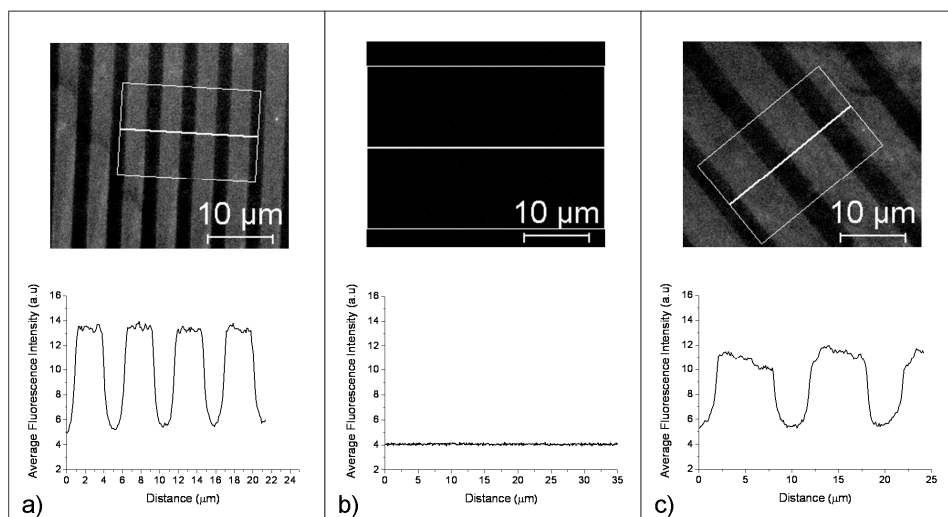

Figure 4.2. Fluorescence images and average fluorescence intensity profiles of the area inside the rectangle of His-EGFP immobilized on Ni(II) patterns created after (a) 1st μCP of 5 μm line features, (b) after rinsing with 0.1M EDTA solution and (c) after 2nd μCP of 10 μm line features. The exposure time of the camera for each of the images is 200 ms.

4.2.3 Fabrication of His-EGFP patterns by dip-pen nanolithography (DPN)

The fabrication of sub-μm scale metal ion patterns on NTA monolayer-functionalized glass was explored by DPN, a technique which is more flexible and can create patterns with smaller feature sizes than μCP.[28] DPN can also modify the surface with different inks whereas μCP is normally a single ink process. The metal-ion patterns were fabricated with DPN, followed by protein incubation, and subsequently monitored by fluorescence spectroscopy and AFM topography *in situ* using the AFFM. The use of this hybrid instrument avoids the intrinsic difficulty of finding the written protein patterns after transferring the sample from the AFM to a fluorescence microscope. For the purpose of scaling down the size of Ni(II) ion patterns, a cleaned Si_3N_4 AFM tip was inked with Ni(II) ions by dipping into a $NiCl_2$ solution, and the ink-loaded tip was brought into contact with

an NTA-functionalized surface for writing dot or line patterns directly above the central focus of the objective lens. The driving forces for the transfer of Ni(II) ions from an AFM tip to a surface are the dissolution of metal ions into the aqueous meniscus formed between tip and surface and the complex formation of Ni(II) ions with NTA molecules functionalized on the glass substrates. The written Ni(II) ion patterns were then immersed in a protein solution and consecutively visualized by fluorescence microscopy.

Metal ions are among the smallest ink "molecules" one can use. It is very difficult to directly characterize the transferred Ni(II) ions on a surface because of the small size of the ions. However, the amount of transfer of Ni(II) ions can be revealed by the subsequent immobilization of His-EGFP and measurement of its intrinsic fluorescence, allowing the systematic investigation of metal-ion deposition by DPN. Therefore, DPN experiments were carried out in which either an ink-coated AFM tip was held at different fixed positions for different times (dot patterns), or in which the AFM tip was moved at different, but constant, writing speeds (line patterns).

4.2.3.1 Writing with different contact times

A Ni(II) ion pattern of 18 dots was written with different tip-surface contact times for each dot, varying between 1 and 60 s. A commercial Si_3N_4 AFM tip was incubated into 10 mM Tris-HCl buffer (pH 8.0) containing 0.1 M $NiCl_2$ for coating Ni(II) ions and then blown dry with N_2. Subsequently, the ink-coated tip was brought into contact with the surface for a given time and was retracted after writing each dot. The contact time was monotonically increased, and the whole writing sequence was completed without reinking the tip. The written area was immediately incubated in a 100 nM His-EGFP solution for 30 minutes and then rinsed with 10 mM Tris-HCl buffer (pH 8) and Milli-Q water before drying with N_2. The fluorescence image of the His-EGFP dot patterns is shown in Figure 4.3a. The observed His-EGFP dot patterns are consistent with the written Ni(II) ion patterns, which indicates that Ni(II) ions have been transferred from the AFM tip onto the surface. To elucidate the relationship between the fluorescence intensity and tip-surface contact time, the fluorescence intensities of a 32x32 pixel area covering each dot were averaged. It is known that there is a correlation between the tip-substrate contact time and the amount of deposited ink molecules.[9, 28, 29] Normally, longer contact times between the tip and the substrate on a certain area, or using slower scanning speeds, should result in higher amount of ink transferred to the substrate. In Figure 4.3a, dots deposited for longer

times show higher fluorescence intensity, indicating that more His-EGFP molecules were attached to the written area. In figure 4.3b, a plot of the averaged fluorescence intensities *versus* the tip-surface contact time shows a linear relationship, suggesting that the amount of Ni(II) ions transferred onto the NTA-functionalized surface increases linearly with the tip-surface contact time.

One important factor in determining the resolution in DPN experiments is how ink molecules diffuse from a tip to a surface *via* a water meniscus.[30] Our DPN experiments were carried out at ~ 60% relative humidity (RH), and it has been reported that, at this RH, a water meniscus of ~ 1.5 μm in diameter is formed between tip and substrate.[31] The size of the water meniscus may suggest that the maximum size of the Ni(II) ion spot and its corresponding His-EGFP pattern is also ~ 1.5 μm in diameter.[31] The diameters of His-EGFP dot patterns written with tip-surface contact times longer than 10 seconds shown in Figure 4.3a are in fact between ~ 1.0 and ~ 1.4 μm. Besides, a gradient in fluorescence intensity was observed; that is each dot exhibits higher emission in the center and a lower emission at the borders; one example is exhibited in Figure 4.3c, which is the enlargement of the fluorescent dot pattern written with a tip-surface contact time of 60 s. Figure 4.3d shows the average fluorescence intensity profile of the area inside the rectangle as indicated in Figure 4.3c, and clearly highlights the gradient of fluorescence intensity. This profile can be fit well with a Gaussian function, which suggests that the gradient phenomenon may be attributed to the radial diffusion of the nickel ions from the contact position of the tip and surface to the border of the spot.

AFM imaging reveals topographic information of the protein patterns adhered to metal-ion sites. To avoid contaminations, a new Si_3N_4 AFM tip was brought to the original position in the DPN experiments, directly above the central focus of the objective lens. The topography measurements were performed in tapping mode and are shown in Figure 4.4a. The 18-dots protein pattern shown in the AFM height image corresponds well to the pattern in the fluorescence image. It can be observed that the spots with higher fluorescence intensity have more distinct AFM patterns, suggesting the denser packing of His-EGFP. The diameters of these more densely packed protein dots are between ~ 300 nm and ~ 800 nm. The height profile of protein patterns generated with tip-surface contact times of 10 s, 28 s and 48 s is shown in Figure 4.4b. The reported size of EGFP in literature is ~ 2 nm in width and ~ 4 nm in height.[32] The data in Figure 4.4b thus suggest that a monolayer of patterned proteins was achieved.
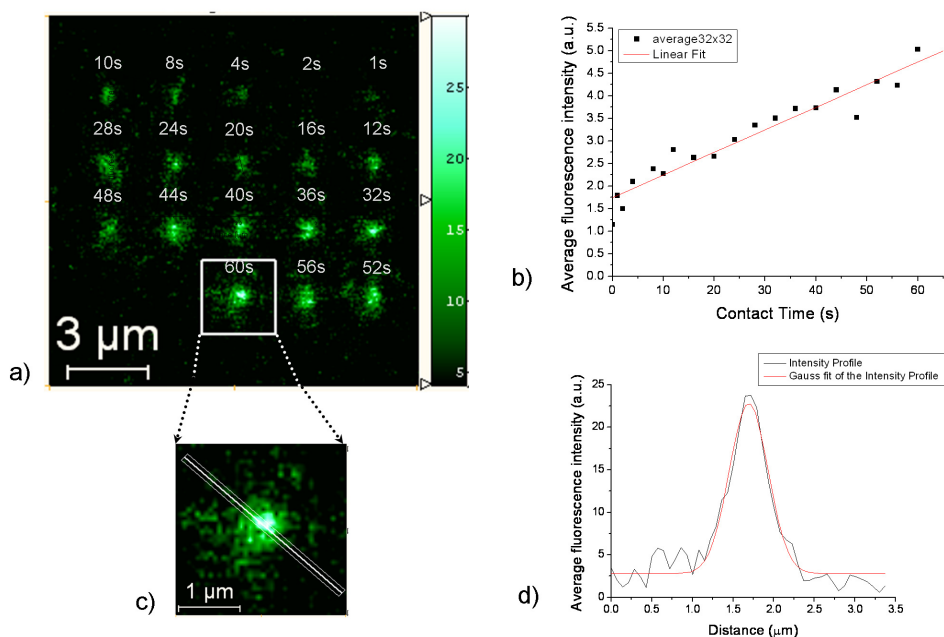
Figure 4.3. *(a) Fluorescence images of His-EGFP patterns acquired after incubating slides, with deposited metal ions areas, with the protein solution. The dot patterns were generated by using an AFM tip inked with Ni(II) ion using tip-surface contact times listed above the dot patterns. The exposure time used for obtaining the images was 0.25 ms per pixel. (b) Plot of average fluorescence intensity of each dot within a 32x32 pixel region around the dot versus tip-surface contact time. The intensity with a contact time of 0 second was obtained by averaging a 32x32 pixel area which had not been in contact with the ink-coated tip; the observed fluorescence can be attributed to the non-specific binding effect of protein on the NTA functionalized surface. A linear fit to the data is plotted in red. (c) Zoom-in of the His-EGFP dot written with tip-surface contact time of 60 seconds shown in (a). (d) Average fluorescence intensity profile of the area inside the rectangle indicated in (c) (black line) and its Gaussian fit profile (red line).*
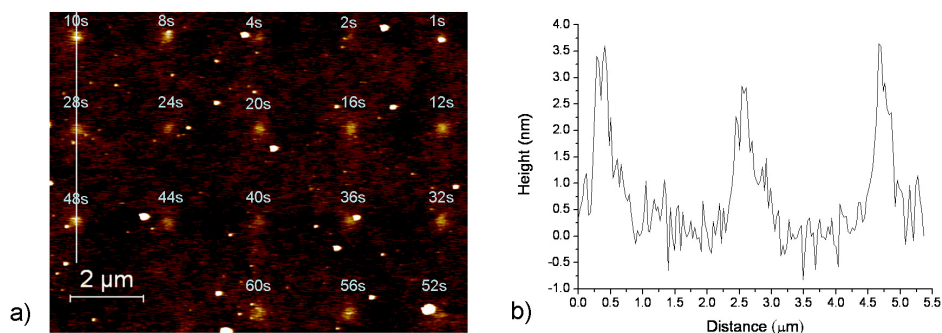
Figure 4.4. (a) AFM tapping mode height image of His-EGFP attached to Ni(II) ion patterns fabricated with dip-pen nanolithography. Some (white) spots shown in the image may result from dust particles or dried salt crystals from the buffer solution. (b) The height profile of protein dots generated with the tip-surface contact times of 10 s, 28 s and 48 s (from left to right).

4.2.3.2 Writing at various speeds

Also line features of His-EGFP were successfully generated by fabricating Ni(II) ion patterns as a template. A Ni(II) ion pattern of five 10 μm long lines with five different scan speeds varying between 10 μm/s and 0.1 μm/s was written. Each line was scanned once, and the tip was retracted after finishing each line. The same tip was used without re-inking to fabricate a second, identical, 5-line pattern. The written area was incubated with a His-EGFP solution to develop the Ni(II) ion pattern. The fluorescence image of the fabricated His-EGFP lines is shown in Figure 4.5a. It was again observed that the protein line patterns correspond to the designed metal ion patterns. A gradient, in-plane and orthogonal to the writing direction, in the fluorescence intensity could also be observed in the line patterns, suggesting that a similar diffusion of Ni(II) ions takes place as observed in the dot patterning. Figure 4.5b shows the average fluorescence intensity profiles of each line in the first 5-line pattern which were fit well with Gaussian functions. The lines with higher fluorescence intensity have more distinct AFM line patterns with a line width of ~ 700 nm.
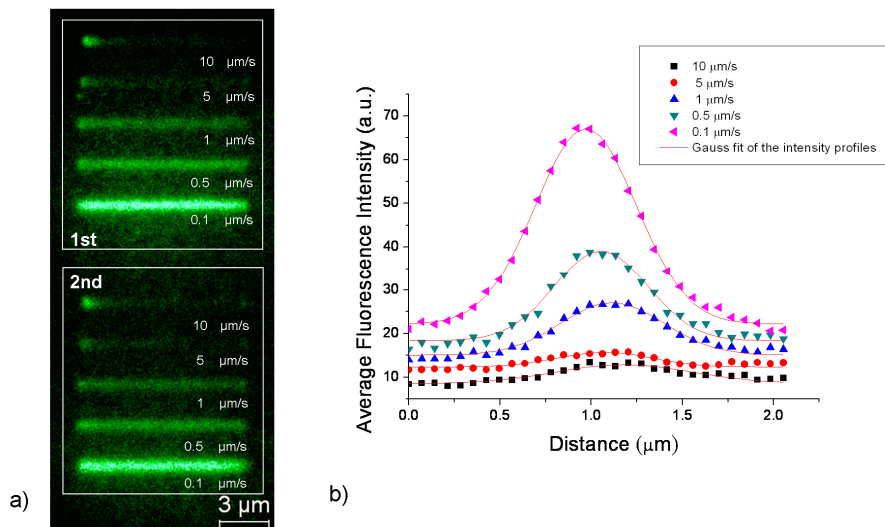
Figure 4.5. *(a) Fluorescence images of His-EGFP patterns acquired after incubating metal-ion written areas with protein solution. The upper 5-line pattern was written first. The pattern includes five horizontal lines (10μm in length) that were successively generated by using an AFM tip inked with Ni(II) ions, using scanning speeds of 10, 5, 1, 0.5, and 0.1 μm/s, from top to bottom. A second 5-lines pattern was generated by using the same tip without re-inking. The camera exposure time for these images is 0.25 ms per pixel. (b) Average fluorescence intensity profiles and Gaussian fit (in red) of each line in 1ˢᵗ 5-line pattern.*

The relationship between the amount of deposited Ni(II) ions and scanning speeds derived by measuring the average fluorescence intensity of each line *versus* writing speed is shown in Figure 4.6a. Comparing the average fluorescence intensities of these two 5-line patterns, we note that the lines written with lower speeds in the first 5-line pattern have slightly higher fluorescence intensity than the ones in the second 5-line pattern. This decrease of fluorescence intensity might result from the depletion of Ni(II) ions coated on the AFM tip surface while performing DPN experiments continuously, that is, without reinking. From Figure 4.5 and 4.6a, it is clear that Ni(II) ion lines written at a lower scanning rate show higher fluorescence intensity, which indicates that more His-EGFP molecules were attached to the written area. To convert the relation between the

fluorescence intensity *versus* writing speed to the fluorescence intensity *versus* tip-surface contact time, the fluorescence intensities over the area of each line (142 x 14 pixels) were averaged. The tip-surface contact time is the time taken to finish the scan of one line. Figure 4.6b shows the average fluorescence intensity *versus* tip-surface contact time of these two 5-line patterns. A close to saturation fluorescence intensity was observed while depositing Ni(II) ions with the slowest scanning speed. A similar result has been reported by Deng *et al.*, observing the saturation of fluorescence emitted from His_6-GFP when the Cu(II) ion density on polyether-functionalized glass substrates is more than $\sim 1.5 \times 10^{14}$ cm^{-2}.[33]

It is interesting to notice the difference between Figure 4.3b (steady state) and Figure 4.6b (writing), although the values of the fluorescence intensity in these two figures are not easily compared with each other due to different experimental conditions. Figure 4.6b shows that the average fluorescence intensity saturates gradually, while the average fluorescence intensity in Figure 4.3b does not show a tendency to saturate even after depositing Ni(II) ions for 60 seconds. This difference is probably due to the different amounts of Ni(II) ions deposited onto the tip surface at the beginning of DPN experiments. There was a practical difficulty to make tips be coated with the same amount of Ni(II) ions. To allow a more thorough investigation of the fundamental DPN parameters, it would be useful to overcome the ink depletion and imperfect coating of ink molecules, for example, by exploiting fountain pen nanolithography[34] or functionalized tip surfaces[35, 36] as an alternative approach for future experiments.
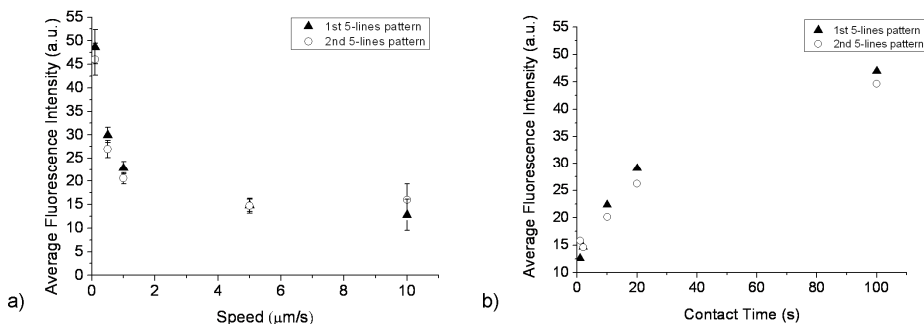

Figure 4.6. (a) Average fluorescence intensities of each line in Fig. 4.5a versus the writing speeds. (b) Plot of average fluorescence intensity of each line within 142x14 pixels (~ 10 μm in length and ~ 1 μm in width) in Fig. 4.5a versus tip-surface contact time.

4.2.4 Fabrication of His-DsRed patterns by μCP and DPN

Monomeric His-EGFP was used to demonstrate successfully that proteins could be immobilized onto metal-ion templates fabricated with μCP and DPN. To further demonstrate the general applicability of this method, the tetrameric reef coral fluorescent protein incorporating a His-tag (His-DsRed) was also used for patterning. Figure 4.7a and 4.7b show that His-DsRed was attached well onto the Ni(II) ion patterns fabricated by μCP and DPN, respectively. A tapping mode AFM topography image of the region displayed in Figure 4.7b is shown in Figure 4.7c. From the cross section profile of the AFM height image (Figure 4.7d), it can be seen clearly that the line width and height of His-DsRed line pattern is ~ 400 nm and ~ 4 nm, respectively. The AFM topographic information again demonstrates the monolayer formation of proteins. In principle, this indirect writing method puts no limits regarding the molecular weight of the molecule (*e.g.*, protein) to be immobilized, which offers an important flexibility and advantage as a patterning technique. Besides, this approach may provide the possibility of generating multiple protein patterns, for example, using EDTA to selectively remove some regions of pre-immobilized proteins and then back filling with another kind of His-tagged protein.
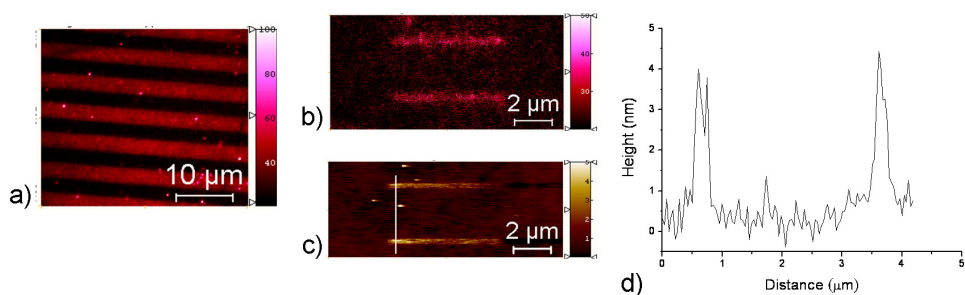

Figure 4.7. *Fluorescence images of His-DsRed immobilized on Ni(II) ion pattern created by (a) microcontact printing and (b) dip-pen nanolithography. (c) AFM tapping mode height image of (b). (d) The cross section profile of His-DsRed line pattern shown in (c).*

4.3 Conclusions

In summary, a general method of fabricating Ni(II) ion patterns on NTA-terminated monolayer-functionalized glass substrates as templates has been developed for the immobilization of His-tagged biomolecules at micrometer and sub-micrometer scale by microcontact printing (μCP) or dip-pen nanolithography (DPN). The advantage of this method is that it allows the oriented and reversible attachment of biomolecules while avoiding protein denaturation because no direct printing or writing of biomolecules is needed. Moreover, this method furnishes well-defined single-protein layers. The driving force for the transfer of Ni(II) ions from an AFM tip to a substrate is the dissolution of metal ions into the aqueous meniscus formed between tip and surface and the complex formation of Ni(II) ions with NTA molecules functionalized on the glass substrates.

The smallest size in diameter or width of His-EGFP or His-DsRed patterns that we can presently achieve by using DPN is around 400 nm. This indirect approach may enable us to fabricate multiple protein patterns in the near future. We have used a hybrid atomic force and fluorescence microscope to perform direct write-read DPN experiments and obtained *in situ* fluorescence images and AFM topography information of the fabricated patterns. By utilizing the intrinsic fluorescence property of His-EGFP, we could study the relationship between tip-surface contact time and deposited amount of Ni(II) ions.

4.4 Experimental

General procedures.
All glassware used to prepare the monolayers was cleaned by sonicating for 60 minutes in a 2% v/v Hellmanex II solution in high purity water (Milli-Q, 18.2 MΩcm), and then rinsed thoroughly with Milli-Q water, and dried in an ambient environment. Microscope glass slide substrates were cleaned in piranha solution for 20 minutes, (concentrated H_2SO_4 and 33% aqueous H_2O_2 in a 3:1 ratio). [Warning: Piranha solution should be handled with caution: it has been reported to detonate unexpectedly.] The glass slides were then rinsed several times with Milli-Q water, and dried gently under a nitrogen stream before forming the monolayer.

NTA and Ni-NTA monolayer preparation.[26]
The freshly cleaned substrates were immersed into a distilled toluene solution containing 1% (vol/vol) 3-glycidyloxypropyl trimethoxysilane under argon for two days. After the substrates were removed from the solution, they were rinsed with distilled toluene and dried under a nitrogen stream. The substrates functionalized with epoxy-terminated monolayer were incubated in 10 mM Tris-HCl

buffer (pH 8.0) containing 2.5 mM *N,N*-bis(carboxymethyl)-L-lysine (NTA) at 60 °C for 4 hours. The substrates were rinsed with Milli-Q water and dried in preparation for μCP and DPN experiments. Ni-NTA surfaces were obtained by immersing the NTA-functionalized substrates into 10 mM Tris-HCl buffer (pH 8.0) containing 0.1 M $NiCl_2$ for 30 minutes. They were then rinsed several times with Milli-Q water, and dried under a nitrogen stream. The formation of the monolayers was examined by water contact-angle goniometry and ellipsometry. The results are consistent with the values reported in literature.[12, 27]

Microcontact printing (μCP).
The preparation procedure of PDMS stamps was described in Chapter 3. The non-oxidized PDMS stamps with 5 μm line features, with a spacing of 3 μm and 10 μm line features, with a spacing of 5 μm were incubated in 10 mM Tris-HCl buffer (pH 8.0) containing 0.1 M $NiCl_2$ for ~ 1 hour and then dried with a nitrogen stream. The stamps were brought into contact with a NTA-terminated substrate for 3 minutes. After peeling off the stamp, the Ni(II) ions-printed substrates were incubated in ~ 200 μl of 25 mM Tris-HCl buffer (pH 7.5) containing 100 nM of His-EGFP or His-DsRed for 30 minutes and then rinsed with 10 mM Tris-HCl buffer (pH 8.0) and Milli-Q water to remove excess protein.

Acquisition of fluorescent images.
The substrates with protein patterns were dried under a nitrogen stream before imaging with a fluorescence microscope (TE2000-U, Nikon) equipped with a mercury lamp as light source and a digital camera (Nikon digital Sight DS-Qi1Mc). The fluorescence images of His-EGFP and His-DsRed patterns were obtained by using filter cubes with blue excitation light (λ=470/22 nm)/ green emission light (λ=520/35 nm)/ dichroic (λ=495 nm) and green excitation light (λ=510/40 nm)/ red emission light (λ=617/73 nm)/ dichroic (λ=562 nm), respectively. The fluorescence images obtained were analyzed with the commercial software SPIP (Image Metrology, Version 4.4.3.0) and ImageJ (Version 1.40g).

Dip pen nanolithography (DPN) and visualization with AFFM.
A custom-built atomic force fluorescence microscope (AFFM) was used to perform dip-pen nanolithography and to observe the results of patterning in situ without having to change to another instrument. Commercial Si_3N_4 AFM cantilevers (Veeco Probes) with nominal spring constant of 0.54 Nm^{-1} were used. Immediately before a DPN experiment, the cantilever was rinsed rigorously with ethanol and dried under a stream of N_2. Cleaned cantilevers were then immersed into 10 mM Tris-HCl buffer (pH 8.0) containing 0.1 M $NiCl_2$ for at least 15 minutes and dried with N_2. The Ni(II) ions-coated cantilever was mounted on the AFM head and used to carry out DPN experiments on NTA-terminated monolayer-functionalized substrates in contact mode inside a custom-built chamber with a controlled humidity (~ 60 %) at a temperature between 20 and 22 °C.[18, 37]

Immediately after DPN, ~ 5 μl of 100 nM His-EGFP or His-DsRed solution was placed onto the written area for 30 minutes, and rinsed with 10 mM Tris-HCl buffer (pH 8.0) and water to remove excess protein. Before fluorescence imaging of the DPN patterns, the substrate was carefully dried with a N_2 stream *in situ* to avoid displacement of the patterned area from the observation range of the objective. The His-EGFP and His-DsRed patterns were excited with the 488 nm line of an argon-ion laser (163-D Laser System, Spectra Physics), and the emission of the fluorescence was recorded by an avalanche photodiode (APD) (SPCM-AQR-14, Perkin Elmer Optoelectronics). The original ink-coated tip was replaced by a new Si_3N_4 AFM tip to prevent contamination of the patterned areas during subsequent imaging. AFM-tapping mode was used to obtain topographic information of the protein patterns. The images were obtained with 512 x 512 pixels acquisitions and scanning speeds of 1000 pixels per second. Fluorescence and topographic images were analyzed with the commercial software SPIP (Image Metrology, Version 4.4.3.0).

4.5 Acknowledgements

Dr. Martin Bennink and Kees van der Werf are acknowledged for their kind help with the modification of the AFM setup and Dr. Francesca Costantini for generously sharing her knowledge of preparing the monolayer.

4.6 References

1. Christman, K. L.; Enriquez-Rios, V. D.; Maynard, H. D. Nanopatterning Proteins and Peptides. *Soft Matt.* **2006,** *2*, 928-939.

2. Mendes, P. M.; Yeung, C. L.; Preece, J. A. Bio-Nanopatterning of Surfaces. *Nanoscale Res. Lett.* **2007,** *2*, 373-384.

3. Weibel, D. B.; DiLuzio, W. R.; Whitesides, G. M. Microfabrication Meets Microbiology. *Nat. Rev. Microbiol.* **2007,** *5*, 209-218.

4. Kane, R. S.; Takayama, S.; Ostuni, E.; Ingber, D. E.; Whitesides, G. M. Patterning Proteins and Cells Using Soft Lithography. *Biomaterials* **1999,** *20*, 2363-2376.

5. Li, H. W.; Muir, B. V. O.; Fichet, G.; Huck, W. T. S. Nanocontact Printing: A Route to Sub-50-Nm-Scale Chemical and Biological Patterning. *Langmuir* **2003,** *19*, 1963-1965.

6. Nam, J. M.; Han, S. W.; Lee, K. B.; Liu, X. G.; Ratner, M. A.; Mirkin, C. A. Bioactive Protein Nanoarrays on Nickel Oxide Surfaces Formed by Dip-Pen Nanolithography. *Angew. Chem., Int. Ed.* **2004,** *43*, 1246-1249.

7. Kenseth, J. R.; Harnisch, J. A.; Jones, V. W.; Porter, M. D. Investigation of Approaches for the Fabrication of Protein Patterns by Scanning Probe Lithography. *Langmuir* **2001,** *17*, 4105-4112.

8. Kim, K. H.; Kim, J. D.; Kim, Y. J.; Kong, S. H.; Jung, S. Y.; Jung, H. Protein Immobilization without Purification Via Dip-Pen Nanolithography. *Small* **2008,** *4*, 1089-1094.

9. Ginger, D. S.; Zhang, H.; Mirkin, C. A. The Evolution of Dip-Pen Nanolithography. *Angew. Chem., Int. Ed.* **2004,** *43*, 30-45.

10. Salaita, K.; Wang, Y. H.; Mirkin, C. A. Applications of Dip-Pen Nanolithography. *Nat. Nanotechnol.* **2007,** *2*, 145-155.

11. Tinazli, A.; Piehler, J.; Beuttler, M.; Guckenberger, R.; Tampe, R. Native Protein Nanolithography That Can Write, Read and Erase. *Nat. Nanotechnol.* **2007,** *2*, 220-225.

12. Maury, P.; Escalante, M.; Peter, M.; Reinhoudt, D. N.; Subramaniam, V.; Huskens, J. Creating Nanopatterns of His-Tagged Proteins on Surfaces by Nanoimprint Lithography Using Specific Ninta-Histidine Interactions. *Small* **2007,** *3*, 1584-1592.

13. Falconnet, D.; Pasqui, D.; Park, S.; Eckert, R.; Schift, H.; Gobrecht, J.; Barbucci, R.; Textor, M. A Novel Approach to Produce Protein Nanopatterns by Combining Nanoimprint Lithography and Molecular Self-Assembly. *Nano Lett.* **2004,** *4*, 1909-1914.

14. Escalante, M.; Zhao, Y. P.; Ludden, M. J. W.; Vermeij, R.; Olsen, J. D.; Berenschot, E.; Hunter, C. N.; Huskens, J.; Subramaniam, V.; Otto, C. Nanometer Arrays of Functional Light Harvesting Antenna Complexes by Nanoimprint Lithography and Host-Guest Interactions. *J. Am. Chem. Soc.* **2008,** *130*, 8892-8893.

15. Hong, Y.; Krsko, P.; Libera, M. Protein Surface Patterning Using Nanoscale Peg Hydrogels. *Langmuir* **2004,** *20*, 11123-11126.

16. Rundqvist, J.; Hoh, J. H.; Haviland, D. B. Directed Immobilization of Protein-Coated Nanospheres to Nanometer-Scale Patterns Fabricated by Electron Beam Lithography of Poly(Ethylene Glycol) Self-Assembled Monolayers. *Langmuir* **2006,** *22*, 5100-5107.

17. Christman, K. L.; Schopf, E.; Broyer, R. M.; Li, R. C.; Chen, Y.; Maynard, H. D. Positioning Multiple Proteins at the Nanoscale with Electron Beam Cross-Linked Functional Polymers. *J. Am. Chem. Soc.* **2009,** *131*, 521-527.

18. Basabe-Desmonts, L.; Wu, C. C.; van der Werf, K. O.; Peter, M.; Bennink, M.; Otto, C.; Velders, A. H.; Reinhoudt, D. N.; Subramaniam, V.; Crego-Calama, M. Fabrication and Visualization of Metal-Ion Patterns on Glass by Dip-Pen Nanolithography. *Chemphyschem* **2008,** *9*, 1680-1687.

19. Kassies, R.; Van der Werf, K. O.; Lenferink, A.; Hunter, C. N.; Olsen, J. D.; Subramaniam, V.; Otto, C. Combined Afm and Confocal Fluorescence Microscope for Applications in Bio-Nanotechnology. *J. Microsc.* **2005,** *217*, 109-116.

20. Vega, R. A.; Maspoch, D.; Shen, C. K. F.; Kakkassery, J. J.; Chen, B. J.; Lamb, R. A.; Mirkin, C. A. Functional Antibody Arrays through Metal Ion-Affinity Templates. *Chembiochem* **2006,** *7*, 1653-1657.

21. Cha, T.; Guo, A.; Jun, Y.; Pei, D. Q.; Zhu, X. Y. Immobilization of Oriented Protein Molecules on Poly(Ethylene Glycol)-Coated Si(111). *Proteomics* **2004,** *4*, 1965-1976.

22. Porath, J.; Carlsson, J.; Olsson, I.; Belfrage, G. Metal Chelate Affinity Chromatography, a New Approach to Protein Fractionation. *Nature* **1975,** *258*, 598-599.

23. Paborsky, L. R.; Dunn, K. E.; Gibbs, C. S.; Dougherty, J. P. A Nickel Chelate Microtiter Plate Assay for Six Histidine-Containing Proteins. *Anal. Biochem.* **1996,** *234*, 60-65.

24. Ludden, M. L. W.; Mulder, A.; Schulze, K.; Subramaniam, V.; Tampe, R.; Huskens, J. Anchoring of Histidine-Tagged Proteins to Molecular Printboards: Self-Assembly, Thermodynamic Modeling, and Patterning. *Chem. Eur. J.* **2008,** *14*, 2044-2051.

25. Lee, K. B.; Lim, J. H.; Mirkin, C. A. Protein Nanostructures Formed Via Direct-Write Dip-Pen Nanolithography. *J. Am. Chem. Soc.* **2003,** *125*, 5588-5589.

26. Paik, H. J.; Kim, Y. R.; Orth, R. N.; Ober, C. K.; Coates, G. W.; Batt, C. A. End-Functionalization of Poly(3-Hydroxybutyrate) Via Genetic Engineering for Solid Surface Modification. *Chem. Commun.* **2005**, 1956-1958.

27. Luzinov, I.; Julthongpiput, D.; Liebmann-Vinson, A.; Cregger, T.; Foster, M. D.; Tsukruk, V. V. Epoxy-Terminated Self-Assembled Monolayers: Molecular Glues for Polymer Layers. *Langmuir* **2000,** *16*, 504-516.

28. Piner, R. D.; Zhu, J.; Xu, F.; Hong, S. H.; Mirkin, C. A. "Dip-Pen" Nanolithography. *Science* **1999,** *283*, 661-663.

29. Noy, A.; Miller, A. E.; Klare, J. E.; Weeks, B. L.; Woods, B. W.; DeYoreo, J. J. Fabrication of Luminescent Nanostructures and Polymer Nanowires Using Dip-Pen Nanolithography. *Nano Lett.* **2002,** *2*, 109-112.

30. Salazar, R. B.; Shovsky, A.; Schonherr, H.; Vancso, G. J. Dip-Pen Nanolithography on (Bio)Reactive Monolayer and Block-Copolymer Platforms: Deposition of Lines of Single Macromolecules. *Small* **2006,** *2*, 1274-1282.

31. Weeks, B. L.; Vaughn, M. W.; DeYoreo, J. J. Direct Imaging of Meniscus Formation in Atomic Force Microscopy Using Environmental Scanning Electron Microscopy. *Langmuir* **2005,** *21*, 8096-8098.

32. Tsien, R. Y. The Green Fluorescent Protein. *Annual Review of Biochemistry* **1998,** *67*, 509-544.

33. Deng, Y.; Zhu, X. Y.; Kienlen, T.; Guo, A. Transport at the Air/Water Interface Is the Reason for Rings in Protein Microarrays. *J. Am. Chem. Soc.* **2006,** *128*, 2768-2769.

34. Kim, K. H.; Sanedrin, R. G.; Ho, A. M.; Lee, S. W.; Moldovan, N.; Mirkin, C. A.; Espinosa, H. D. Direct Delivery and Submicrometer Patterning of DNA by a Nanofountain Probe. *Adv. Mater.* **2008,** *20*, 330-334.

35. Wu, C. C.; Xu, H. P.; Otto, C.; Reinhoudt, D. N.; Lammertink, R. G. H.; Huskens, J.; Subramaniam, V.; Velders, A. H. Porous Multilayer-Coated AFM Tips for Dip-Pen Nanolithography of Proteins. *J. Am. Chem. Soc.* **2009,** *131*, 7526-7527.

36. Senesi, A. J.; Rozkiewicz, D. I.; Reinhoudt, D. N.; Mirkin, C. A. Agarose-Assisted Dip-Pen Nanolithography of Oligonucleotides and Proteins. *Acs Nano* **2009,** *3*, 2394-2402.

37. Stukalov, O.; Murray, C. A.; Jacina, A.; Dutcher, J. R. Relative Humidity Control for Atomic Force Microscopes. *Rev. Sci. Instrum,* **2006,** *77*, 033704.

Chapter 5

Reactive Microcontact Printing and Dip-Pen Nanolithography: a strategy towards patterning submicrometer-sized orthogonal functional groups [*]

Abstract

   A reactive microcontact printing (μCP) and dip-pen nanolithography (DPN) approach is described to create covalently immobilized nanoparticle and supramolecular host patterns. Amine functionalized β-cyclodextrin (βCD-NH$_2$) and quantum dots (QD-NH$_2$) have been printed and written onto *N,N*-carbonyldiimidazole-activated amino monolayer (IM monolayer)-functionalized glass slides, *via* the covalent formation of urethane bonds. The quantum dots patterns were directly imaged by exploiting their intrinsic fluorescence. To confirm the covalent formation of βCD-NH$_2$ patterns, adamantyl-labeled fluorophores and ferrocenyl-labeled fluorescent proteins were used to image the obtained patterns. Additionally, orthogonal microcontact printing of β-CD and QD-NH$_2$ patterns is succesfully demonstrated, furnishing a viable chemical strategy for the generation of patterns of different functional groups through reactive DPN for selective immobilization of multiple desired molecules with complementary functionalities.

---

[*]Manuscript in preparation

5.1 Introduction

Introducing reactive functional units on monolayers offers the opportunity of anchoring desired molecules onto solid support surfaces *via* the formation of covalent bonds and therefore attracts enormous attention. By combining lithography techniques with reactive monolayers, patterns of desired ligand molecules at micro- or nanometer scale can be obtained, with potential applications in different fields.[1-6] These processes may include single or multiple steps. The Whitesides group has utilized microcontact printing (μCP) to respectively generate poly(ethylene-imine) patterns on carboxylic anhydride-terminated self-assembled monolayers (SAMs),[7] and amino derivatives of biotin and benzenesulfonamide patterns on pentafluorophenylesters-terminated SAMs,[8] *via* formation of amide bonds. We have also demonstrated patterning through microcontact printing amines on aldehyde-terminated SAMs *via* imine formation,[9] and acetylene-containing molecules on azide-terminated SAMs *via* triazole formation.[10, 11] Several results have been reported where dip-pen nanolithography (DPN) is used to generate patterns on reactive monolayers. Mirkin's group demonstrated the Michael addition reaction of thiols and acrylamide moieties for covalently immobilizing oligonucleotides.[12] Collier and co-workers also used the Michael addition reaction between thiols and maleimides for the generation of biotin patterns.[13] In addition, the Diels–Alder reaction,[14] borohydride reduction,[15] triazole reaction,[16, 17] and amide-coupling reactions using *N*-hydroxysuccinimidyl ester[18, 19] and carboxylic anhydride[20] are representative covalent organic reactions that have been applied with DPN.

N,N-carbonyldiimidazole (CDI)-activated amino monolayers (IM monolayers) developed in our group have been demonstrated by μCP to react with various functional groups including amino-, carboxyl- and alcohol groups, *via* the formation of urethane, amide and carbamate covalent bonds respectively.[21] The rapid and efficient covalent reaction between amines and imidazolide groups is thought to be an advantage for efficient reactive DPN experiments. These IM monolayers can be used as platforms to immobilize a variety of functional molecules and β-cyclodextrin (βCD) is one good candidate. βCD is a water soluble cyclic oligosaccharide consisting of seven glucose units linked through α-1,4 bonds to form a toroidal structure.[22] The interior of the βCD toroid is relatively hydrophobic. This specific geometrical shape and chemical anisotropy of βCD molecules enable hosting of hydrophobic guest molecules within the toroid in aqueous media based on hydrophobic interactions.[23] We have developed a platform, the so-called molecular printboard, that consists of β-cyclodextrin-terminated monolayers (βCD

monolayers) on different surfaces *e.g.* gold and glass substrates.[24] A wide range of guest molecules or macromolecules containing suitable guest moieties, *e.g.* adamantyl moiety-labeled fluorescent molecules[25] and proteins[26] or ferrocene-labeled dendrimers[27, 28] have been placed onto the molecular printboard. β-cyclodextrin (βCD) patterns on silicon oxide substrates have been fabricated by using nanoimprint lithography (NIL).[29] The disadvantage of this technique is that it is difficult to introduce a second functional group onto reactive SAMs. However, by using µCP or DPN, the orthogonal printing or writing of molecules can be achieved relatively easily.

In this chapter, we first use µCP to print amine containing βCD and quantum dots (QDs-NH$_2$) onto IM monolayer-functionalized glass slides, because of the simplicity and high-throughput production of µCP. Fluorophores equipped with adamantyl moieties were used to confirm the formation of βCD patterns. Subsequently, the atomic force fluorescence microscope (AFFM) was used to perform DPN accompanied by direct visualization of the results by atomic force microscopy (AFM) and confocal fluorescence microscopy. The experimental procedures are illustrated in Scheme 5.1. This is the first demonstration of using DPN to covalently anchor molecules onto IM monolayers. Additionally, the orthogonal printing of βCD and QD-NH$_2$ on IM monolayers is also demonstrated, setting the first step towards submicrometer patterns of orthogonal functional groups, including supramolecular cyclodextrin patterns.
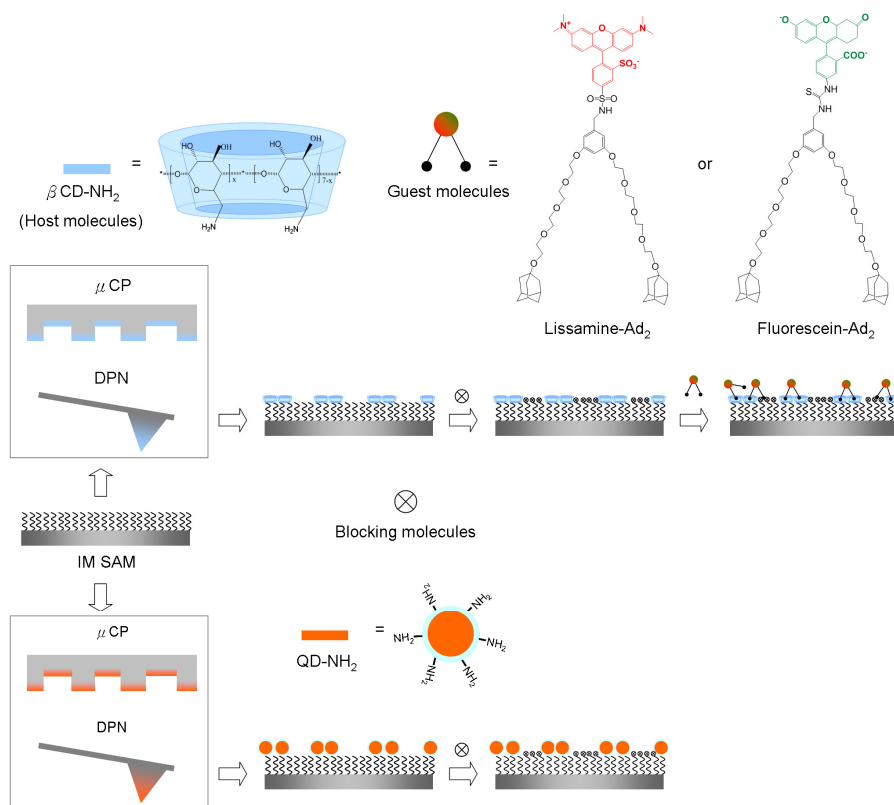
Scheme 5.1. *Illustration of fabricating β-cyclodextrin (βCD) and quantum dot (QD) patterns onto N,N-carbonyldiimidazole (CDI)-activated amino monolayers (IM monolayers) on glass substrates, with microcontact printing (μCP) and dip-pen nanolithography (DPN). Lissamine and fluorescein-linked with adamantyl units were used to confirm formation of βCD patterns.*

5.2 Results and Discussion

N,N-carbonyldiimidazole (CDI)-activated amino monolayers utilized for μCP and DPN experiments were prepared by following the procedures reported by Hsu *et al.* and its synthesis process is depicted in Scheme 5.2 (see Experimental section 5.4).[21] A two-step procedure was followed. Amino-terminated (TPEDA) monolayers were first formed by silylation of the cleaned glass substrates with (*N*-[3-(trimethoxysilyl)propyl]-ethylenediamine). Subsequently the TPEDA monolayers were converted into imidazolide

monolayers (IM monolayers) by reacting CDI with the amino groups. By measuring the advancing water contact angles (θ_a) of monolayers, a clear change in the polarity between TPEDA monolayers (θ_a: ~ 64°) and IM monolayers (θ_a: ~ 55°) was observed, which corresponds to reported values in the literature.[21]

5.2.1 Fabrication of patterns with microcontact printing (μCP)

5.2.1.1 Fabricating β-cyclodextrin (βCD) patterns

Per-7-amino-β-cyclodextrin (βCD-NH$_2$) (Scheme 5.1) was used as ink molecule. Non-oxidized poly(dimethylsiloxane) (PDMS) stamps with 10 μm line features and a spacing of 5 μm, inked with βCD-NH$_2$, were brought into conformal contact with IM monolayer-functionalized glass slides for 5 minutes. After peeling off the stamps, the microcontact printed substrates were vigorously rinsed with MilliQ water to remove excess physisorbed βCD-NH$_2$ and then incubated into 0.1 M ethanolamine aqueous solution for 30 minutes to passivate the non-reacted imidazolide groups. These substrates were rinsed with MilliQ water and then dried with nitrogen before examining with AFM. For measurements of the topography of the surfaces, the AFM was operated in contact mode. The height image and its average profile are shown in Figure 5.1a and 5.1b, respectively. The height of the pattern is ~ 0.7 nm which indicates a single layer of βCD-NH$_2$ lying flat on the surface.[30] To confirm the reactivity of the βCD-NH$_2$ patterns and their ability to exhibit host-guest interactions, lissamine equipped with two adamantyl moieties linked *via* flexible tetra(ethylene glycol) spacers (lissamine-Ad$_2$, Scheme 5.1) were used for fluorescent signaling. The fluorescence image and its average fluorescence intensity profile (Figure 5.1c and 5.1d) show that the lissamine-Ad$_2$ area is consistent with the expected feature size of the microcontact printed βCD region, indicating the quick immobilization of βCD-NH$_2$ onto IM monolayers since the microcontact printing time is only 5 minutes.
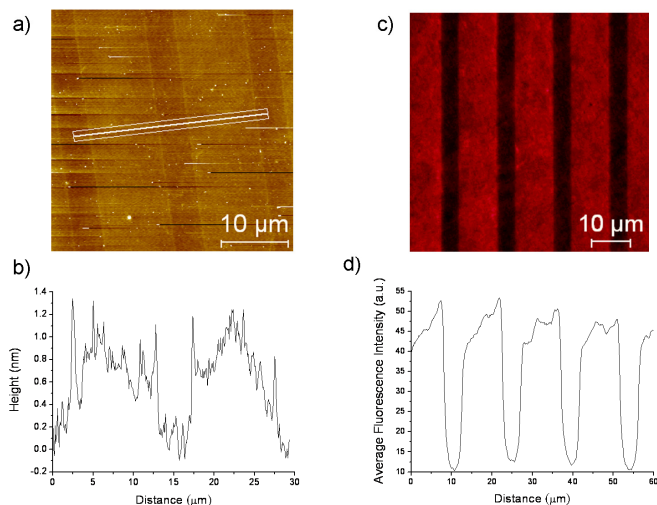
Figure 5.1. *(a) AFM contact mode height image of βCD-NH$_2$ (μCP patterns) covalently bound to IM monolayers. (b) Average height profile of the area defined by the white lines in (a). (c) Fluorescence images of lissamine-Ad$_2$ adhered to βCD-NH$_2$ via host-guest interaction. (d) Average fluorescence intensity profile of (c). Exposure time of the camera was 400 ms.*

Fabricated βCD patterns can also be used as an indirect strategy to immobilize guest moieties-labeled proteins with controlled orientation, which provides potential applications described in the introductions of Chapter 2 and Chapter 4. Non-oxidized βCD-NH$_2$ inked PDMS stamps with 5 μm line features and a spacing of 3 μm were brought into conformal contact with IM monolayers-functionalized glass slides for 20 minutes. The remaining active imidazolide groups were blocked by incubating the substrate with aqueous ethanolamine solution for 30 minutes. Yellow fluorescent protein labeled with a ferrocenyl moiety (Fc-YFP) was used to adhere to printed βCD-NH$_2$ patterns. The longer microcontact printing time (20 minutes) was used in order to have more βCD-NH$_2$ adhered to IM-monolayers, in accordance with previous reports that the maximum fluorescence intensity was obtained after printing 4-(2-aminoethylamino)-7-(*N,N*-dimethylsulfamoyl)benzofurazan (ADF) with IM monolayers for 20 minutes.[21] The fluorescent image of Fc-YFP (Figure 5.2a) shows the protein patterns with the expected feature size.
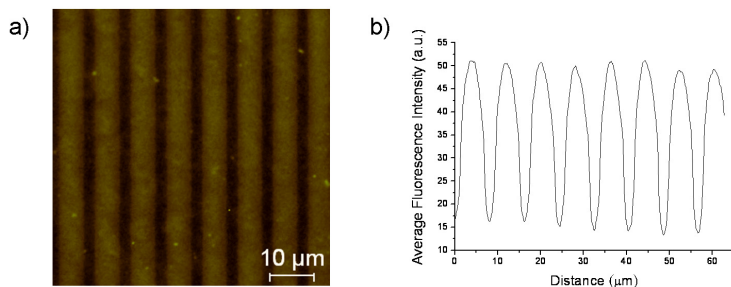
Figure 5.2. *(a) Fluorescence images of Fc-YFP adhered to βCD-NH$_2$ patterns via host-guest interaction. (b) The average fluorescence intensity profile of (a). The exposure time of the camera to obtain the image is 2 s.*

5.2.1.2 Fabricating quantum dot patterns

Amine-containing quantum dots (QDs-NH$_2$, eBioscience Inc.) (Scheme 5.1) were also used as ink. The emission wavelength of QDs-NH$_2$ is 605 nm. Non-oxidized poly(dimethylsiloxane) (PDMS) stamps with 5 µm line features and a spacing of 3 µm, inked with QDs-NH$_2$ were brought into conformal contact with IM monolayers-functionalized glass slides for 20 minutes. After removing the stamps, the microcontact printed substrates were vigorously rinsed with Milli-Q water and then examined with a fluorescence microscope. Figure 5.3 shows the successful transfer of QDs-NH$_2$ from the PDMS stamp to IM monolayers.
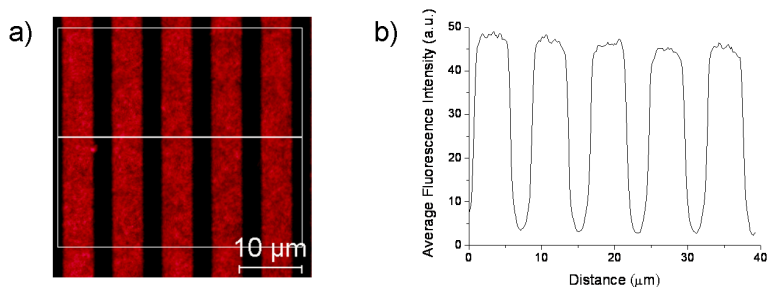

Figure 5.3. *a) Fluorescence image of QD-NH$_2$ patterns via covalent bonding between amine and imidazolide groups. b) Average fluorescence intensity profile of the area inside the rectangle indicated in (a). Exposure time was 100 ms.*

5.2.1.3 Fabricating β-cyclodextrin and quantum dot patterns together

The remaining active imidazolide groups after patterning QDs-NH$_2$ on IM monolayers can subsequently react with βCD-NH$_2$. To have clear fluorescent patterns a non-oxidized PDMS stamp with 10 μm diameter circular features separated with a distance of 5 μm was used. After 20 minutes of printing QDs-NH$_2$, the patterned substrate was rinsed with water, dried with N$_2$ and then immediately incubated with 0.5 mM βCD-NH$_2$ aqueous solution for 30 minutes. To distinguish the βCD-NH$_2$ region from QDs-NH$_2$, fluorescein equipped with two adamantyl moieties (fluorescein-Ad$_2$, Scheme 5.1) was used to visualize the βCD-NH$_2$ area. (Figure 5.4a-c) This experimental procedure was also performed in the opposite sequence, *i.e.* printing βCD-NH$_2$ first and then functionalizing the unprinted region with QDs-NH$_2$ (Figure 5.4 d-e). Fluorescence images of QD-NH$_2$ (Figure 5.4a and 5.4d) and fluorescein-Ad$_2$ (Figure 5.4b and 5.4e) patterns were obtained separately using suitable filter cubes.

Figure 5.4 demonstrates the successful surface modification of non-printed areas of the IM monolayers and indicates the potential of orthogonal microcontact printing of different inks. To explore this further, a PDMS stamp with 10 μm line features and a spacing of 5 μm inked with QDs-NH$_2$ was first brought into conformal contact with the IM monolayer-functionalized surface for 20 minutes. Another stamp inked with βCD-NH$_2$ was subsequently brought into contact with the same substrate in the orthogonal direction for 20 minutes. After blocking the remaining active imidazolide groups with ethanolamine, this substrate was incubated into fluorophore solution to fill printed βCD-NH$_2$ area with fluorescein-Ad$_2$. Clear fluorescence line patterns of QDs-NH$_2$ (Figure 5.5a) and well-defined areas of fluorescein-Ad$_2$ (Figure 5.5b) were obtained, demonstrating successful orthogonal microcontact printing of the two inks.
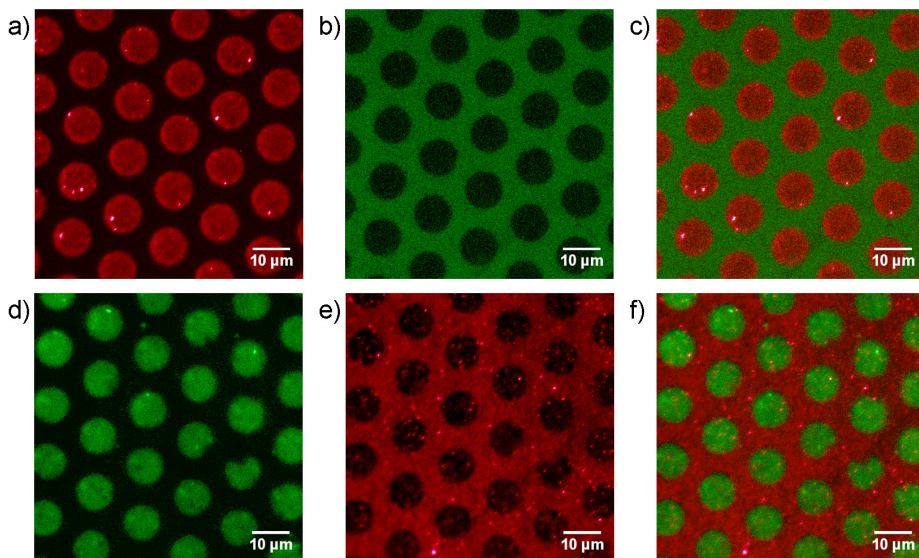
Figure 5.4. *Fluorescence images (exposure time 100 ms). Top, (a) microcontact printed QD-NH$_2$ patterns, (b) unprinted QD-NH$_2$ regions reacted with βCD-NH$_2$ and then filled with fluorescein-Ad, and (c) the added result of (a) and (b). Bottom, (d) microcontact printed βCD-NH$_2$ patterns consecutively filled with fluorescein-Ad$_2$, (e) the unprinted βCD-NH$_2$ region shown in (d) functionalized with QD-NH$_2$, and (f) the added result of (d) and (e). .*
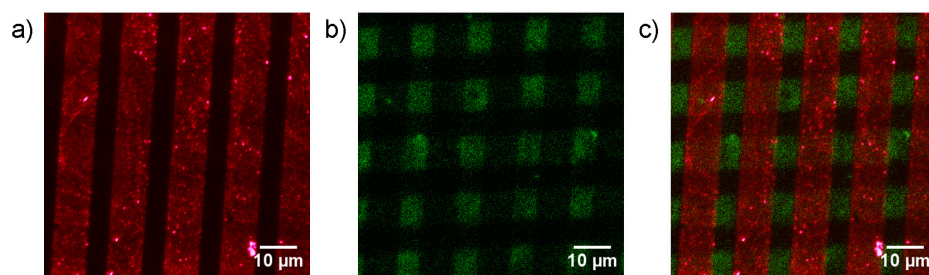

Figure 5.5. *Fluorescence images of (a) QD-NH$_2$ patterns via the covalent bonding between amine and imidazolide groups, (b) Fluorescein-Ad$_2$ reacted with microcontact printed region of βCD-NH$_2$. (c) The added result of (a) and (b). The exposure time of (a) and (b) is 100ms.*

5.2.2 Fabrication of patterns with dip-pen nanolithography (DPN)

5.2.2.1 Fabricating quantum dot patterns

Here, QDs-NH$_2$ were used as ink first for DPN experiments because their intrinsic fluorescence enables immediate visualization of the patterning results *in situ* on the atomic force fluorescence microscope (AFFM). To prove the reactive covalent bond formation of urethane, commercial Si$_3$N$_4$ AFM tips incubated in a 2 μM QDs-NH$_2$ solution were used to generate quantum dot patterns on both IM monolayer-functionalized and cleaned bare glass substrates. The QDs-NH$_2$-coated tip was brought into contact with an IM monolayer-functionalized surface to continuously generate 5 single vertical lines of ~ 7.2 μm in length without re-inking the tip. The 5 lines (from left to right) were written with a scan rate of ~ 28 μm/s for 1, 2, 3, 4 and 5 minutes at ~ 40 % relative humidity (RH). The fluorescence image of the 5-lines pattern was acquired by the confocal microscope of the AFFM immediately after writing (Figure 5.6a) and the average fluorescence intensity profile (Figure 5.6c) was extracted, which indicated the successful transfer of QDs-NH$_2$ from the tip to the substrate. The width of the quantum dot line is ~ 1 μm. The written area was subsequently rinsed with HPLC water carefully and imaged (Figure 5.6b). The average fluorescence intensity of each line acquired after rinsing decreases showing some physisorbed QDs-NH$_2$ were removed (Figure 5.6d). Nevertheless, the 5-lines quantum dot pattern still can be clearly observed in Figures 5.6b and 5.6d confirming the formation of irreversible covalent bonds through reactive DPN.

A control DPN experiment was performed by bringing a QDs-NH$_2$-coated tip into contact with a cleaned bare glass substrate to write a ~ 1.5 μm wide square in one move with a writing speed of ~ 7 μm/s. A bright square pattern was obtained immediately after writing showing the deposition of QDs-NH$_2$ (Figure 5.6e). However, the QD-NH$_2$ pattern did not stay on the substrate after rinsing with HPLC water, which indicated the lack of strong interactions between quantum dots and substrate (Figure 5.6f).
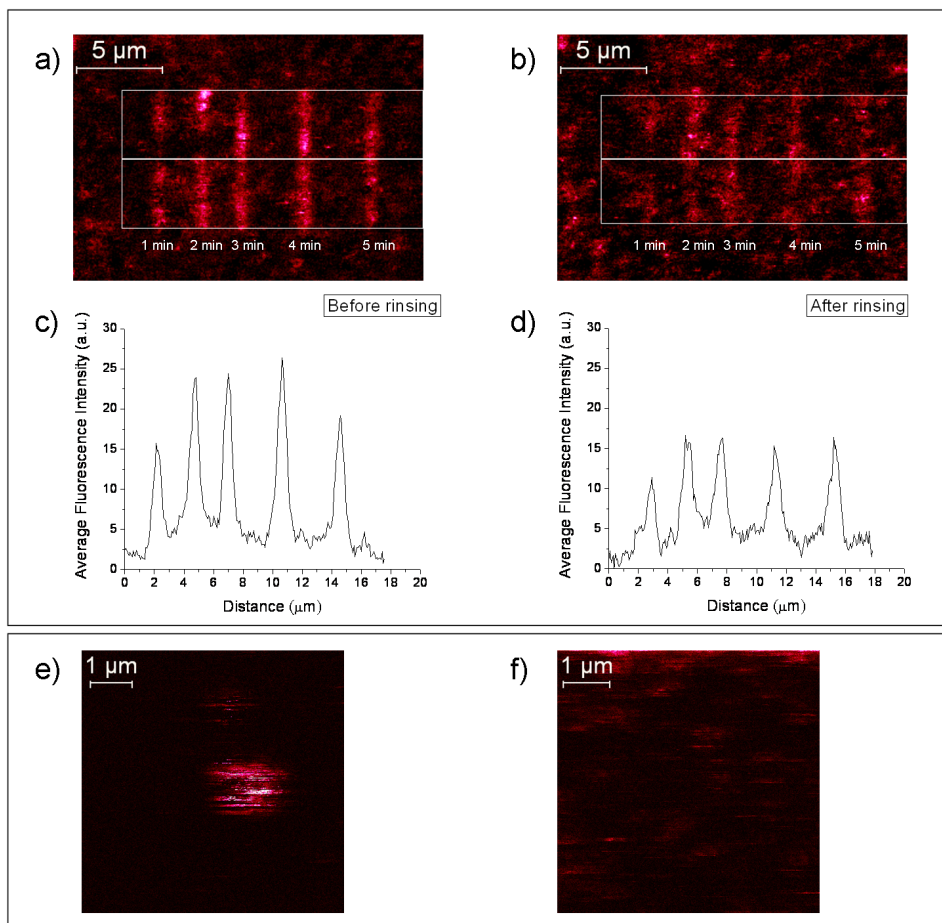
Figure 5.6. *Fluorescence image of five vertical lines (~ 7.2 µm in length) were successively generated from left to right by using an AFM tip inked with QDs-NH₂ using a scanning speed of 28 µm/s for varied times (a) before and (b) after rinsing with HPLC water. The scanning time of each line is listed on the images. (c) and (d) The average fluorescence intensity profile of the area inside the rectangle indicated in (a) and (b), respectively. Fluorescence images of a square QD-NH₂ pattern (~ 1.5 x 1.5 µm²) written onto a cleaned bare glass substrate (e) before and (f) after rinsing with HPLC water. The exposure time of all images is 0.25 ms per pixel.*

5.2.2.2 Fabricating β-cyclodextrin (βCD) patterns

Commercial Si_3N_4 AFM tips incubated in filtered saturated $βCD-NH_2$ aqueous solution overnight were used to fabricate βCD patterns which were confirmed by complexing with fluorescein-Ad_2 for fluorescent signaling *via* host-guest interaction. Using the AFFM at ~ 40 % relative humidity (RH), the $βCD-NH_2$-coated tip was brought into contact with an IM monolayer-functionalized and a cleaned bare glass substrate to scan a ~ 3.6 μm wide square once with a writing speed of ~ 1.4 μm/s. After DPN, the topographic information of the βCD patterns was revealed by AFM imaging. To avoid contaminations, a new Si_3N_4 AFM tip was brought to the original position in the DPN experiments, directly above the central focus of the objective lens. The topography measurements were performed in tapping mode and are shown in Figure 5.7a and 5.7b indicating the transfer of material from the tip to the substrate. The corresponding average height profiles (Figures 5.7c and 5.7d) show that multilayers of $βCD-NH_2$ adhered to both substrates.

After passivation of the remaining imidazolide groups on the IM monolayer with 0.1 M ethanolamine aqueous solution, fluorescein-Ad_2 solution was placed onto the written area on both bare and IM monolayer-functionalized glass substrates for confirming the immobilization of CD by reactive DPN. After removing fluorescein-Ad_2 solution and rinsing the written areas with saturated β-cyclodextrin (βCD) aqueous solution and HPLC water, the written areas were subsequently imaged with AFFM (Figures 5.8a and 5.8b). It can be clearly observed that the fluorescent square pattern is only observed on the IM monolayer-functionalized glass substrate, again indicating the formation of covalent bonds that have been successfully obtained using DPN. The average fluorescence intensity profile of the fluorescein-Ad_2 pattern is shown in Figure 5.8c.
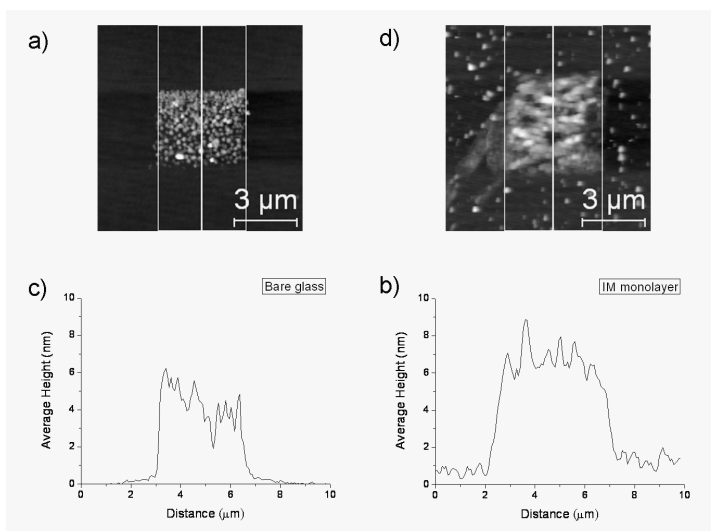
Figure 5.7. *(a) AFM tapping mode height image of βCD patterns fabricated by depositing βCD-NH₂ with dip-pen nanolithography onto (a) a cleaned bare glass substrate and (b) IM monolayer-functionalized glass substrate. Some white spots shown outside of the square area in (a) result from the N,N-carbonyldiimidazole (CDI) adsorbed onto the surface while preparing IM monolayer. (c) and (d) Average height profile of the area inside the rectangle indicated in (a) and (b), respectively.*
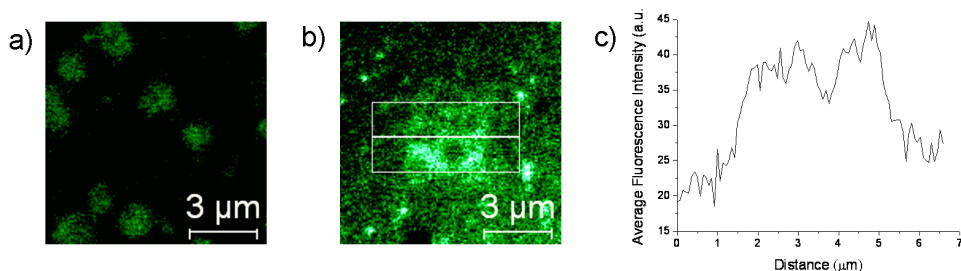

Figure 5.8. *Fluorescence image of βCD-NH₂ pattern generated by dip-pen nanolithography on (a) a cleaned bare glass substrate and (b) a IM monolayer-functionalized glass substrate after reacting with fluorescein-Ad₂ via host-guest interaction. The exposure time of the fluorescence image obtained by AFFM is 0.25 ms per pixel. The excitation laser power for obtaining figure (a) is 10 times higher than for figure (b). (c) The average fluorescence intensity profile of the area defined by the white lines shown in (b).*

In Figure 5.8, the βCD-NH$_2$ pattern was generated with a writing speed of ~ 1.4 μm/s. To demonstrate that the patterns can be fabricated within a shorter time, another βCD-NH$_2$-coated tip was brought into contact with an IM monolayer-functionalized surface to continuously generate 2 squares of ~ 3.6 μm in width without re-inking the tip. The 2 squares (from right to left) were written once with a scan rate of ~ 28 and ~ 14 μm/s respectively, at ~ 40 % relative humidity (RH),. After passivating the un-patterned area and filling the CD area with fluorescein-Ad$_2$, the fluorescence image and its average fluorescence intensity profile (Figure 5.9a and 5.9b) show that fluorescein-Ad$_2$ patterns are consistent with the expected feature sizes of the written βCD-NH$_2$ region. This result indicates that ~ 3.6 μm wide patterns of covalently immobilized βCD can be fabricated within a minute. Comparing with the fluorescent images obtained by μCP (Figures 5.1 and 5.2), much higher background signals are obtained while performing DPN experiments (Figures 5.8b and 5.9a). This difference may be attributed to the difficulty of rinsing written areas right above the objective lens without moving the substrate.
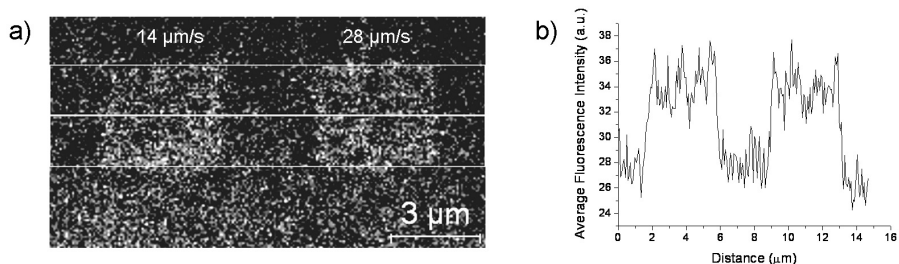

Figure 5.9. (a)Fluorescence image of 2 βCD-NH$_2$ square pattern generated by dip-pen nanolithography with a scanning speed of ~ 28 and ~ 14 μm/s (from right to left) respectively on a IM monolayer-functionalized glass substrate after reacting with fluorescein-Ad$_2$ via host-guest interaction. The exposure time of the fluorescence image obtained by AFFM is 0.25 ms per pixel. (b) The average fluorescence intensity profile of the area defined by the white lines shown in (a).

Although the DPN results are still clearly not optimized, section 5.2.2 demonstrates preliminary DPN results showing that the covalent reaction between imidazolide groups and amine groups can be obtained after DPN. Since DPN allows one to create patterns with a feature size of tens of nanometers, we expect to be able to achieve sub-micrometer patterns of βCD-NH$_2$ and QDs-NH$_2$ in the near future. Additionally, it has been demonstrated in Section 5.2.1.3 that βCD-NH$_2$ and QDs-NH$_2$ patterns can be fabricated together using orthogonal microcontact printing. Therefore, we believe that this chemical approach can be used with DPN to generate different types of amino-containing functional groups onto IM monolayer-functionalized surfaces for selectively anchoring desired molecules.

5.3 Conclusions

In summary, a covalent reaction approach has been developed for immobilizing amine-containing β-cyclodextrin and quantum dots (βCD-NH$_2$ and QD-NH$_2$) at micrometer scale onto *N,N*-carbonyldiimidazole-activated amino monolayer (IM monolayer)- functionalized glass slides via the covalent formation of urethane bonds by microcontact printing (μCP) and dip-pen nanolithography (DPN). Fluorophores equipped with adamantyl moieties (fluorecein-Ad$_2$ and lissamine-Ad$_2$) and yellow fluorescent proteins labeled with ferrocenyl moieties (Fc-YFP) were used for fluorescence microscopy confirmation of the formation of covalently immobilized βCD-NH$_2$ patterns. The orthogonal microcontact printing of βCD-NH$_2$ and QD-NH$_2$ has also successfully been demonstrated. Therefore this chemical strategy provides the possibility of writing different types of amino-containing functional groups with DPN onto IM monolayer-functionalized surfaces at sub-micrometer scales for selective anchoring of desired molecules in the near future, *e.g.* as an indirect DPN approach to generate multiple protein patterns.

5.4 Experimental

General procedures

All glassware used to prepare the monolayers was cleaned by sonicating for 60 minutes in a 2% v/v Hellmanex II solution in high purity water (Milli-Q, 18.2 MΩcm), and then rinsed thoroughly with Milli-Q water, and dried in an ambient environment. Microscope glass slide substrates were cleaned in piranha solution for 20 minutes, (concentrated H_2SO_4 and 33% aqueous H_2O_2 in a 3:1 ratio). [**Warning:** Piranha solution should be handled with caution: it has been reported to detonate unexpectedly.] The glass slides were then rinsed several times with Milli-Q water, and dried gently under a nitrogen stream before forming the monolayer.

Imidazolide monolayer preparation.

The freshly cleaned microscope glass slide substrates were placed in a desiccator under vacuum overnight for the gas-phase evaporation of *N*-[3-(trimethoxysilyl)propyl]ethylenediamine to form amino-terminated monolayer (TPEDA monolayer). After the TPEDA monolayer-functionalized substrates were taken out from the desiccator, they were rinsed carefully with ethanol and dichloromethane to remove physisorbed materials and then dried under a stream of N_2. In order to obtain more stable TPEDA monolayer, the substrates were placed in an oven at 110 °C for 3 hours before reacting with *N,N*-carbonyldiimidazole (CDI). The TPEDA monolayer-functionalized substrates were then incubated with saturated CDI solution in freshly distilled Tetrahydrofuran (THF) under Argon overnight.[21] After the formation of imidazolide monolayer, the substrates were rinsed with THF, followed by nitrogen drying. All samples were freshly prepared and used immediately after drying.

Glass   TPEDA monolayer   IM monolayer
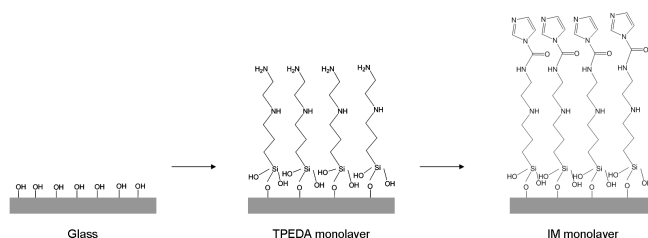
Scheme 5.2. *Illustration of the preparation procedure for an imidazolide-terminated monolayer (IM monolayers) on glass.*

Microcontact printing (μCP).

The preparation procedure of PDMS stamps were described in Chapter 3. The non-oxidized PDMS stamps were incubated in 0.5 mM per-7-amino-β-cyclodextrin (βCD-NH₂) aqueous solution or 500 nM amine-containing quantum dots (QDs-NH₂, eFluor™ 605^{NC} (Amine), eBioscience, Inc. USA)

aqueous solution for at least 20 minutes and then dried with a nitrogen stream. The inked stamps were subsequently brought into contact with IM monolayers-functionalized glass slides for defined time without the use of external pressure. After removing the stamps, the printed substrates were rinsed vigorously with Milli-Q water and then dried. The βCD-NH$_2$ printed substrates were immediately incubated into 0.1 M ethanolamine aqueous solution for 30 minutes to block the remaining active imidazolide groups and then rinsed with MilliQ water to remove excess physisorbed materials before drying with N$_2$. These printing procedures were also applied in the experiment of cross printing.

The βCD-NH$_2$ printed substrates were incubated into an ~ 1μM aqueous solution of lissamine equipped with two adamantyl moieties linked *via* flexible tetra(ethylene glycol) spacers (lissamine-Ad$_2$) for 10 minutes. After removing substrates from the fluorophore solution, they were rinsed vigorously with 1 mM β-cyclodextrin (βCD) aqueous solution and Milli-Q water mixed with 1% (v/v) ethanol to remove the excess physisorbed fluorophores and then dried. The βCD-NH$_2$ patterned substrates were also incubated into ~ 1μM solution in PBS buffer (pH 7.4) of ferrocene derivative yellow fluorescent protein (Fc-YFP) for 30 minutes and then rinsed with pH 7.4 PBS buffer and Milli-Q water to remove excess proteins and then dried.

The printed QDs-NH$_2$ patterns were also incubated into 0.5 mM βCD-NH$_2$ aqueous solution for 30 minutes to backfill the unprinted region and then vigorously rinsed with Milli-Q water. These substrates were incubated into an ~ 1μM aqueous solution of fluorescein equipped with two adamantyl moieties linked *via* flexible tetra(ethylene glycol) spacers (fluorescein-Ad$_2$) for 10 minutes. After removing substrates from the fluorophore solution, they were rinsed with 1 mM βCD aqueous solution and Milli-Q water mixed with 1% (v/v) ethanol and then dried. This experimental procedure was also performed when printing βCD-NH$_2$ and then backfilling with QDs-NH$_2$.

Acquisition of fluorescent images.

All these pattered surfaces with μCP were imaged with a fluorescence microscope (TE2000-U, Nikon) equipped with a mercury lamp as light source and a digital camera (Nikon digital Sight DS-Qi1Mc). To obtain fluorescence images of QD-NH$_2$ and lissamine-Ad$_2$ patterns, a filter cube with green excitation light (λ=510/40 nm), red emission light (λ=617/73 nm) and dichroic (λ=562 nm) was used. To obtain fluorescence images of Fc-YFP and fluorescein-Ad$_2$ patterns, a filter cube with blue excitation light (λ=470/22 nm), green emission light (λ=520/35 nm) and dichroic (λ=495 nm) was used. The fluorescence images obtained were analyzed with the commercial software SPIP (Image Metrology, Version 4.4.3.0) and ImageJ (Version 1.40g).

AFM imaging of microcontact printed patterns.

AFM topography measurements in height were carried out with a custom-built atomic force fluorescence microscope (AFFM) in contact mode, with 512 x 512 pixels acquisitions. Commercial

Si$_3$N$_4$ AFM cantilevers (Veeco Probes) with nominal spring constant of 0.54 N/m were used. The scan speed is 500 pixels per second.

Dip pen nanolithography (DPN) and visualization with AFFM.

AFFM was also used to perform dip-pen nanolithography and to observe the results of patterning *in situ* without having to change to another instrument. Commercial Si$_3$N$_4$ AFM cantilevers (Veeco Probes) with nominal spring constant of 0.32 N/m were used. Immediately before a DPN experiment, the cantilever was rinsed rigorously with ethanol and dried under a stream of N$_2$. Cleaned cantilevers were then immersed into 2 μM QD-NH$_2$ solution for at least 15 minutes or filtered saturated βCD-NH$_2$ aqueous solution overnight and then dried with N$_2$. The QDs-NH$_2$ or βCD-NH$_2$-coated cantilever was mounted on the AFM head and used to carry out DPN experiments on IM monolayers-functionalized or cleaned bare glass substrates in contact mode inside a custom-built chamber with a controlled humidity (~ 40 %) at a temperature between 20 and 22 °C.

After depositing QDs-NH$_2$, the fluorescence image of the generated quantum dot pattern was obtained by exciting with the 488 nm line of an Argon-ion laser (163-D Laser System, Spectra Physics) and then recording the fluorescent signals with an avalanche photodiode (APD) (SPCM-AQR-14, Perkin Elmer Optoelectronics). The same area was imaged again after carefully rinsing with HPLC water to remove the physisorbed materials and then drying under a stream of N$_2$ *in situ* to avoid displacement of the patterned area from the observation range of the objective.

Before complexing βCD-NH$_2$ with fluorescein-Ad$_2$ for fluorescent imaging, the topography of generated βCD-NH$_2$ square patterns on either IM monolayers-functionalized or cleaned bare glass substrates was characterized by AFM in tapping mode. The original ink-coated tip was replaced by a new Si$_3$N$_4$ AFM tip (Veeco Probes) with nominal spring constant of 0.54 N/m to prevent contamination of the patterned areas during subsequent imaging. The image was obtained with 256 x 256 pixels acquisitions and scanning speeds of 2000 pixels per second. Subsequently, the written βCD-NH$_2$ pattern on the IM monolayer-functionalized substrate was incubated with 5 μl of 0.1 M ethanolamine aqueous solution for 30 minutes to block the remaining active imidazolide groups and then rinsed with a few drops of HPLC water before drying with N$_2$. 5 μl of 200 nM fluorescein-Ad$_2$ solution was placed onto the written area on both substrates for 5 minutes. To remove the excess fluorescein-Ad$_2$ adsorbed onto the surface, 5 μl of filtered saturated β-cyclodextrin (βCD) aqueous solution was placed onto the written region for 5 minutes. After removing βCD solution, the βCD-NH$_2$ deposited areas were subsequently rinsed with few drops of HPLC water before drying with N$_2$. The fluorescein-Ad$_2$ patterns were also excited with the 488 nm line of an Argon-ion laser and the emission of the fluorescence was recorded using an APD. Both fluorescence and AFM topographic images were analyzed and prepared with the commercial software SPIP (Image Metrology, Version 4.4.3.0).

5.5 Acknowledgements

5.6 References

1. Smith, R. K.; Lewis, P. A.; Weiss, P. S. Patterning Self-Assembled Monolayers. *Prog. Surf. Sci.* **2004,** *75*, 1-68.

2. Li, X. M.; Huskens, J.; Reinhoudt, D. N. Reactive Self-Assembled Monolayers on Flat and Nanoparticle Surfaces, and Their Application in Soft and Scanning Probe Lithographic Nanofabrication Technologies. *J. Mater. Chem.* **2004,** *14*, 2954-2971.

3. Arya, S. K.; Solanki, P. R.; Datta, M.; Malhotra, B. D. Recent Advances in Self-Assembled Monolayers Based Biomolecular Electronic Devices. *Biosensors & Bioelectronics* **2009,** *24*, 2810-2817.

4. Gooding, J. J.; Mearns, F.; Yang, W. R.; Liu, J. Q. Self-Assembled Monolayers into the 21(St) Century: Recent Advances and Applications. *Electroanalysis* **2003,** *15*, 81-96.

5. Kramer, S.; Fuierer, R. R.; Gorman, C. B. Scanning Probe Lithography Using Self-Assembled Monolayers. *Chem. Rev.* **2003,** *103*, 4367-4418.

6. Rosa, L. G.; Liang, J. Atomic Force Microscope Nanolithography: Dip-Pen, Nanoshaving, Nanografting, Tapping Mode, Electrochemical and Thermal Nanolithography. *Journal of Physics-Condensed Matter* **2009,** *21*, 483001.

7. Yan, L.; Huck, W. T. S.; Zhao, X. M.; Whitesides, G. M. Patterning Thin Films of Poly(Ethylene Imine) on a Reactive Sam Using Microcontact Printing. *Langmuir* **1999,** *15*, 1208-1214.

8. Lahiri, J.; Ostuni, E.; Whitesides, G. M. Patterning Ligands on Reactive Sams by Microcontact Printing. *Langmuir* **1999,** *15*, 2055-2060.

9. Rozkiewicz, D. I.; Ravoo, B. J.; Reinhoudt, D. N. Reversible Covalent Patterning of Self-Assembled Monolayers on Gold and Silicon Oxide Surfaces. *Langmuir* **2005,** *21*, 6337-6343.

10. Rozkiewicz, D. I.; Janczewski, D.; Verboom, W.; Ravoo, B. J.; Reinhoudt, D. N. "Click" Chemistry by Microcontact Printing. *Angew. Chem., Int. Ed.* **2006,** *45*, 5292-5296.

11. Scaramuzzo, F. A.; González-Campo, A.; Wu, C. C.; Velders, A. H.; Subramaniam, V.; Doddi, G.; Mencarelli, P.; Barteri, M.; Jonkheijm, P.; Huskens, J. Pyrylium Monolayers as Amino-Reactive Platform. *Chem. Commun.* **2010**, in press.

12. Demers, L. M.; Ginger, D. S.; Park, S. J.; Li, Z.; Chung, S. W.; Mirkin, C. A. Direct Patterning of Modified Oligonucleotides on Metals and Insulators by Dip-Pen Nanolithography. *Science* **2002,** *296*, 1836-1838.

13. Jung, H.; Dalal, C. K.; Kuntz, S.; Shah, R.; Collier, C. P. Surfactant Activated Dip-Pen Nanolithography. *Nano Lett.* **2004,** *4*, 2171-2177.

14. Matsubara, S.; Yamamoto, H.; Oshima, K.; Mouri, E.; Matsuoka, H. Fabrication of Nano-Structure by Diels-Alder Reaction. *Chem. Lett.* **2002**, 886-887.

15. Blasdel, L. K.; Banerjee, S.; Wong, S. S. Selective Borohydride Reduction Using Functionalized Atomic

Force Microscopy Tips. *Langmuir* **2002,** *18*, 5055-5057.

16. Long, D. A.; Unal, K.; Pratt, R. C.; Malkoch, M.; Frommer, J. Localized "Click" Chemistry through Dip-Pen Nanolithography. *Adv. Mater.* **2007,** *19*, 4471-4473.

17. Paxton, W. F.; Spruell, J. M.; Stoddart, J. F. Heterogeneous Catalysis of a Copper-Coated Atomic Force Microscopy Tip for Direct-Write Click Chemistry. *J. Am. Chem. Soc.* **2009,** *131*, 6692-+.

18. Degenhart, G. H.; Dordi, B.; Schonherr, H.; Vancso, G. J. Micro- and Nanofabrication of Robust Reactive Arrays Based on the Covalent Coupling of Dendrimers to Activated Monolayers. *Langmuir* **2004,** *20*, 6216-6224.

19. Pena, D. J.; Raphael, M. P.; Byers, J. M. "Dip-Pen" Nanolithography in Registry with Photolithography for Biosensor Development. *Langmuir* **2003,** *19*, 9028-9032.

20. Chi, Y. S.; Choi, I. S. Dip-Pen Nanolithography Using the Amide-Coupling Reaction with Interchain Carboxylic Anhydride-Terminated Self-Assembled Monolayers. *Adv. Funct. Mater.* **2006,** *16*, 1031-1036.

21. Hsu, S. H.; Reinhoudt, D. N.; Huskens, J.; Velders, A. H. Imidazolide Monolayers for Reactive Microcontact Printing. *J. Mater. Chem.* **2008,** *18*, 4959-4963.

22. Kham, K.; Guerrouache, M.; Carbonnier, B.; Lazerges, M.; Perrot, H.; Millot, M. C. Suprarnolecular Interactions between Beta-Cyclodextrin and Hydrophobically End-Capped Poly(Ethylene Glycol)S: A Quartz Crystal Microbalance Study. *J. Colloid Interface Sci.* **2007,** *315*, 800-804.

23. Park, I. K.; Von Recum, H. A.; Jiang, S. Y.; Pun, S. H. Supramolecular Assembly of Cyclodextrin-Based Nanoparticles on Solid Surfaces for Gene Delivery. *Langmuir* **2006,** *22*, 8478-8484.

24. Huskens, J. Multivalent Interactions at Interfaces. *Curr. Opin. Chem. Biol.* **2006,** *10*, 537-543.

25. Mulder, A.; Onclin, S.; Peter, M.; Hoogenboom, J. P.; Beijleveld, H.; ter Maat, J.; Garcia-Parajo, M. F.; Ravoo, B. J.; Huskens, J.; van Hulst, N. F*., et al.* Molecular Printboards on Silicon Oxide: Lithographic Patterning of Cyclodextrin Monolayers with Multivalent, Fluorescent Guest Molecules. *Small* **2005,** *1*, 242-253.

26. Ludden, M. J. W.; Reinhoudt, D. N.; Huskens, J. Molecular Printboards: Versatile Platforms for the Creation and Positioning of Supramolecular Assemblies and Materials. *Chem. Soc. Rev.* **2006,** *35*, 1122-1134.

27. Nijhuis, C. A.; Yu, F.; Knoll, W.; Huskens, J.; Reinhoudt, D. N. Multivalent Dendrimers at Molecular Printboards: Influence of Dendrimer Structure on Binding Strength and Stoichiometry and Their Electrochemically Induced Desorption. *Langmuir* **2005,** *21*, 7866-7876.

28. Dorokhin, D.; Hsu, S. H.; Tomczak, N.; Reinhoudt, D. N.; Huskens, J.; Velders, A. H.; Vancso, G. J. Fabrication and Luminescence of Designer Surface Patterns with Beta-Cyclodextrin Functionalized Quantum Dots Via Multivalent Supramolecular Coupling. *Acs Nano* **2010,** *4*, 137-142.

29. Maury, P.; Peter, M.; Crespo-Biel, O.; Ling, X. Y.; Reinhoudt, D. N.; Huskens, J. Patterning the Molecular Printboard: Patterning Cyclodextrin Monolayers on Silicon Oxide Using Nanoimprint Lithography and Its Application in 3d Multilayer Nanostructuring. *Nanotechnology* **2007,** *18*, -.

30. Onclin, S.; Mulder, A.; Huskens, J.; Ravoo, B. J.; Reinhoudt, D. N. Molecular Printboards: Monolayers of Beta-Cyclodextrins on Silicon Oxide Surfaces. *Langmuir* **2004,** *20*, 5460-5466.

Chapter 6

Porous Multilayer-coated AFM Tips for Dip-Pen Nanolithography of Proteins[*]

Abstract

A simple and novel method was developed for fabricating porous multilayer-coated silicon nitride tips for dip-pen nanolithography (DPN) by using Layer-by-Layer (LbL) technique. The pore sizes can be adjusted by treating the poly4-(vinylpyridine)/ poly(acrylic acid) (P4VP/PAA) films coated onto amino-terminated monolayer (NH_2-monolayer)-functionalized AFM tip surfaces with a base solution for different periods of time. This hydrophilic porous material can easily absorb biomolecules, and provides a larger volume ink reservoir compared to a bare silicon nitride tip. Proof-of-concept of the porous AFM tip is demonstrated by using fluorescent proteins as ink molecules to fabricate protein patterns at micrometer and sub-micrometer length scale.

6.1 Introduction

It has been pointed out in Chapter 2 that generally two strategies can be discerned to pattern biomolecules with the DPN technique, namely an indirect method and a direct method.[1] In the indirect method first a suitable molecular functionality at a surface is prepared by DPN, which is followed by the immobilization of proteins from a solution. One great advantage of this indirect method is avoiding the denaturation of fragile biomolecules while directly writing.[2] One indirect approach has been described in Chapter 4 by fabricating nickel ions patterns to immobilize proteins. A disadvantage of the indirect approach is its relatively low efficiency because one or more chemical reaction steps have to be carried out before immobilizing biomolecules.

For efficient patterning, especially for non-fragile biomolecules, directly depositing from the ink-coated tip onto a surface is simpler and more straightforward. Unlike writing small organic or inorganic molecules, transferring high molecular weight molecules, *e.g.* biomolecules, onto solid surfaces is much more challenging because of the slow diffusion rate, the limited amount of ink, and the difficulty of maintaining functional biological properties of molecules.[3] Several modifications of tip surfaces[2-4] have been reported in order to overcome these restrictions. For instance, Lee *et al.* modified the tip surface with a PEG monolayer in order to facilitate the diffusion process from the tip to the substrate.[2] Choi *et al.* utilized the polymerization method to grow a thin porous film on the tip surface and create a sponge-like tip.[3] More recently, Senesi *et al.* utilized the porous property of agarose to encapsulate biomolecules for performing DPN experiments.[5]

In this chapter, a new and simple approach is presented, using Layer-by-Layer (LbL) self-assembly of poly4-(vinylpyridine)/poly(acrylic acid) (P4VP/PAA), to form hydrophilic porous structures on the surface of Si_3N_4 AFM tips. This porous thin film coated on an AFM tip can act as an ink reservoir with increased volume. LbL self-assembly has increasingly attracted attention due to its simplicity, versatility, and systematic control over the thickness and underlying structure of the resulting layer.[6-8] By immersing the LbL multilayer in solutions with different pH or ionic strengths, porous structures at micrometer and nanometer length scales have been formed attributing to the re-conformation or aggregation of remained polymer on the surface.[9, 10] An attractive feature of this method is that the pore size and the thickness of the porous films can be tuned by altering parameters such as polymer concentrations, pH value of the alkaline solutions, and duration of base treatment. Such porous structures have also been applied onto poly(dimethylsiloxane) (PDMS) stamps to function as a reservoir for multiple

microcontact printing (μCP) of immunoglobulin G (IgG) onto a amino-terminated monolayer-functionalized glass substrate.[11]

6.2 Results and Discussion

6.2.1 Fabrication and characterization of porous multilayer-coated AFM tip

LbL films are generally constructed *via* electrostatic interactions[7, 8, 12, 13] between two kinds of polymers. Other interactions, *e.g.* covalent bonding,[14] hydrogen bonding,[15-18] and specific molecular recognition[19] have also been utilized as the driving force for LbL assembly. The preparation of porous multilayer-coated AFM tips in principle followed the procedure published by Fu *et al.*, and is shown in Scheme 6.1.[9] To affix the polymer on the cantilever surface, a cleaned bare Si_3N_4 cantilever was first functionalized with an amino-terminated self-assembled monolayer by gas-phase deposition of *N*-[3-(trimethoxysilyl)propyl]-ethylenediamine (TPEDA monolayer). This TPEDA monolayer allows the interaction with the polymer via hydrogen bonding. The TPEDA monolayer-functionalized AFM cantilevers were alternately incubated in poly (4-vinylpyridine) (P4VP) and poly(acrylic acid) (PAA) methanol solutions for assembling LbL15 films based on hydrogen bonding between the pyridine and carboxylic acid groups (15 denotes the number of P4VP/PAA bilayers). These LbL15-functionalized cantilevers were subsequently immersed into a 0.1 N of KOH solution for 5, 10 or 15 minutes to dissolve the PAA in the multilayer. This dissolution phenomenon of PAA in alkaline solution has been reported previously showing the release of PAA did not remove whole multi-layers away from the tip surface. Due to the poor solubility of P4VP in the alkaline solution, the remaining P4VP led to the formation of porous structures on the cantilever surfaces.[9, 20]
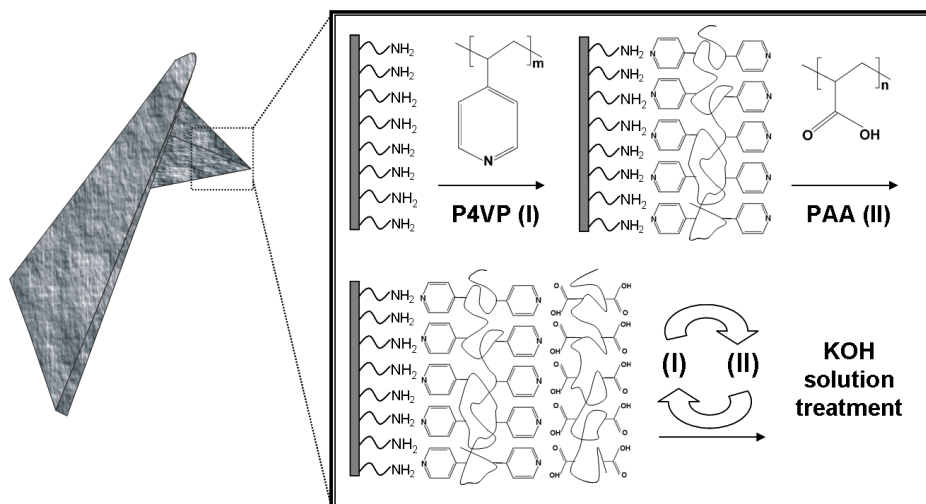
Scheme 6.1. *Preparation procedure of a porous LbL AFM tip.*

The porous LbL15 tips were characterized by scanning electron microscopy (SEM) and atomic force microscopy (AFM). (Figure 6.1a) The SEM images of the porous LbL15 tips, fabricated by varying the duration of the treatment in KOH solution, are shown in Figure 6.1c-e. The corresponding supporting chip areas of the cantilevers used for DPN were examined by AFM in tapping mode, and are shown in Figure 6.1f-h. Larger pore sizes and more apparent porous network structures were obtained upon longer treatment with alkaline solution. The pore sizes ranged from ~ 50 nm to a few hundreds of nm as determined by AFM. The thickness of the porous film is between 20 and 30 nm. The SEM images also show that the LbL structures make the tip blunter than the Si_3N_4 tip functionalized with TPEDA monolayer (Figure 6.1b). Nevertheless, the radius of the porous tip is ~ 100 nm which is still considered within the acceptable length scale for performing DPN experiments.
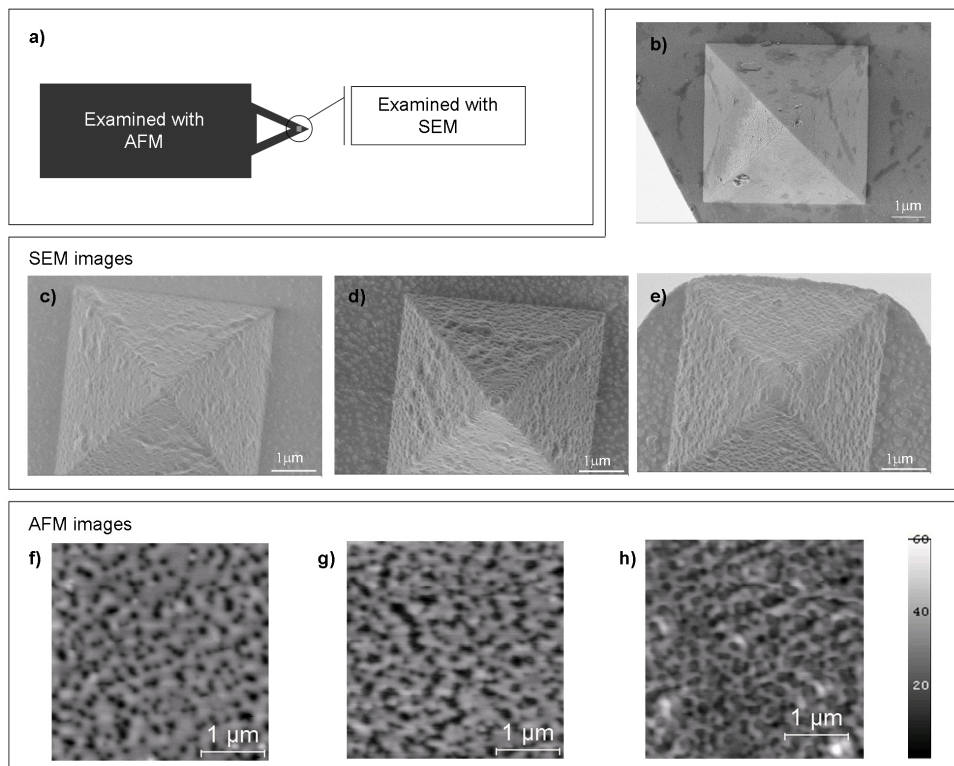
Figure 6.1. *(a) Schematic illustration the position of the cantilever examined with SEM and AFM, respectively. (b) SEM image of a Si₃N₄ AFM tip functionalized with TPEDA monolayer. (c), (d) and (e) SEM images of LbL15-functionalized tips treated with KOH solution for 5, 10 and 15 minutes, respectively. (f), (g) and (h) tapping mode AFM height images of the porous cantilever treated with KOH solution for 5, 10 and 15 minutes, respectively.*

To prove that the prepared porous tip could encapsulate more biomolecular ink than a bare tip, a bare Si_3N_4 AFM tip and a porous LbL15 tip were inked with a small drop of His-tagged tetrameric reef coral fluorescent protein (His-DsRed) solution (2 μM) placed onto an octadecyltrichlorosilane (OTS monolayer)-functionalized glass slide for ~ 10 minutes. The OTS monolayer is hydrophobic and therefore it avoids the spreading of the protein solution. After inking, the tips were blown dry with N_2 and were imaged with fluorescence microscopy (Figure 6.2). It can be seen that the fluorescence intensity of the

porous LbL15 tip is significantly higher than that of the bare tip. This result proves that more fluorescent proteins are encapsulated into the porous tip, which effectively acts as a sponge.
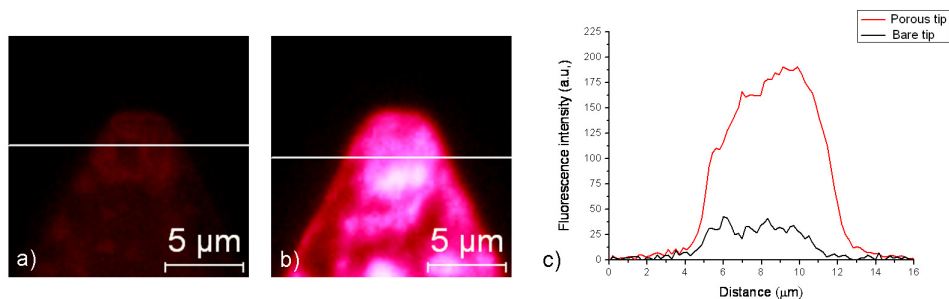

Figure 6.2. *Fluorescence images of (a) a bare AFM tip and (b) a porous LbL15 tip, dipped into His-Ds Red solution (2 μM) for 10 minutes and then dried with N$_2$. The exposure time of both images is 100 ms. (c) The intensity profiles of the line shown in (a) and (b).*

6.2.2 Fabrication of protein patterns with multilayer-coated AFM tip

Porous LbL tips were examined for their potential application in transferring biomolecules *via* DPN. Proof-of concept experiments were performed by generating His-tagged visible fluorescent protein (VFP) patterns on TPEDA monolayer- or nickel(II)-nitrilotriacetic acid-terminated (Ni-NTA) monolayer-functionalized glass substrates through electrostatic interactions or the formation of metal ion-imidazole bonds, respectively. Two proteins with different molecular weights, His-tagged enhanced green fluorescent protein (His-EGFP, ~ 27 kDa) and His-tagged tetrameric reef coral fluorescent protein (His-DsRed, ~ 100 kDa), were used. The intrinsic fluorescence of the VFPs is an indicator of structural and functional integrity, since structurally damaged or misfolded proteins do not fluoresce.

In the procedure of inking metal ions, *i.e.* Ca(II) and Ni(II), as described in Chapter 3 and Chapter 4 respectively, the commercial Si$_3$N$_4$ AFM tips were fully incubated into metal ion solutions for coating. Since proteins are much bigger molecules compared to metal ions, the inking procedure was modified, in order to avoid the proteins adhering to

the backside of the cantilever. This adsorption may obstruct the detection of the laser deflection signal and affect performing further DPN experiments. Scheme 6.2 exhibits how a porous LbL15 tip inked with proteins. A small drop of protein solution (~ 2 μl) was placed onto the OTS monolayer-functionalized glass substrate right above an objective lens. To prevent the ink solution from drying during the inking process, a thin layer of wet tissue paper was placed surrounding the protein drop. Subsequently, a porous LbL15 tip mounted on the AFM head was very gently brought to touch the protein drop for ~ 10 minutes and then carefully dried with N_2.
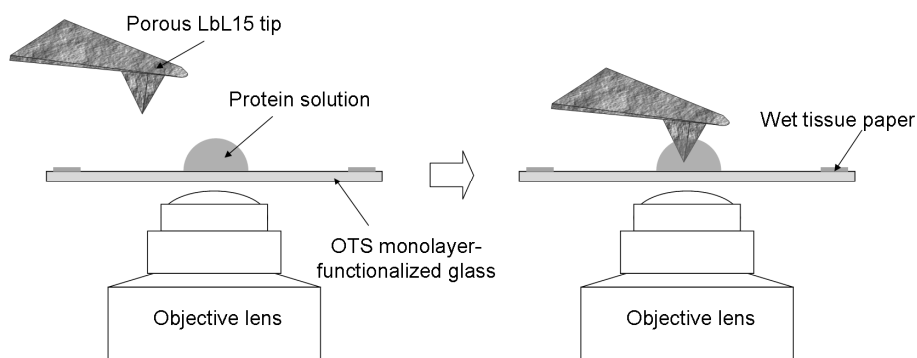
Scheme 6.2. *Illustration of the procedure of inking proteins with a porous LbL15 tip. The schematic is not to scale.*

6.2.2.1 His-EGFP patterns

A His-EGFP-impregnated porous tip was brought into contact with a TPEDA monolayer-functionalized surface to write a 25 μm wide square in one move with an atomic force fluorescence microscope (AFFM)[21] at ~ 60% relative humidity (RH) with a writing speed of 25 μm/s. The resulting fluorescent pattern was immediately imaged in situ by the AFFM. Without a re-inking process, the same His-EGFP square pattern was generated more than 20 times, as shown in Figure 6.3. This series of results again successfully demonstrates that the porous LbL tip acts as a sponge-like reservoir for encapsulating large amounts of aqueous protein solution, maintaining the protein functionality and enabling ink release during the short tip-surface contact period. It can

also be observed that the protein lines became narrower while proceeding with the DPN experiments. This phenomenon indicates that there was a depletion of ink molecules from the tip as the DPN experiments progressed.
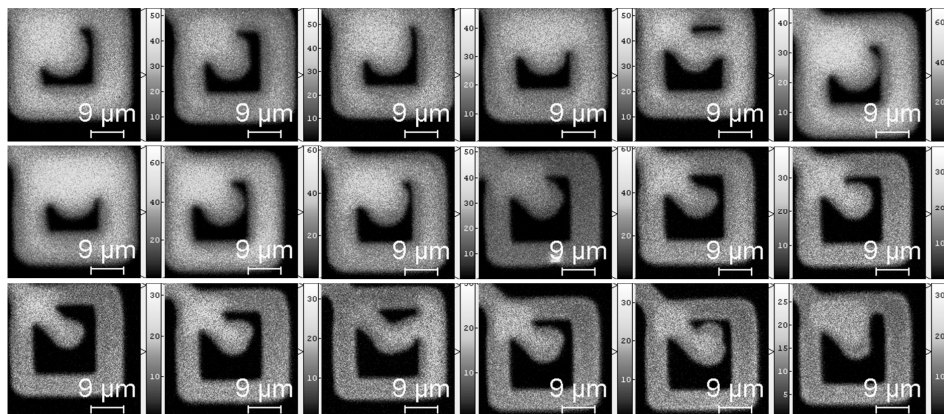

Figure 6.3. *Fluorescence images of His-EGFP square patterns that were generated successively on TPEDA monolayer from left to right and from top to bottom (zigzag). The scale of the color bar for the different images is not uniform.*

6.2.2.2 His-DsRed patterns

To further demonstrate the general applicability of the porous LbL15 tips, His-DsRed, another type of protein with 4 times higher molecular weight than His-EGFP, was also used to create patterns on the Ni-NTA monolayer-functionalized glass substrates. In order to obtain the protein patterns at sub-micron scale, a series of writing experiments at different RH was performed since RH has been reported as one of the important factors in determining the resolution in DPN experiments.[22] A His-DsRed-impregnated porous tip was first brought into contact with a Ni-NTA monolayer-functionalized surface to generate a pattern at ~ 60% RH. Immediately after writing, a fluorescent pattern at micron scale was observed and is shown in Figure 6.4a. The same tip, without re-inking, was subsequently used to generate some dot and line patterns at ~ 30% RH. Figure 6.4b and 6.4c demonstrate that fluorescent patterns at sub-micron scale were successfully obtained. The fluorescence intensity shown in Figure 6.4b is lower than that shown in Figure 6.4a, indicating that less amount of proteins were deposited on the surface. To confirm that the

protein patterns fabricated at sub-micron scale were due to the decrease of RH instead of the depletion of ink molecules, the same tip without re-inking was used again to generate patterns at ~ 45% RH. In Figure 6.4d, fluorescent features at micron scale were observed again. This process can be repeated as shown in Figure 6.4e and 6.4f proving that controlling RH is a significant issue for obtaining protein patterns at the desired length scale. Since our interest is to generate features at sub-micron scale in order to obtain high-density protein patterns, lower RH was applied for the DPN experiments.
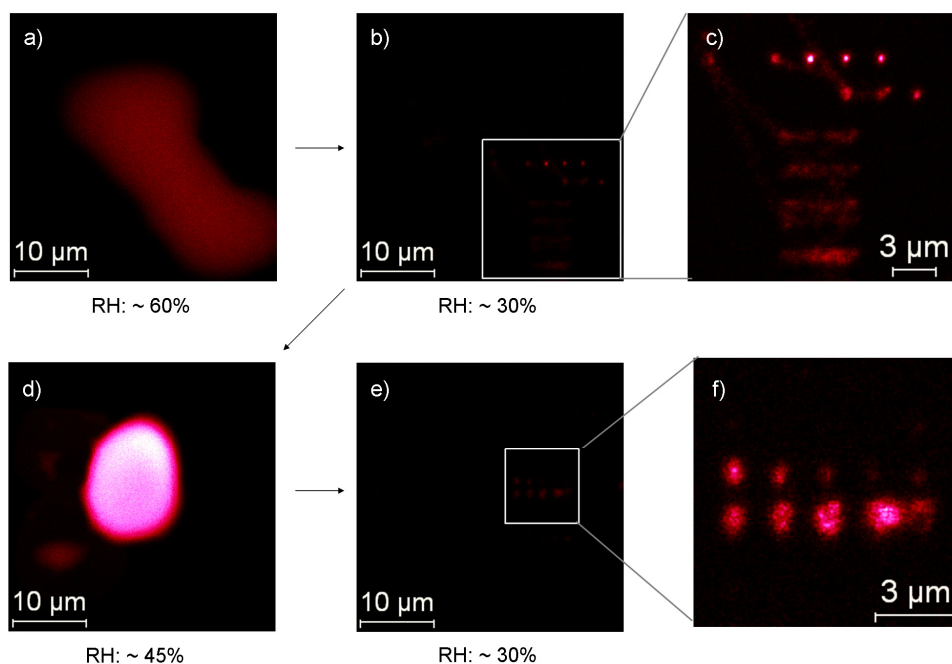

Figure 6.4. *(a), (b), (d) and (e) Fluorescence images of His-DsRed patterns which were generated successively without reinking the tip on Ni-NTA monolayer-functionalized substrates at varied relative humidity. The color scale of (a), (b), (d)and (e) is the same. (c) and (f) are the zoom-in fluorescence image of the white square indicated in (b) and (e), respectively.*

   A porous tip impregnated with His-DsRed was brought into contact with the surface for a given contact time of 10 seconds at ~ 35 % RH. The inked porous tip was used to successively generate 42 spots and was retracted after depositing each dot. No re-inking process occurred during the entire writing sequence. Tapping mode AFM revealed further topographical information about the protein patterns. The fluorescence and topographical information about the protein dot patterns are shown in Figure 6.5a and 6.5b respectively. To avoid contamination, a new Si_3N_4 AFM tip was used for imaging. Despite repeated writing, it was observed that the fluorescence intensity does not decrease gradually, suggesting that the ink flows from the distal end to the tip. Figure 6.5c and 6.5d showed that the diameters of His-DsRed arrays were between 200 nm and 300 nm and did not vary much. The height data suggest that multilayers of proteins were deposited on the surface. Another porous tip impregnated with His-DsRed was utilized to generate two continuous line patterns at ~ 35% RH with a writing speed of 5 μm/s. The resulting fluorescent pattern is shown in Figure 6.6 and also shows that the fluorescence intensity did not decrease gradually despite writing continuously, consistent with the data in Figure 6.5a.
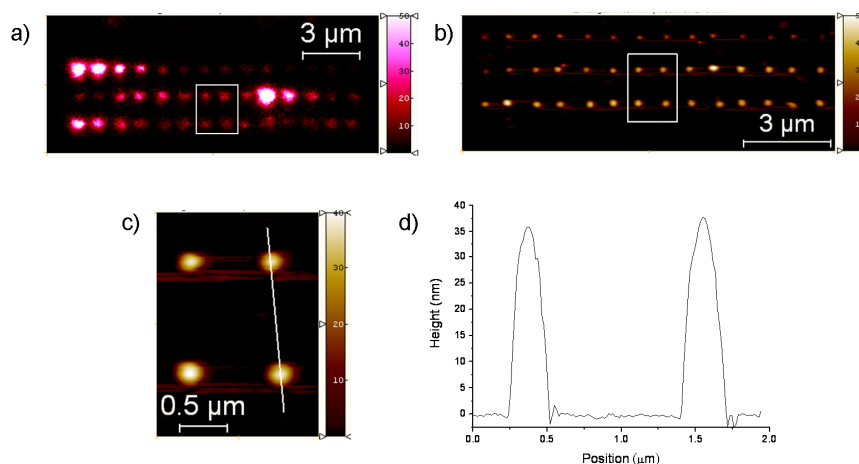

Figure 6.5. *(a) Fluorescence images of His-DsRed square patterns acquired immediately after DPN with a porous LbL15 tip. The dot patterns were successively generated from left to right and from top to bottom (zigzag). (b) AFM tapping mode image in height of His-DsRed dot patterns shown in (a). (c) Zoom-in image of the indicated area shown in (b). (d) Topography information in height of the line indicated in (c).*
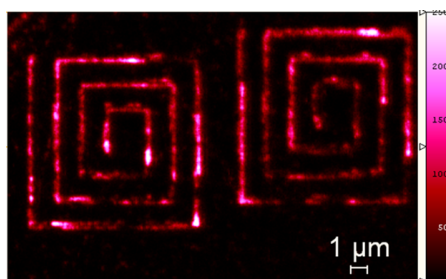
Figure 6.6. *Fluorescence images of His-DsRed continuous line patterns acquired immediately after DPN with a porous LbL15 tip. The lines were written counterclockwise from outside to inside and the left pattern was created first.*

6.2.3 Examining the co-deposition of the porous material

A potential risk was that the porous material coated on an AFM tip might be simultaneously deposited onto the substrate while performing DPN experiments. Therefore, a porous LbL15 tip before use and after writing with His-DsRed and subsequent rinsing with MilliQ water were examined by SEM, shown in Figure 6.7a and 6.7b, respectively. Although the tip was rinsed with MilliQ water, it was very difficult to remove all the remaining His-DsRed and a coating layer (remaining proteins and porous structures) was observed in Figure 6.7b. It can be seen that there was no apparent polymer release from the tip surface after writing. From Figure 6.7, we cannot conclusively exclude this possibility of co-deposition during the DPN experiments and therefore another experiment was performed for a further check.
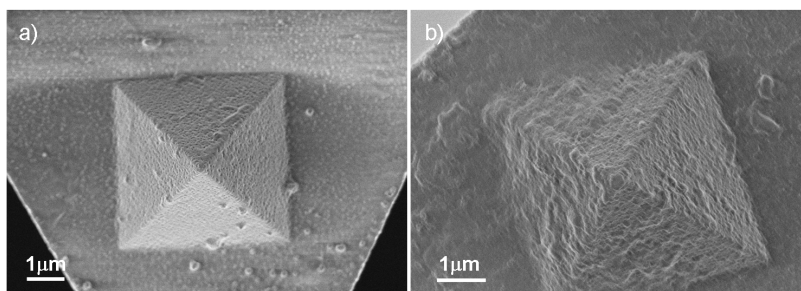

Figure 6.7. *SEM images of an LbL15-functionalized porous tip, (a) before and (b) after writing His-DsRed.*

A cleaned glass substrate was first imaged in contact mode AFM, shown in Figure 6.8a, before performing DPN experiments. A porous LbL15 tip was incubated into MilliQ water for ~ 10 minutes and then blow-dried for writing. Subsequently, several line and dot patterns with varied writing speeds and tip-surface contact time were generated onto the cleaned glass substrate with the porous tip inked with MilliQ water. After writing, a new Si_3N_4 AFM tip was used to image the written area shown in Figure 6.8b. There were no obvious features exhibited in Figure 6.8b, indicating the co-deposition of the porous material can be ignored.
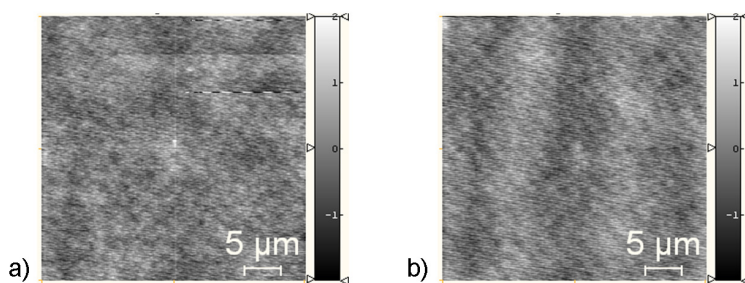

Figure 6.8. AFM contact mode image in height of a cleaned glass substrate (a) before and (b) after writing with a porous LbL15 tip inked with MilliQ water.

6.3 Conclusions

In summary, a simple method for fabricating surface-modified nanoporous AFM tips using the LbL technique has been presented in this chapter. The pore sizes of the porous film can easily be adjusted by varying the incubation time of the LbL15 tips in alkaline solution. We have successfully demonstrated that aqueous fluorescent protein solutions can easily be absorbed into the porous LbL tip while retaining the biological activity of the proteins for extended periods. Furthermore, the pore structures provide a large-volume ink reservoir for DPN experiments. His-EGFP and His-DsRed patterns at micrometer and submicrometer scales were successfully fabricated with the LbL15 porous tips. Different parameters, e.g. the molecular weight of P4VP and the number of bilayers, for tuning the pore sizes and properties will be described in more detail in Chapter 7.

6.4 Experimental

General procedures.

All glassware used to prepare the monolayers was cleaned by sonicating for 60 minutes in a 2% v/v Hellmanex II solution in Milli-Q water, and then rinsed thoroughly with MilliQ water, and dried in an ambient environment. Microscope glass slide substrates and Si_3N_4 AFM cantilevers (NP, Veeco) were cleaned in piranha solution for 20 minutes and 1 minute, respectively, (concentrated H_2SO_4 and 33% aqueous H_2O_2 in a 3:1 ratio). [**Warning:** Piranha solution should be handled with caution: it has been reported to detonate unexpectedly.] The glass slides and cantilevers were then rinsed several times with Milli-Q water, and dried gently under a nitrogen stream before forming the monolayer.

Monolayers preparation.

Preparation of the amino terminated monolayer (TPEDA). The preparation of cleaned microscope glass slide substrates and Si_3N_4 AFM cantilevers were placed in a desiccator under vacuum overnight for the gas-phase evaporation of *N*-[3-(trimethoxysilyl)propyl]ethylenediamine to form amino-terminated monolayer (TPEDA monolayer). After the TPEDA monolayer-functionalized substrates and cantilevers were taken out from the desiccator, they were rinsed carefully with ethanol and dichloromethane to remove physisorbed materials and then dried under a stream of N_2. In order to obtain more stable TPEDA monolayer, the cantilevers and substrates were placed in an oven at 60 °C for 1 hour before performing experiments.

Preparation of OTS monolayer.[23] Cleaned microscope glass slide substrates immersed in a distilled toluene solution of 1 mM octadecyltrichlorosilane (OTS) for 1 hour. After the substrates were taken from the solution, they were rinsed carefully to remove excess physisorbed materials and then dried under a stream of N_2.

Preparation of the Ni-NTA monolayer.[24] The glass substrates functionalized with Ni-NTA monolayers were prepared by following the procedures described in Chapter 4.

Fabrication of multilayer-coated porous tip.[9]

Poly(acrylic acid) 50 wt% solution in water MW 5000 was first freeze dried to obtain pure poly(acrylic acid) (PAA). Poly (4-vinylpyridine) (P4VP), MW 50000 and PAA were dissolved in methanol individually to obtain 1 mg/ml P4VP and PAA methanol solution. The TPEDA monolayer-functionalized AFM cantilevers were first incubated into P4VP solution for 10 minutes and then rinsed several times with methanol before incubating into PAA solution for 10 minutes. This process was repeated for 15 times to obtained Layer-by-Layer (LbL)-functionalized cantilevers. The LbL-functionalized cantilevers were subsequently immersed into KOH solution of 0.1 N for varied periods of time to obtain porous structure coated cantilevers with different sizes of pores. The porous cantilevers were rinsed with Milli-Q water and then dried very gently under a stream of N_2.

Analysis of porous structures.

The surface structures of porous cantilevers were characterized by a scanning electron microscope (SEM) (Zeiss) and a custom-built atomic force microscope (AFM) in tapping mode equipped with a Si_3N_4 AFM cantilever (MSCT, Veeco) with a nominal spring constant of 0.54 N/m.

Acquisition of fluorescent images.

The porous LbL15 tip and the bare Si_3N_4 tip inked with His-DsRed were placed onto a cleaned glass substrate and then examined with a fluorescence microscope (TE2000-U, Nikon) equipped with a mercury lamp as light source and a digital camera (Nikon digital Sight DS-Qi1Mc). To obtain fluorescence images of proteins adhered to tip surfaces, the filter cube with green excitation light (λ=510/40 nm), red emission light (λ=617/73 nm) and dichroic (λ=562 nm) was used. The obtained fluorescence images were analyzed with the commercial software SPIP (Image Metrology, Version 4.4.3.0).

Dip pen nanolithography with multilayer-coated porous tips and visualization with AFFM.

For DPN experiments, the porous LbL tips treated with alkaline solution for 15 minutes were used. Immediately before a DPN experiment, ~ 3 μl of 10 mM Tris-HCl buffer (pH 7.5) containing 5 μM His-EGFP or 2 μM His-DsRed was placed onto OTS monolayer-functionalized glass slide. The porous cantilever mounted on the AFM head was very carefully brought to immerse into the drop of fluorescent proteins ~10 minutes and then dried very gently under a stream of N_2. All DPN experiments were operated inside a custom-built chamber with a controlled humidity system at a temperature between 20 and 22 °C. After creating His-EGFP or His-DsRed patterns on the surface, the fluorescent images of deposited fluorescent proteins were obtained by exciting molecules with 488 nm line of an Argon-ion laser (163-D Laser System, Spectra Physics) and recording the emission of the fluorescence by an avalanche photodiode (APD) (SPCM-AQR-14, Perkin Elmer Optoelectronics). To obtain AFM topography information of the protein patterns, tapping mode was used. The original ink-coated porous tip was replaced by a new Si_3N_4 AFM tip (MSCT, Veeco) with a nominal spring constant of 0.54 N/m to prevent contamination of the patterned areas during subsequent imaging.. Fluorescence and topographic images were analyzed and prepared with the commercial software SPIP (Image Metrology, Version 4.4.3.0).

6.5 Acknowledgements

6.6 References

1. Christman, K. L.; Enriquez-Rios, V. D.; Maynard, H. D. Nanopatterning Proteins and Peptides. *Soft Matter* **2006,** *2*, 928-939.

2. Lee, K. B.; Lim, J. H.; Mirkin, C. A. Protein Nanostructures Formed Via Direct-Write Dip-Pen Nanolithography. *J. Am. Chem. Soc.* **2003,** *125*, 5588-5589.

3. Choi, D. S.; Yun, S. H.; An, Y. C.; Lee, M. J.; Kang, D. G.; Chang, S. I.; Kim, H. K.; Kim, K. M.; Lim, J. H. Nanopatterning Proteins with a Stamp Tip for Dip-Pen Nanolithography. *Biochip J.* **2007,** *1*, 200-203.

4. Lim, J. H.; Ginger, D. S.; Lee, K. B.; Heo, J.; Nam, J. M.; Mirkin, C. A. Direct-Write Dip-Pen Nanolithography of Proteins on Modified Silicon Oxide Surfaces. *Angew. Chem., Int. Ed.* **2003,** *42*, 2309-2312.

5. Senesi, A. J.; Rozkiewicz, D. I.; Reinhoudt, D. N.; Mirkin, C. A. Agarose-Assisted Dip-Pen Nanolithography of Oligonucleotides and Proteins. *Acs Nano* **2009,** *3*, 2394-2402.

6. Decher, G. Fuzzy Nanoassemblies: Toward Layered Polymeric Multicomposites. *Science* **1997,** *277*, 1232-1237.

7. Decher, G.; Hong, J. D.; Schmitt, J. Buildup of Ultrathin Multilayer Films by a Self-Assembly Process.3. Consecutively Alternating Adsorption of Anionic and Cationic Polyelectrolytes on Charged Surfaces. *Thin Solid Films* **1992,** *210*, 831-835.

8. Decher, G.; Hong, J. D. Buildup of Ultrathin Multilayer Films by a Self-Assembly Process.2. Consecutive Adsorption of Anionic and Cationic Bipolar Amphiphiles and Polyelectrolytes on Charged Surfaces. *PCCP* **1991,** *95*, 1430-1434.

9. Fu, Y.; Bai, S. L.; Cui, S. X.; Qiu, D. L.; Wang, Z. Q.; Zhang, X. Hydrogen-Bonding-Directed Layer-by-Layer Multilayer Assembly: Reconformation Yielding Microporous Films. *Macromolecules* **2002,** *35*, 9451-9458.

10. Kim, B. Y.; Bruening, M. L. Ph-Dependent Growth and Morphology of Multilayer Dendrimer/Poly(Acrylic Acid) Films. *Langmuir* **2003,** *19*, 94-99.

11. Xu, H. P.; Gomez-Casado, A.; Liu, Z. H.; Reinhoudt, D. N.; Lammertink, R. G. H.; Huskens, J. Porous Multilayer-Coated Pdms Stamps for Protein Printing. *Langmuir* **2009,** *25*, 13972-13977.

12. Decher, G.; Hong, J. D. Buildup of Ultrathin Multilayer Films by a Self-Assembly Process.1. Consecutive Adsorption of Anionic and Cationic Bipolar Amphiphiles on Charged Surfaces. *Makromolekulare Chemie-Macromolecular Symposia* **1991,** *46*, 321-327.

13. Ariga, K.; Hill, J. P.; Ji, Q. M. Layer-by-Layer Assembly as a Versatile Bottom-up Nanofabrication Technique for Exploratory Research and Realistic Application. *PCCP* **2007,** *9*, 2319-2340.

14. Fang, M. M.; Kaschak, D. M.; Sutorik, A. C.; Mallouk, T. E. A "Mix and Match" Ionic-Covalent Strategy for Self-Assembly of Inorganic Multilayer Films. *J. Am. Chem. Soc.* **1997,** *119*, 12184-12191.

15. Stockton, W. B.; Rubner, M. F. Molecular-Level Processing of Conjugated Polymers.4. Layer-by-Layer Manipulation of Polyaniline Via Hydrogen-Bonding Interactions. *Macromolecules* **1997,** *30*, 2717-2725.

16. Kharlampieva, E.; Kozlovskaya, V.; Sukhishvili, S. A. Layer-by-Layer Hydrogen-Bonded Polymer Films: From Fundamentals to Applications. *Adv. Mater.* **2009,** *21*, 3053-3065.

17. Wang, L. Y.; Fu, Y.; Wang, Z. Q.; Fan, Y. G.; Zhang, X. Investigation into an Alternating Multilayer Film of Poly(4-Vinylpyridine) and Poly(Acrylic Acid) Based on Hydrogen Bonding. *Langmuir* **1999,** *15*, 1360-1363.

18. Wang, L. Y.; Wang, Z. Q.; Zhang, X.; Shen, J. C.; Chi, L. F.; Fuchs, H. A New Approach for the

Fabrication of an Alternating Multilayer Film of Poly(4-Vinylpyridine) and Poly(Acrylic Acid) Based on Hydrogen Bonding. *Macromol. Rapid Commun.* **1997,** *18*, 509-514.

19. Spaeth, K.; Brecht, A.; Gauglitz, G. Studies on the Biotin-Avidin Multilayer Adsorption by Spectroscopic Ellipsometry. *J. Colloid Interface Sci.* **1997,** *196*, 128-135.

20. Xu, H.; Gomez-Casado, A.; Reinhoudt, D. N.; Lammertink, R. G. H.; Huskens, J., Porous Multilayer-Coated Pdms Stamps for Protein Printing. In *Langmuir*, 2009.

21. Kassies, R.; Van der Werf, K. O.; Lenferink, A.; Hunter, C. N.; Olsen, J. D.; Subramaniam, V.; Otto, C. Combined Afm and Confocal Fluorescence Microscope for Applications in Bio-Nanotechnology. *J. Microsc.* **2005,** *217*, 109-116.

22. Ginger, D. S.; Zhang, H.; Mirkin, C. A. The Evolution of Dip-Pen Nanolithography. *Angew. Chem., Int. Ed.* **2004,** *43*, 30-45.

23. Kulkarni, S. A.; Mirji, S. A.; Mandale, A. B.; Gupta, R. P.; Vijayamohanan, K. P. Growth Kinetics and Thermodynamic Stability of Octadecyltrichlorosilane Self-Assembled Monolayer on Si (100) Substrate. *Mater. Lett.* **2005,** *59*, 3890-3895.

24. Paik, H. J.; Kim, Y. R.; Orth, R. N.; Ober, C. K.; Coates, G. W.; Batt, C. A. End-Functionalization of Poly(3-Hydroxybutyrate) Via Genetic Engineering for Solid Surface Modification. *Chem. Commun.* **2005**, 1956-1958.

Chapter 7

Ink Loading of Porous Multilayer-coated AFM Tips[*]

Abstract

This chapter describes the investigation of the morphology variations of porous multilayers-coated silicon nitride AFM tips using the Layer-by-Layer (LbL) technique described in Chapter 6. The porous films were prepared by systematically varying different parameters, including the molecular weight of poly(4-vinylpyridine) (P4VP), the number of assembled layers, and the duration of KOH solution treatment. The morphology variations were characterized using scanning electron microscopy (SEM) and atomic force microscopy (AFM). The porous tips prepared under various conditions were inked with two kinds of fluorescent proteins, *i.e.* histidine-tagged enhanced green fluorescent protein (His-EGFP, ~ 27 kDa) and histidine-tagged tetrameric reef coral fluorescent protein (His-DsRed, ~ 100 kDa), to study the ink reservoir properties of the porous films. The different LbL conditions yielded tips with different ink loading capacities, which indicates tailoring these variable parameters can be of significant value in generating porous tips capable of performing long-term dip-pen nanolithography (DPN) writing.

---

[*]Manuscript in preparation.

7.1 Introduction

Chapter 6 described a simple approach using Layer-by-Layer (LbL) self-assembly techniques to alternately grow multiple poly(4-vinylpyridine) (P4VP) and poly(acrylic acid) (PAA) layers on silicon nitride AFM tip surfaces based on hydrogen bonding.[1-4] By immersing the LbL multilayer into alkaline solutions for different times, hydrophilic porous structures at micrometer and nanometer length scales were formed.[1, 5, 6] These porous thin films can act as a reservoir with increased volume for the ink molecules.[5] In addition to the duration of post-base treatment, many other factors that have an influence on the formation of porous structures such as pH values of alkaline solutions,[1] surface properties of substrates,[7] type of polymers,[8, 9] type and molecular weights of polymers[10] and the number of bilayers grown on tip surfaces[1] have been described. Bai *et al.* have demonstrated that the strong attractive interaction between P4VP and substrates has led to slower variation of microporous morphology.[7] Zhang *et al.* assembled PAA and poly(2-vinylpyridine) (P2VP) of different molecular weight onto amino-terminated monolayer-functionalized substrates followed by the post-base treatment and found that that the rate of micropore formation increases with increasing molecular weight of P2VP.[10] Upon comparing the assembly of P4VP and P2VP of almost the same molecular weight, micropore formation in P2VP/PAA was found to be faster than in P4VP/PAA.[10]

In Chapter 6, a comparison of the ink reservoir capacity of a bare silicon nitride tip and a LbL15 multilayer-coated AFM tip (15 denotes the number of P4VP/PAA bilayers) was presented. Here in this chapter, we first describe the characterization of porous tips prepared under different conditions while varying parameters including molecular weight of P4VP, number of P4VP/PAA bilayers and duration of KOH solution treatment. The porous cantilevers were all characterized by scanning electron microscopy (SEM) and atomic force microscopy (AFM). It is interesting to investigate how these parameters result in differences in the functionality of the porous structure as an ink reservoir. Tailoring these parameters enables one to select the best protocol to prepare porous tips for performing long-term dip-pen nanolithography (DPN) experiments. The results obtained may also be applied to porous multilayer-coated poly(dimethylsiloxane) (PDMS) stamps for multiple microcontact printing (μCP).[11] To study the ink reservoir properties of the porous films prepared under different conditions, two kinds of ink molecules, histidine-tagged enhanced green fluorescent protein (His-EGFP, ~ 27 kDa) and histidine-tagged tetrameric reef coral fluorescent protein (His-DsRed, ~ 100 kDa), were used.

7.2 Results and Discussion

7.2.1 Fabrication of porous multilayer-coated AFM tips

The procedure for preparing multilayer-coated porous AFM tips was in principle the same as that illustrated in Scheme 6.1. Briefly, amino-terminated monolayer (*N*-[3-(trimethoxysilyl) propyl]-ethylenediamine)-functionalized silicon nitride cantilevers were alternately incubated into P4VP (1 mg/ml) and PAA (1 mg/ml) methanol solutions to assemble LbL films. These LbL film-coated cantilevers were subsequently immersed into a KOH solution to form porous structures. Table 7.1 summarizes the different conditions that were applied to prepare a range of porous tips, including different molecular weight (MW) of P4VP (50,000 and 160,000 Da), number of bilayers (15 and 25) and duration of KOH (0.1 N) solution treatment (15, 30, 45 and 60 minutes).

Table 7.1. *Summary of porous tips prepared at different conditions. Three parameters were utilized to tune the variations of porous morphology, including molecular weight of P4VP, number of bilayers and duration of KOH solution treatment.*

	Molecular weight of P4VP	Number of bilayers	Duration of KOH (0.1 N) treatment
Porous tips	P4VP (50,000)	15	15 min
			30 min
			45 min
			60 min
		25	15 min
			30 min
			45 min
			60 min
	P4VP (160,000)	15	15 min
			30 min
			45 min
			60 min
		25	15 min
			30 min
			45 min
			60 min

In Chapter 6, the porous tips were prepared one by one, which is not an efficient procedure and which may result in differences of porous morphology between tips. To minimize any variations between individual porous tips, the preparation procedure was modified to ensure the tips were fabricated under the same conditions and that the tip surfaces were functionalized in a parallel fashion simultaneously. Instead of a single cantilever, an array of AFM cantilevers cut from a wafer (380 tips) of silicon nitride probes (Veeco, NP) was used. (Figure 7.1)
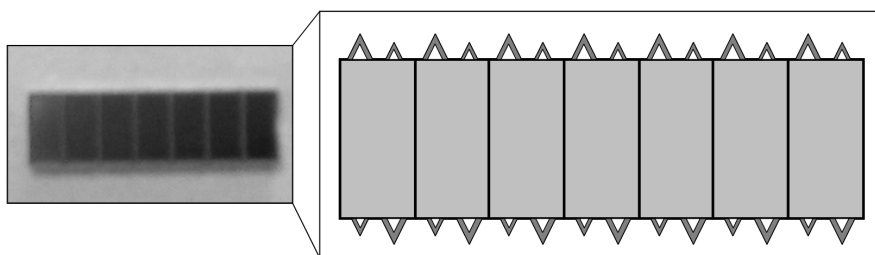
Figure 7.1. *Photograph and schematic illustration of an array of AFM Si$_3$N$_4$ cantilevers (Veeco, NP) used for preparing porous multilayer-coated tips.*

The morphological variations of the P4VP50000/PAA or P4VP160000/PAA (50000 and 160000 denote the molecular weight of P4VP) LbL films-coated AFM cantilevers upon immersion in the alkaline solution were examined using SEM and AFM. The SEM images of the porous tips fabricated under varied conditions are shown in Figure 7.2a-d. The corresponding supporting chip areas of the cantilevers were examined by AFM in contact mode, and are shown in Figure 7.3.
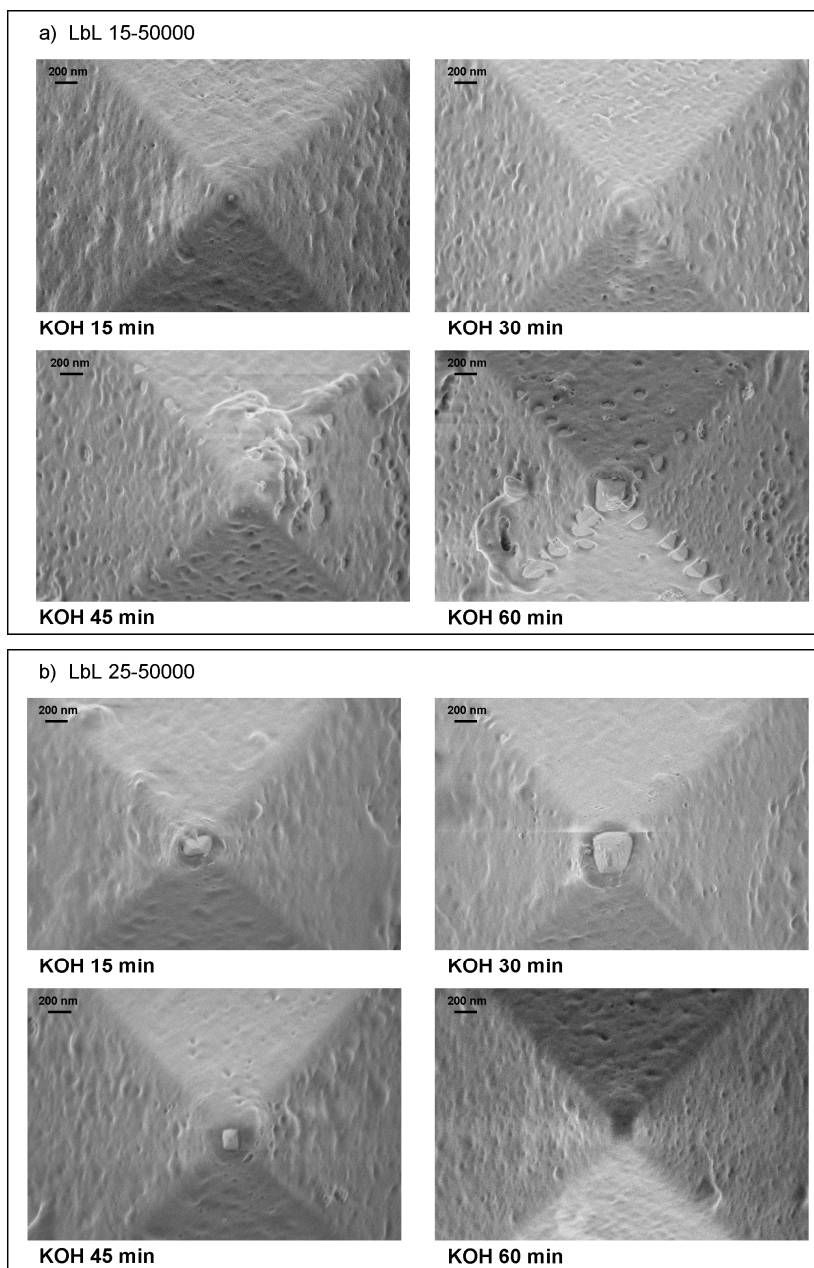
Figure 7.2. *SEM images of LbL multilayer-coated porous tips prepared under the conditions of (a) 15 bilayers of P4VP 50000/PAA, (b) 25 bilayers P4VP 50000/PAA, (c) 15 bilayers of P4VP 160000/PAA, (d) 25 bilayers P4VP 160000/PAA with four different durations of KOH solution (0.1N) treatment varying from 15 minutes to 60 minutes.*
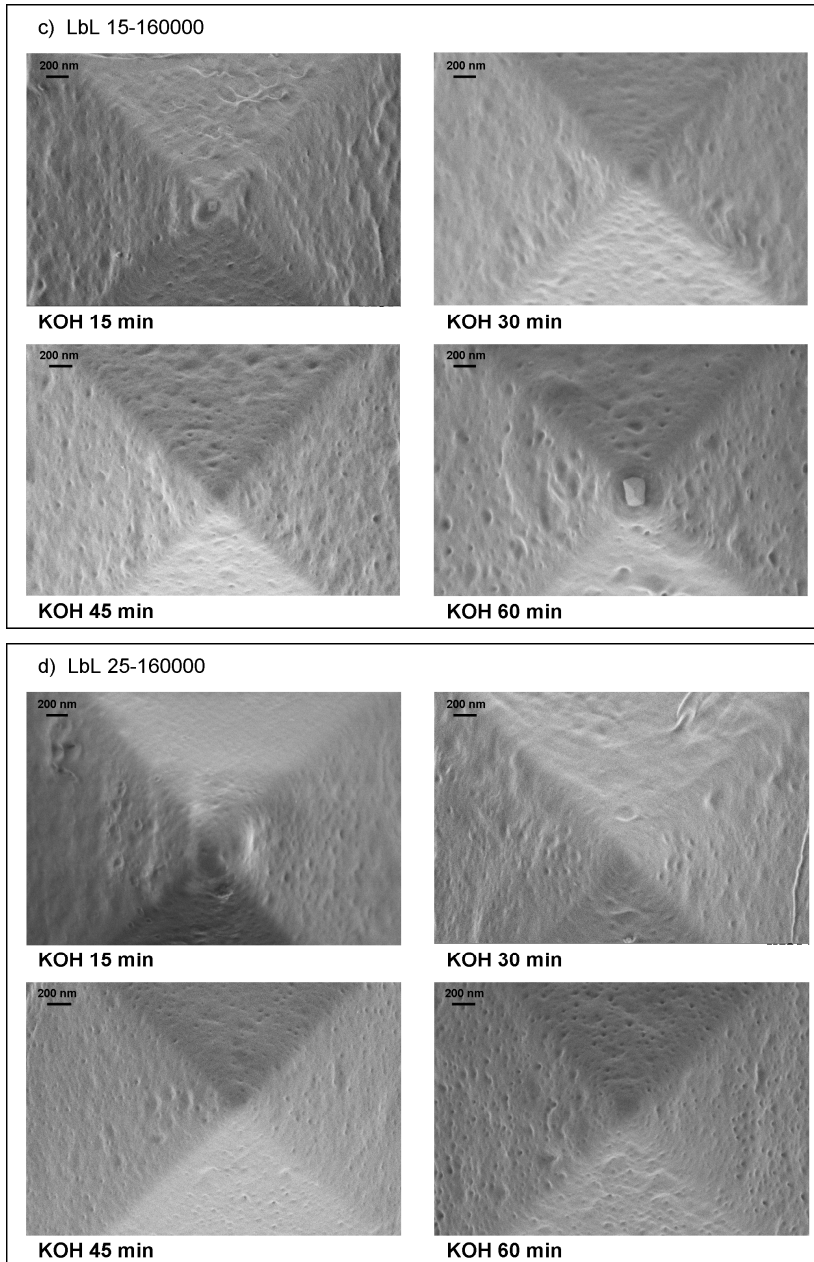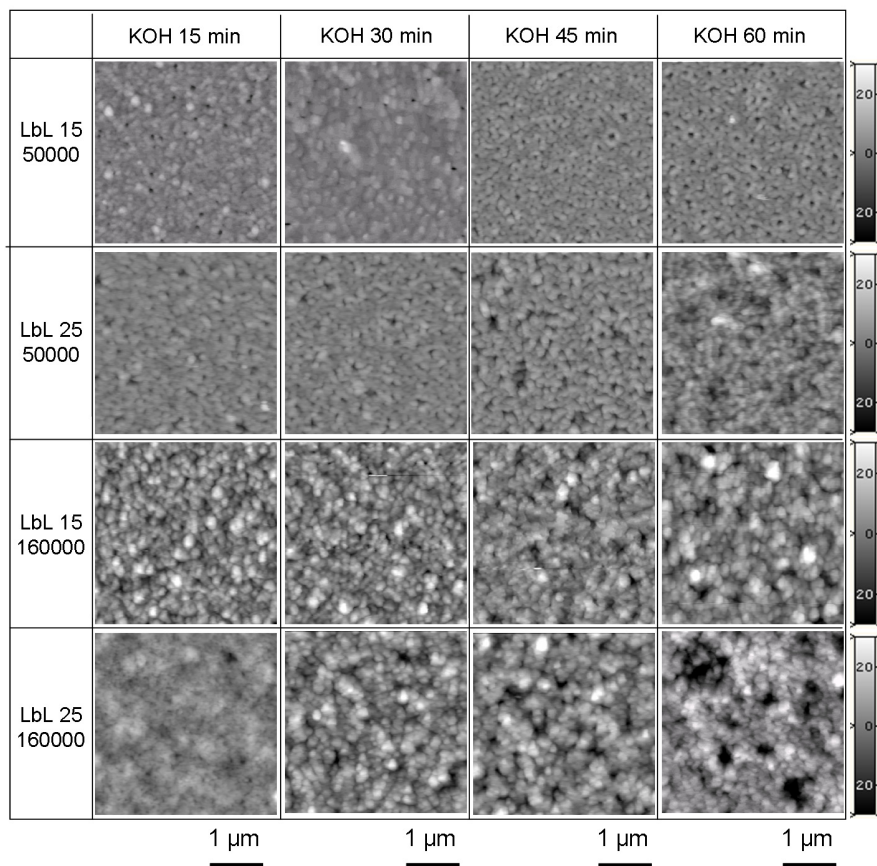
Figure 7.2. SEM images of LbL multilayer-coated porous tips prepared under the conditions of (a) 15 bilayers of P4VP 50000/PAA, (b) 25 bilayers P4VP 50000/PAA, (c) 15 bilayers of P4VP 160000/PAA, (d) 25 bilayers P4VP 160000/PAA with four different durations of KOH solution (0.1N) treatment varying from 15 minutes to 60 minutes.

Figure 7.3. *Contact mode AFM height images of the LbL-functionalized porous cantilever prepared under various conditions.*

The morphologies of the LbL multilayers prepared under different conditions are not the same, but the porous films homogeneously cover the tip and chip surfaces of the cantilevers as shown in Figures 7.2 and 7.3. From both SEM and AFM results, we concluded that the molecular weight of P4VP and the duration of post-base treatments are both important parameters in determining surface morphologies. Except for the porous films prepared with 25 bilayers P4VP 160000/PAA, there are no apparent changes of porous structures after 15 or 30 minutes treatment with KOH solution. The morphology of LbL multilayers is apparently rather insensitive to the duration of post-base treatment, which allows us to prepare porous tips with certain tolerance. Nevertheless, larger and

deeper holes were obtained by treating LbL multilayers with the base solution for longer times, which enables us to tune the pore sizes. Compared with SEM images, AFM images (Figure 7.3) exhibit more obvious differences between porous films using P4VP 50000 and P4VP 160000. By using P4VP with higher molecular weight, larger grainy structures of re-conformed P4VP are obtained. In contrast, smoother porous morphology can be obtained by using P4VP with lower molecular weight. All the prepared porous multilayer-coated silicon nitride tips described above were used to study the ink loading properties.

7.2.2 Ink loading study of porous multilayer-coated AFM tips

Histidine-tagged enhanced green fluorescent protein (His-EGFP, ~ 27 kDa) and histidine tagged-tetrameric reef coral fluorescent protein (His-DsRed, ~ 100 kDa) were used as ink molecules to study the ink reservoir properties of the porous multilayers. Tris-HCl buffer (10 mM, pH 7.5) containing 1 µM His-EGFP or His-DsRed solution was applied onto each multilayer-coated porous cantilever, as well as on a *N*-[3-(trimethoxysilyl)propyl]-ethylenediamine (TPEDA) monolayer-functionalized cantilever and a bare Si_3N_4 cantilever for 10 minutes. After the loading of ink, the drops of protein solution were removed with a pipette; the cantilevers were rinsed with few drops of Milli-Q water, and dried carefully under a stream of N_2 before imaging with a fluorescence microscope. The intrinsic fluorescence of the visible fluorescent proteins enables facile quantification of the amounts of fluorescent proteins encapsulated into the porous films by measuring the fluorescence intensities of the protein-infiltrated functionalized tips.

The exposure time for all the acquired fluorescence images of cantilevers inked with either His-EGFP or His-DsRed was fixed at 600 ms. In order to compare the ink reservoir properties of different porous films, the average fluorescence intensities over 10 different areas with a size of 90 x 90 pixels (15 x 15 µm^2) from each fluorescence image obtained were first corrected for the background signal and then averaged. Figures 7.4a and 7.5a are bar charts of the average fluorescence intensities for the His-EGFP and His-DsRed loaded porous multilayers-coated silicon nitride cantilevers prepared under different conditions respectively. One representative image of the ten fluorescence images of His-EGFP and His-DsRed acquired at each condition are shown in Figures 7.4b and 7.5b, respectively.
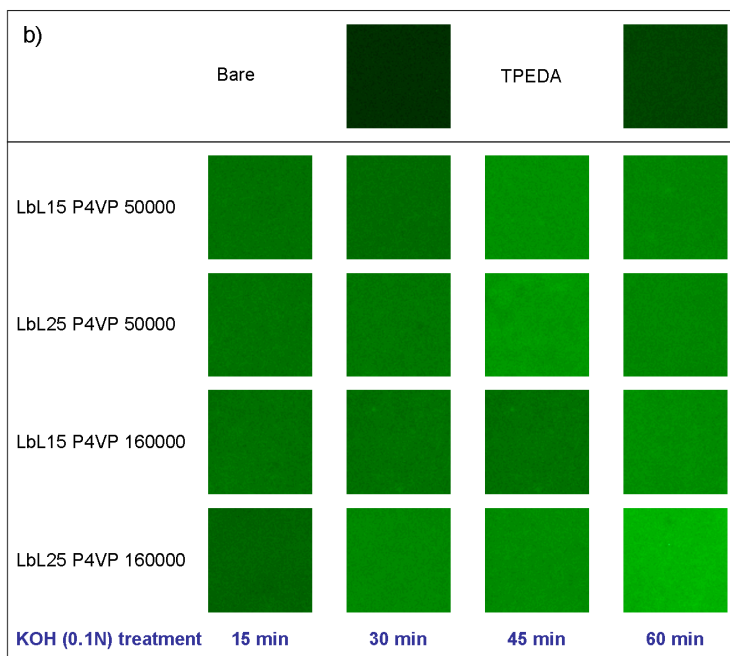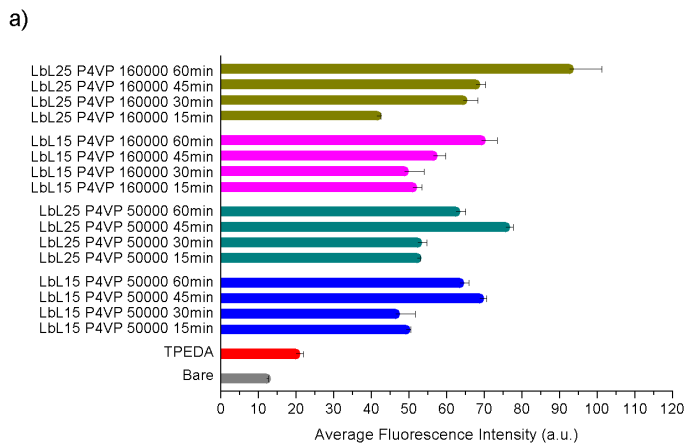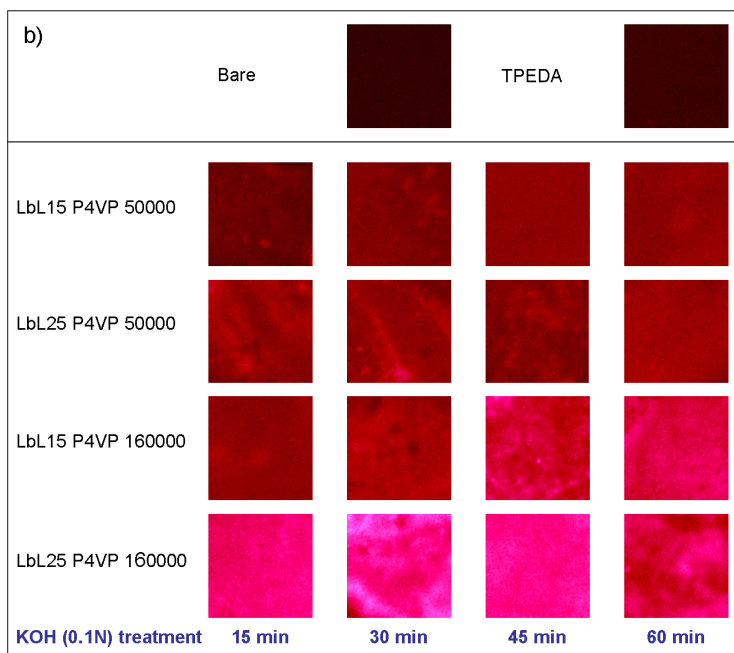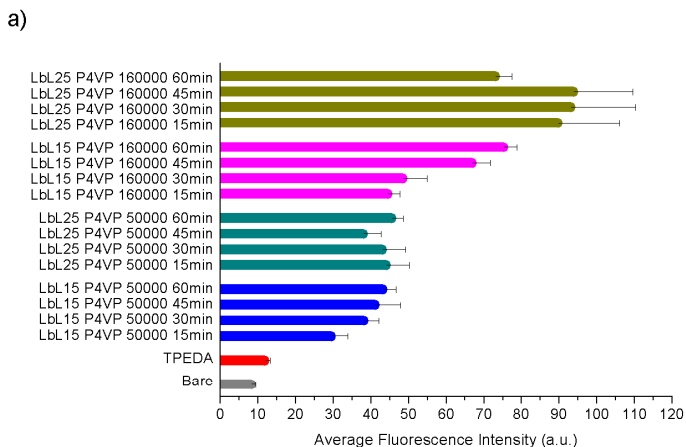
a)

b)

Figure 7.4. *(a) Bar charts of average fluorescence intensities of the His-EGFP loaded porous multilayers-coated silicon nitride cantilevers prepared under different conditions. Error bars indicate standard deviation. (b) Representative fluorescence images of His-EGFP loaded porous multilayers-coated silicon nitride cantilevers prepared under different conditions. The image size is 15 x 15 μm² and the color scale of each image is the same.*

a)

b)

Figure 7.5. *(a) Bar charts of the average fluorescence intensities of the His-DsRed loaded porous multilayers-coated silicon nitride cantilevers prepared under different conditions. Error bars indicate standard deviation. (b) Representative fluorescence images of His-DsRed loaded porous multilayers-coated silicon nitride cantilevers prepared under different conditions. The image size is 15 x 15 μm^2 and the color scale of each image is the same.*

From Figures 7.4 and 7.5, it is clear that when using P4VP with lower molecular weight (P4VP 50000), the number of assembling P4VP/PAA bilayers does not strongly influence the average fluorescence intensities of His-EGFP or His-DsRed. Compared with His-EGFP, His-DsRed has a greater tendency to adhere to the porous film formed by the remaining P4VP with higher molecular weight (P4VP 160000). This result suggests that in order to encapsulate more His-DsRed, P4VP 160000 should be used for assembling bilayers onto the surfaces of the cantilever. Therefore, the properties of the inks used, *e.g.* molecular weights and hydrophobicity, also play an important role in optimizing the amount of ink in the porous reservoir.

The changes in the average fluorescence intensities obtained by imaging encapsulated His-EGFP generally correspond to the morphology variations of the porous films shown in Figure 7.3. That is, when the porous films with bigger and deeper pores are inked with His-EGFP, higher average fluorescence intensities are observed in general. However, this observation is not obvious while loading His-DsRed into porous films prepared from 25 bilayers of P4VP and PAA.

Figures 7.4 and 7.5 show that tuning all parameters is necessary in order to encapsulate the highest amount of ink molecules and that all the porous cantilevers inked with His-EGFP or His-DsRed have at least more than threefold increase in the fluorescence intensities than those of the bare cantilevers. In addition, inking a LbL25 P4VP 160000 (KOH 60 minutes) porous tip with His-EGFP or LbL25 P4VP 160000 (KOH 45 minutes) with His-DsRed shows ~ 9 times higher fluorescence intensities than inking with bare tips. These results successfully demonstrate that more fluorescent proteins can be encapsulated into the porous films, which effectively act as a sponge for long-term DPN writing.

7.3 Conclusions

In summary, this chapter deals with a systematic investigation of surface-modified porous AFM tips using the LbL technique presented in Chapter 6. The morphology variations of porous films prepared upon varying different parameters, including molecular weight of P4VP, numbers of P4VP/PAA bilayers and duration of KOH treatment have been investigated using SEM and AFM. These porous tips prepared under various conditions can be used for studying the ink reservoir capacities by loading

His-EGFP and His-DsRed as ink molecules. We observe that larger amounts of His-EGFP can be encapsulated into the porous films with bigger and deeper pores, and that His-DsRed tends to adhere better to the porous films prepared using P4VP with higher molecular weight. The ink reservoir properties of the porous films loaded with various ink molecules behave differently, a phenomenon that is complex and not fully understood. Nevertheless, this chapter demonstrates that tuning all the parameters is an important procedure to select the best protocol to prepare tips that can encapsulate the largest amount of ink molecules for performing long-term DPN experiments.

7.4 Experimental

General procedures.

All glassware used to prepare the monolayers was cleaned by sonicating for 60 minutes in a 2% v/v Hellmanex II solution in high purity water (Milli-Q, 18.2 MΩcm), and then rinsed thoroughly with Milli-Q water, and dried in an ambient environment. Arrays of Si_3N_4 AFM cantilevers (NP, Veeco) were cleaned in piranha solution for 1 minute, (concentrated H_2SO_4 and 33% aqueous H_2O_2 in a 3:1 ratio). [**Warning:** Piranha solution should be handled with caution: it has been reported to detonate unexpectedly.] The cantilevers were then rinsed several times with Milli-Q water, and dried carefully with N_2 before forming the amino-terminated monolayer (*N*-[3-(trimethoxysilyl)propyl]-ethylenediamine, TPEDA). The preparation of TPEDA monolayer on the surfaces of AFM tips was described in detail in Chapter 6.

Fabrication of multilayer-coated porous tip.

The multilayer-coated AFM tips were prepared by following the procedures described in Chapter 6.[1] Poly(acrylic acid) (PAA), m.w. 5000, 50 wt% solution in water was first freeze-dried to obtain pure PAA. Commercially available Poly (4-vinylpyridine) (P4VP), MW 50,000 and MW 160,000 was used directly without further purifications. P4VP 50000, P4VP 160000 and PAA were dissolved in methanol individually to obtain 1 mg/ml P4VP and PAA methanol solutions. The TPEDA monolayer-functionalized AFM cantilevers were first incubated into either P4VP 50000 or P4VP 160000 solution for 10 minutes and then rinsed with methanol several times before being incubated into PAA solution for 10 minutes. This process was repeated for a defined number of times to obtain LbL-functionalized cantilevers. The LbL-functionalized cantilevers were subsequently immersed into KOH solution of 0.1 N for various durations to obtain porous structures coated cantilevers. The porous cantilevers were rinsed with Milli-Q water and dried very gently under a stream of N_2 before characterizing porous structures and loading ink molecules.

Analysis of porous structures

The surface structures of porous cantilevers were characterized by a scanning electron microscope (SEM) (Zeiss) and a custom-built atomic force microscope (AFM) in contact mode equipped with a Si_3N_4 AFM cantilever (MSCT, Veeco) with a nominal spring constant of 0.54 N/m. The scan speed of all AFM images is 1000 pixels per second with a scan range of ~ 3400 nm in width. The obtained AFM height images were analyzed using the commercial software SPIP (Image Metrology, Version 4.4.3.0).

Acquisition of fluorescent images.

The porous tip and the bare Si_3N_4 tip inked with His-EGFP or His-DsRed were placed onto a cleaned glass substrate and then examined with a fluorescence microscope (TE2000-U, Nikon) equipped with a mercury lamp as light source and a digital camera (Nikon digital Sight DS-Qi1Mc). To obtain fluorescence images of His-EGFP adhered to tip surfaces, the filter cube with blue excitation light (λ=470/22 nm), green emission light (λ=520/35 nm) and dichroic (λ=495 nm) was used. To obtain fluorescence images of His-DsRed, the filter cube with green excitation light (λ=510/40 nm), red emission light (λ=617/73 nm) and dichroic (λ=562 nm) was used. The exposure time for all the acquired fluorescence images of cantilevers inked with fluorescent proteins was fixed at 600 ms. The fluorescence images obtained were analyzed using the commercial software SPIP (Image Metrology, Version 4.4.3.0).

7.5 References

1. Fu, Y.; Bai, S. L.; Cui, S. X.; Qiu, D. L.; Wang, Z. Q.; Zhang, X. Hydrogen-Bonding-Directed Layer-by-Layer Multilayer Assembly: Reconformation Yielding Microporous Films. *Macromolecules* **2002,** *35*, 9451-9458.
2. Wang, L. Y.; Fu, Y.; Wang, Z. Q.; Fan, Y. G.; Zhang, X. Investigation into an Alternating Multilayer Film of Poly(4-Vinylpyridine) and Poly(Acrylic Acid) Based on Hydrogen Bonding. *Langmuir* **1999,** *15*, 1360-1363.
3. Wang, L. Y.; Wang, Z. Q.; Zhang, X.; Shen, J. C.; Chi, L. F.; Fuchs, H. A New Approach for the Fabrication of an Alternating Multilayer Film of Poly(4-Vinylpyridine) and Poly(Acrylic Acid) Based on Hydrogen Bonding. *Macromol. Rapid Commun.* **1997,** *18*, 509-514.
4. Zhang, X.; Chen, H.; Zhang, H. Y. Layer-by-Layer Assembly: From Conventional to Unconventional Methods. *Chem. Commun.* **2007**, 1395-1405.
5. Wu, C. C.; Xu, H. P.; Otto, C.; Reinhoudt, D. N.; Lammertink, R. G. H.; Huskens, J.; Subramaniam, V.; Velders, A. H. Porous Multilayer-Coated Afm Tips for Dip-Pen Nanolithography of Proteins. *J. Am. Chem. Soc.* **2009,** *131*, 7526-7527.
6. Kharlampieva, E.; Kozlovskaya, V.; Sukhishvili, S. A. Layer-by-Layer Hydrogen-Bonded Polymer Films: From Fundamentals to Applications. *Adv. Mater.* **2009,** *21*, 3053-3065.

7.   Bai, S. L.; Wang, Z. Q.; Gao, J.; Zhang, X. Hydrogen-Bonding-Directed Layer-by-Layer Polymer Films: Substrate Effect on the Microporous Morphology Variation. *Eur. Polym. J.* **2006,** *42*, 900-907.

8.   Bai, S. L.; Wang, Z. Q.; Zhang, X.; Wang, B. Hydrogen-Bonding-Directed Layer-by-Layer Films: Effect of Electrostatic Interaction on the Microporous Morphology Variation. *Langmuir* **2004,** *20*, 11828-11832.

9.   Zhang, H. Y.; Fu, Y.; Wang, D.; Wang, L. Y.; Wang, Z. Q.; Zhang, X. Hydrogen-Bonding-Directed Layer-by-Layer Assembly of Dendrimer and Poly(4-Vinylpyridine) and Micropore Formation by Post-Base Treatment. *Langmuir* **2003,** *19*, 8497-8502.

10.   Zhang, H. Y.; Wang, D.; Wang, Z. Q.; Zhang, X. Hydrogen Bonded Layer-by-Layer Assembly of Poly(2-Vinylpyridine) and Poly(Acrylic Acid): Influence of Molecular Weight on the Formation of Microporous Film by Post-Base Treatment. *Eur. Polym. J.* **2007,** *43*, 2784-2791.

11.   Xu, H. P.; Gomez-Casado, A.; Liu, Z. H.; Reinhoudt, D. N.; Lammertink, R. G. H.; Huskens, J. Porous Multilayer-Coated Pdms Stamps for Protein Printing. *Langmuir* **2009,** *25*, 13972-13977.

Appendix

In addition to using visible fluorescent proteins as ink molecules, amine-containing quantum dots (QDs-NH$_2$, eBioscience, Inc.) were also used to compare the ink reservoir property of the porous multilayer-coated AFM tips. From Figure A7.1, it can be seen that the porous LbL15 tips can encapsulate more QDs-NH$_2$ than a bare or amino-terminated monolayer (TPEDA monolayer)-functionalized tip.
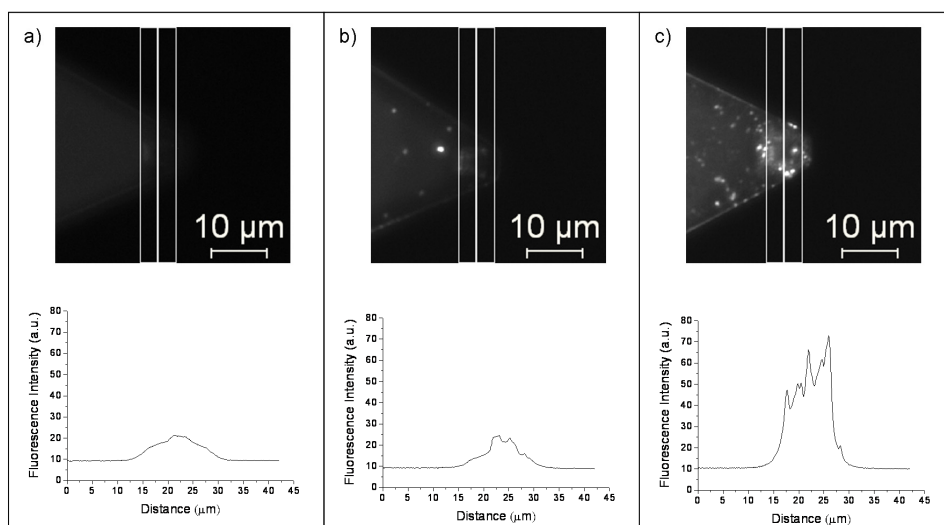

Figure A7.1. *Fluorescence images and average fluorescence intensity profiles of the area inside the rectangle of (a) a bare AFM tip, (b) an amino-terminated monolayer (TPEDA monolayer)-functionalized tip, and (c) a porous LbL15 tip, dipped into amine-containing quantum dots (QDs-NH$_2$) solution (200 nM) for 10 minutes and then dried with N$_2$. The exposure time of each image is 400 ms.*

Summary

Dip-pen nanolithography (DPN) is an atomic force microscopy (AFM)-based lithography technique offering the possibility of fabricating patterns with feature sizes ranging from micrometers to tens of nanometers, utilizing either top-down or bottom-up strategies. Although during its early development stages the serial nature of operation of DPN restricted the patterning efficiency, the successful design and fabrication of AFM probe arrays have increased the throughput of DPN dramatically by enabling generation of patterns in parallel. Several advantages of DPN including (1) ease of generation of arbitrary patterns, (2) application to a variety of ink-substrate combinations, and (3) lower cost relative to other lithographic techniques, have led to many applications in different fields and the establishment of DPN as a popular tool for nanofabrication.

This thesis contributes to the continuing development of the DPN technique, mainly focusing on two aspects. The first aspect, presented in Chapters 3-5, is to use DPN to fabricate metal-ion and (bio)-molecular patterns at micrometer or sub-micrometer scale onto monolayer-functionalized solid surfaces with different chemical immobilization strategies. Before performing all DPN experiments, microcontact printing (μCP), a well-known and understood simple and rapid soft lithography technique, was used first to confirm the usefulness of the ink-substrate interactions. The second aspect of interest is to develop an AFM tip surface-modification method for long-term DPN writing, as described in Chapters 6 and 7. A brief synopsis of all chapters follows:

In **Chapter 1**, a general introduction to this thesis is given.

In **Chapter 2** the development of the DPN technique in the past decade and the related chemical strategies are reviewed, classified into indirect DPN and direct DPN, which have been reported to fabricate biomolecular (proteins, peptides, and DNA) architectures onto solid surfaces. In addition, some other AFM-based lithography techniques, such as nanoshaving/nanografting, bias AFM lithography and fountain pen lithography, used for bio-patterning, are also briefly described at the end of this chapter.

In **Chapter 3** first a brief introduction of a custom-built instrument, the atomic force fluorescence microscope (AFFM) is given and the simple relative humidity (RH) control

system is described that was designed for implementation with the AFFM. In this thesis, all DPN experiments were performed with the AFFM, which combines an atomic force microscope and a confocal fluorescence microscope and therefore allows one to write patterns and subsequently visualize the written results *in situ* in a sequential write-read mode. Subsequently, a modification of the protocol for preparing fluorescent monolayers sensitive to metal ions is described. The controlled delivery of Ca(II) ions with DPN onto fluorescent sensitive monolayer-functionalized glass substrates is demonstrated by visualizing the enhancement of the fluorescence intensity. The driving force for the transfer of these ions from an AFM tip to the surface is their complexation to the organic ligands on the monolayer.

Metal ions represent the smallest sized ink molecules for DPN. A potential application of metal ion patterns is that they can be utilized as a template to immobilize biomolecules. **Chapter 4** demonstrates the possibility of this application by generating Ni(II) ion patterns at micro- and submicrometer scale onto nitrilotriacetic acid (NTA)-terminated monolayers-functionalized glass substrates with μCP and DPN, respectively. The patterned Ni(II)-NTA monolayers allow a single layer of histidine-tagged visible fluorescent proteins *via* a specific metal-protein interaction, which was characterized by AFM topography measurements. This is an indirect DPN method of fabricating protein patterns that can prevent denaturation of fragile biomolecules caused by direct printing or writing. We have also demonstrated by μCP that the metal ions complexed with His-tagged proteins can be easily removed by rinsing with an EDTA solution for reusing the functionalized substrates. The property of being able to regenerate and reuse the substrate is potentially useful for the fabrication of multiple protein patterns. Additionally, complexing with His-tagged fluorescent proteins offers the possibility of fundamental parameters of DPN regarding the dependence of transfer of Ni(II) ink ions, such as writing speeds and tip-surface contact times, since the small size of Ni(II) ions is practically extremely difficult to characterize directly.

In Chapter 3 and Chapter 4, non-covalent interactions have been described to generate patterns. In **Chapter 5**, a reactive μCP and DPN approach is presented for immobilizing amine containing β-cyclodextrin (βCD-NH$_2$) and quantum dots (QD-NH$_2$) onto *N, N*-carbonyldiimidazole-activated amino monolayer (IM monolayer) at micrometer scale *via* the covalent formation of urethane bonds. To confirm the covalent formation of βCD-NH$_2$ patterns, adamantyl-labeled fluorophores or ferrocenyl-labeled fluorescent proteins were used to image the patterns obtained. This is the first demonstration of using

DPN to covalently anchor molecules onto IM monolayers. In addition, orthogonal microcontact printing of βCD-NH$_2$ and QD-NH$_2$ patterns is succesfully demonstrated, suggesting a viable chemical approach for fabricating patterns of different functional groups through reactive DPN for selective immobilization of multiple desired molecules with complementary functionalities to be available in the near future.

One of the limitations of DPN is ink depletion from the tip, which limits the amount of ink molecules that can be written. In **Chapter 6**, a rather simple method is presented to coat the surfaces of AFM tips with a thin layer of porous film by using Layer-by-Layer (LbL) techniques. The pore sizes can be adjusted by treating the poly4-(vinylpyridine)/poly(acrylic acid) (P4VP/PAA) films coated onto amino-terminated monolayer (NH$_2$-monolayer)-functionalized AFM tip surfaces with a base solution for different periods of time. This hydrophilic porous film can easily absorb biomolecules and act as a larger volume ink reservoir compared to a bare AFM tip. Proof-of-concept of the porous AFM tip is demonstrated by using fluorescent proteins as ink molecules to fabricate protein patterns at micrometer and sub-micrometer length scales.

A further investigation of the morphology variations of porous films-coated silicon nitride AFM tips, prepared under various conditions, is described in **Chapter 7**. The variable parameters include the molecular weight of poly(4-vinylpyridine) (P4VP), the number of assembled layers, and duration of base solution treatment. These porous tips prepared under different conditions have been investigated for their ink reservoir properties by loading two different kinds of proteins, histidine-tagged enhanced green fluorescent protein (His-EGFP) and histidine-tagged tetrameric reef coral fluorescent protein (His-DsRed), as ink molecules. We find that, as expected, larger amounts of His-EGFP can be encapsulated into the porous films with bigger and deeper pores, and that His-DsRed tends to adhere to the porous films prepared using P4VP with higher molecular weight. This chapter demonstrates that one can tune all the parameters in order to select the best protocol to prepare tips that can encapsulate the largest amount of ink molecules for performing long-term DPN experiments.

Collectively, the results presented in this thesis illustrate a range of new ink-substrate combinations that can be applied with DPN to create patterns at micro- and sub-micrometer scale. The fabrication of Ni(II) ion patterns onto NTA-terminated monolayers *via* coordinating interactions is a general indirect DPN approach to immobilize a monolayer of His-tagged proteins, with the advantage of avoiding denaturation of fragile biomolecules readily observed when printing or writing proteins

directly. The preliminary demonstration of reactive DPN by utilizing the quick covalent formation of urethane bonds between imidazolide and amine groups may become a potential chemical strategy to generate patterns of various functional groups for selective immobilization of multiple desired molecules with complementary functionalities. Surface modification of AFM tips with a hydrophilic porous film prepared by LbL technique enhances the loading capacities of the tip, demonstrated using biomolecules and amine-containing quantum dots. The simplicity and ease of adjusting the pore sizes enable us to optimize the porosity for encapsulating the maximum amount of specific ink molecules. Therefore, the multilayer-coated porous tips show the potential to be a universal approach for long-term production of (bio)molecular patterns onto surfaces at hundreds of nanometers scale.

Samenvatting

Dip-pen nanolithografie (DPN) is een lithografietechniek gebaseerd op atomaire kracht microscopie (*atomic force microscopy,* AFM) die de mogelijkheid levert voor het maken van patronen in de ordegrootte van micrometers tot tientallen nanometers, middels een *top-down* of *bottom-up* strategie. Alhoewel de efficiëntie van het maken van de patronen in het begin van de ontwikkeling werd belemmerd door de seriële aard van de DPN operaties, heeft het ontstaan van AFM tip array, waarmee patronen in parallel gemaakt kunnen worden, de snelheid van DPN aanzienlijk verbeterd. De voordelen van DPN zijn, onder andere, (1) het gemak van het genereren van willekeurige patronen, (2) veel inkt-substraat combinaties zijn mogelijk, en (3) kost minder dan andere lithographietechnieken. Deze voordelen hebben voor veel applicaties van DPN in verschillende velden gezorgd en DPN tot een populaire methode voor nanofabricage gemaakt.

Dit proefschrift levert een bijdrage aan de verdere ontwikkelingen van de DPN techniek, gericht op twee aspecten. Het eerste aspect, geïntroduceerd in hoofdstukken 3-5, betreft het gebruik maken van DPN voor het genereren van metaal-ion en (bio)-moleculaire patronen op micrometer- of submicrometerschaal op monolaag-bewerkte oppervlakken met verschillende chemische immobilisatie strategieën. Vóór het uitvoeren van alle DPN experimenten, was eerst microcontact-drukken (µCP), een bekende en goed begrepen simpele en snelle zacht-lithografische techniek, gebruikt om de geschiktheid van de inkt-substraat interacties te bevestigen. Het tweede aspect betreft het ontwikkelen van een oppervlak-modificatie methode die langdurig DPN schrijven mogelijk maakt, zoals beschreven in hoofdstukken 6 en 7. Een kleine samenvatting van de afzonderlijke hoofdstukken is als volgt:

In **hoofdstuk 1** wordt een algemene inleiding tot dit proefschrift gegeven.

In **hoofdstuk 2** worden de ontwikkeling van DPN techniek in het afgelopen decennium en gerelateerde chemische strategiën behandeld, geclassificeerd als *indirect* DPN en *direct* DPN, die bekend zijn vanwege het fabriceren van biomoleculaire (eiwitten, peptides, en DNA) strukturen op oppervlakken. Bovendien zijn andere

lithografietechnieken die op AFM zijn gebasseerd en die gebruikt worden om bio-patronen te maken, zoals nanoscheren/nanoschuren bias AFM lithografie en vulpen lithografie, ook kort beschreven aan het einde van dit hoofdstuk.

In **hoofdstuk 3** wordt eerst een zelfgemaakt instrument, de *atomic force fluorescence microscope* (AFFM), geintroduceerd en ook een beschrijving van een simpel relatieve vochtigheid controlesysteem dat ontworpen is om met de AFFM te kunnen samenwerken. In dit proefschrift zijn alle DPN experimenten uitgevoerd met de AFFM, die een combinatie is van een atomair kracht microscope en een confocaal fluorescentie microscoop. Deze combinatie geeft de mogelijkheid om na het schrijven van een patroon meteen *in situ* het schrijfresultaat te kunnen observeren in een sequentiële schrijf-lees modus. Vervolgens is een modificatie van het protocol beschreven voor het voorbereiden van fluorescerende monolagen die gevoelig zijn voor metaalionen. De gecontroleerde afgave van Ca(II) ionen met DPN op fluorescerende gevoelige monolaag-bewerkte glassubstraten is aangetoond door het visualiseren van de versterking van de fluorescentie-intensiteit. De drijfkracht voor het overdragen van de ionen van een AFM tip naar de oppervlakte is hun complexatie met de organische liganden op de monolaag.

Metaalionen vertegenwoordigen de kleinst mogelijke inktmoleculen voor DPN. Een potentiële toepassing van metaalionen-patronen is dat ze gebruikt kunnen worden als een template om biomoleculen te immobiliseren. **Hoofdstuk 4** laat de mogelijkheid van deze toepassing zien door het genereren van Ni(II) ion patronen op micro- en submicrometer schaal op nitrilotriazijnzuur (NTA)-eindigende monolaag-bewerkte glassubstraten met, respectievelijk, µCP en DPN. De volgens patroon bewerkte monolagen laten een enkele laag van met histidine gelabelde zichtbare fluorescerende eiwitten toe *via* een specifieke metaal-eiwit interactie, die gekarakteriseerd is door AFM topografiemetingen. Dit is een indirecte DPN methode van eiwitpatronen-fabricage die denaturatie van zwakke biomoleculen veroorzaakt door direct printen of schrijven kan voorkomen. We hebben ook middels µCP laten zien dat de metaalionen complexeerd met His-gelabelde eiwitten gemakkelijk verwijderd kunnen worden door ze af te spoelen met een EDTA oplossing voor het herbruiken van de bewerkte substraten. De eigenschap dat de substraten hergegenereerd en hergebruikt kunnen worden is handig voor het fabriceren van meerdere eiwitpatronen. Bovendien geeft het complexeren met fluorescerende eiwitten gelabeled met His de mogelijkheid van bestuderen van fundamentele parameters van DPN betreffende de afhankelijkheid van Ni(II) ionen transportatie, zoals schrijfsnelheid en

tip-oppervlakte aanrakingstijd. De Ni(II) ionen zijn namelijk heel moeilijk direct te karakteriseren door hun kleine formaat.

In hoofdstuk 3 en hoofdstuk 4 zijn niet-covalente interacties beschreven om patronen te genereren. In **hoofdstuk 5** wordt een reactieve µCP and DPN aanpak gepresenteerd voor de immobilisatie van amine-gefunctionaliseerde β-cyclodextrin (βCD-NH$_2$) en quantum dots (QD-NH$_2$) op N, N-carbonyldiimidazole-geactiveerde amino monolagen (IM monolagen) op micrometer schaal, *via* de covalente formatie van urethaan-bindingen. Om de covalente formatie van βCD-NH$_2$ vast te stellen zijn fluoroforen met adamantyl of fluorescerende eiwitten met ferrocenyl gebruikt om de gekregen patronen af te beelden. Dit is de eerste demonstratie van het gebruiken van DPN om moleculen op IM monolayers te verankeren op een covalente manier. Additioneel is orthogonale microcontact printing van βCD-NH$_2$ and QD-NH$_2$ met succes gedemonstreerd. Dit suggereert een toepasbare chemische aanpak voor het fabriceren van patronen van verschillende functionele groepen door reactieve DPN voor selectieve immobilisatie van meerdere gewenste moleculen met complementaire functionaliteiten die in de nabije toekomst verkrijgbaar zal zijn.

Een van de limitaties van DPN is het opraken van inkt op de tip, waardoor de hoeveelheid inktmoleculen die gebruikt kunnen worden voor het schrijven wordt beperkt. In **hoofdstuk 6** wordt een simpele methode gepresenteerd om op de oppervlaktes van AFM tippen met een dunne laag poreuze film te bekleden door middel van laag-op-laag (*Layer-by-Layer*, LbL) technieken. De formaten van de poriën kunnen ingesteld worden door de met poly4-(vinylpyridine)/poly(acrylzuur) (P4VP/PAA) films beklede amino-monolaag (NH2-monolaag)-behandelde AFM tip oppervlakken met een basische oplossing te behandelen voor verschillende tijdsspannes. Deze hydrofiele film met poriën kan gemakkelijk biomoleculen absorberen en fungeren als een inktreservoir met grotere inhoud vergeleken met een kale AFM tip. *Proof-of-concept* van de poreuze AFM tip is gedemonstreerd door lichtgevende eiwitten te gebruiken als inktmoleculen om eiwitpatronen te fabriceren op micrometer en sub-micrometer schaal.

Een nader onderzoek van de morphologische variaties van silicon-nitride AFM tips bekleed met poreuze films, gemaakt onder verschillende condities, wordt beschreven in **hoofdstuk 7**. De variabele parameters betreffen het moleculaire gewicht van poly(4-vinylpyridine) (P4VP), het aantal gemonteerde lagen, en de tijdsduur van de behandeling met de basisoplossing. Deze poreuze tippen, voorbereid onder verschillende condities, zijn onderzocht voor hun inktreservoir eigenschappen door het laden van twee

verschillende soorten eiwitten, histidine-gemerkte versterkte groen lichtgevende eiwitten (His-EGFP) en histidine-gemerkte tetrameric koraalrif lichtgevende eiwitten (His-DsRed), als inktmoleculen. Zoals verwacht kan een grotere hoeveelheid His-EGFP ingekapseld worden in de poreuze films met grotere en diepere poriën, en heeft His-DsRed de neiging om aan poreuze films te plakken die voorbehandeld zijn met P4VP met een hoger molecuulgewicht. Dit hoofdstuk toont aan dat men verschillende combinaties van parameters kan uitproberen om het beste protocol te kiezen voor het voorbereiden van tippen zodat die de grootste hoeveelheid inktmoleculen kunnen opnemen voor lange-termijn DPN experimenten.

De resultaten gepresenteerd in dit proefschrift illustreren een reeks van nieuwe inkt-substraat combinaties die gebruikt kunnen worden met DPN om patronen te produceren op micrometer en sub-micrometer schaal. Het fabriceren van Ni(II)-ion patronen op NTA-eindigende monolagen *via* gecoördineerde interacties is een algemene indirecte DPN aanpak om een monolaag van His-gemerkte eiwitten vast te zetten, met het voordeel dat denaturatie van zwakke biomoleculen, vaak geobserveerd tijdens direct printen of schrijven van eiwitten, wordt vermeden. De voorafgaande demonstratie van reactieve DPN bij het gebruiken van de snelle covalente formatie van urethaanbindingen tussen imidazolide en amine groepen kan een potentiële chemische strategie zijn om patronen van verschillende functionele groepen voor selectieve vastlegging van meerdere moleculen met aanvullende functionaliteiten te genereren. Modificatie van de oppervlakken van de AFM tippen met een hydrofiele poreuze film die voorbereid is met LbL techniek versterkt de laadcapaciteit van de tip, gedemonstreerd door het gebruiken van biomoleculen en amine-bevattende quantum dots. Het gemak waarmee de poriëngroottes aangepast kunnen worden staat ons toe om de poreusheid voor het opnemen van de maximale hoeveelheid specifieke inktmoleculen te optimaliseren. Daardoor tonen de multilagen-beklede poreuze tippen de potentie om een universele aanpak te worden voor het produceren van lange-termijn (bio)moleculen patronen op oppervlakten op een schaal van honderden nanometers.

Abbreviations

AFM: Atomic Force Microscope

AFFM: Atomic Force Fluorescence Microscope

βCD: β-cyclodextrin

CDI: *N,N*-carbonyldiimidazole

DPN: Dip-Pen Nanolithography

DsRed: Tetrameric Reef Coral Fluorescent Protein

EGFP: Enhanced Green Fluorescent Protein

(E)SEM: (Environmental) Scanning Electro Microscope

His$_6$: Hexahistidine

IM: Imidazolide

LbL: Layer-by-Layer

µCP: Microcontact Printing

MHA: 16-Mercaptohexadecanoic Acid

Ni-NTA: Nickel(II)-Nitrilotriacetic Acid

ODT: 1-Octadecanethiol

QDs: Quantum Dots

OTS: Octadecyltrichlorosilane

P4VP: Poly(4-vinylpyridine)

PAA: Poly(acrylic acid)

PDMS: Poly(dimethylsiloxane)

RH: Relative Humidity

SAMs: Self-Assembled Monoalyers

SPL: Scanning Probe Lithography

TAMRA: 5-(and-6)-Carboxytetramethylrhodamine, succinimidyl ester

THF: Tetrahydrofuran

TPEDA: *N*-[3-(trimethoxysilyl)propyl]ethylenediamine

VFP: Visible Fluorescent Protein

Acknowledgements

I would like to express my gratitude to colleagues and friends in BPE, SMCT, and MnF. Because of your contributions, supports and accompanying, I had great time not just in the work part but also in the private life during all these years in Enschede.

Technicians are the first persons I ran to when I encountered difficulties in handling equipments and needed practical support. Kees, thanks for the AFM training and keeping the AFM alive until now. I enjoyed discussing with you on design of the humidity chamber and all the AFM experiments a lot. Aufried, thanks for your help on the optical part of AFFM, I learned a lot from you. Mark, thank you for the high-resolution SEM measurements and chat. Gerard, thanks for the XPS measurements. Marcel and Kirsten, thanks for ordering the chemicals for me. Richard, thanks for all the support on my computer and network problems. Yvonne, Frans, Erwin, Christian Breukers and Marloes of BPE and Bianca and Tieme of SMCT, thanks for all of your kind help all this time.

Dear Sylvia, the secretary in BPE, thank you so much for your help and support all the time. Your smile and big hug always warm me up; I'll miss them. I would also like to thank the secretaries from SMCT: Izabel, and ex-secretaries, Gerardine, Melissa, Danielle, Marieke for handling all the administrative works.

For the collaborations, I would like to thank Lourdes for being the first one to show me how to prepare monolayer and perform dip-pen nanolithography. I enjoyed all the discussions through Internet while writing the manuscript together and had great time with you and Fernando in Enschede and Dublin. Thank Prof. Jurriaan Huskens and Huaping, for all the useful discussions on the preparing of porous AFM tips. Huaping, thanks for your warm greetings after you went back to China. Dr. Pascal Jonkheijm and Francesca Scaramuzzo, thank you for the collaboration. Francesca, I especially enjoyed the late nights working with you.

Thanks all my officemates in Zuidhorst: Marieke *(also my dear paranimf, I really cherish all the moments of chat, watering plants, sharing sweets…etc. with you.)*, Cicerone *(for sharing Romanian information and jokes)*, Daniele *(for the nice pizza and chat)* and Malte *(for letting me believe there is Santa Claus in the world)* and officemates in Hogekamp: Christian Blum *(for all the useful discussions and offering me fluorescent proteins)*, Dianwen *(for always willing to share your experience on aligning laser.)*, Cynthia, Constantin, Raja *(especially for your help on the design of thesis cover)*.

In BPE, I would also like to thank Maryana *(for all the nice chat, discussions and help)*, Yujie *(for all the FLIM measurements, help and advises on delivering my concept thesis and the nice chat)*, Vishnu *(for Raman measurements and advises on printing thesis)*, Tom *(for the confocal fluorescence microscope training)*, Martijn van Raaij *(for showing me how to use AFFM)*, Lily *(for all the nice chat and your hospitality)*, Lanti *(for your help on AFM and all the nice chat in both BPE and MnF)*, Kim *(for showing me how to use BioScope AFM)*, Ine, Mireille, Dodo, Shrirang, Yanina, Alma, Aurel, Hank-Jan, Arun, Roy, Chandra, Tomasz,

Felicia, Bart, Alex, Liesbeth, Shashank, Remco, Peter, Martijn Stopel, Dirk, Niels and all of you great colleagues in BPE.

In SMCT and MnF, I would also like to thank Shu-Han *(for your always energetic laugh and help. I also enjoyed the time with you in Bulgaria)*, Yiping *(also my dear paranimf, thanks for your help on thesis printing, all the nice chat and dinners)*, Martine *(for sharing your experiences and the great time together)*, Albert *(for the solutions of chemistry problems)*, Denis *(for QDs information)*, Kim *(for training me how to use AFM and nice tips on traveling to USA)*, Arántzazu *(for sharing your experiences on experiments)*, Xing Yi *(for all the nice discussions and chat)*, Xuexin *(especially for accompanying to go to NanoNed flagship meetings and conferences)*, Alessandro *(for your kind help on aldehyde monolayer)*, Alberto *(for all the discussions about AFM and also nice travel tips to Madrid)*, Dorota *(for all the porous stamps experiments)*, Sachine, Huaping, Victoria, Raluca, Laura, Jealemy, Vijay, Srinidhi, Ignacio, Riccardo, Roberto, Peter, Janet, Oya, Tian, Dae Jun, Elisabetta, Francesca Costantini, Francesca Scaramuzzo, Andras, Pieter, Oktay, Nicolai, Musassir, Jordi, Anna, Deniz, Carlo, Melanie, Carmen, Veera, Xuemei, Alessio, Fernando, Lourdes, Soco, Mirko, Henk, Rik and all of you great colleagues in SMCT, MnF and BNT.

Ming Ni, Hsiao-Lei and Li-Hsin, thanks for your support and encouragements during all these years (even more than one third of my life) although we are in different countries. Also thank my friends in Enschede: Amy, Dongpo, Yi-Tzu, Lorraine & Yung-Ching, Chia-Chi, Chou-Yen, Lelia, Jen Hsuan, Sheng-He, Chin-Huang, Richard Hsieh, Hsiang-Hsu, Hao Gu & Lanti Yang, Xiao Li & Zheng Zhang, Tian Gang & Xin Wan, Qi Chen & Yujie Ma, Jun Liu & Nan Li, Yixuan & Vincent, Yiping, Xiaoying, Jeroen and Eric, I enjoyed all the moments which we chatted, had breakfast/lunch/dinners and played games together. Friends in Delft and Leiden: Bill & Pei-Hui, Haibo, Chung-Kai, Yan Liu, Vijay and Jan and friends in USA: Briana & Martin, Cindy & Kenny, Ching-Hsuan & Ching-Chih, Noemie, Frank, Chun-Chieh and Wei-Min, thanks for all the nice moments we had been together. In addition, I would like to thank Intervocaal members, especially Marijke, Lon, Ning, Piet and Yulan who always give me encouragements. I had great time while singing together with you on the stage.

Kai-Fan, thank you very much for writing samenvatting and your immense support and love. I am so glad that I can share all my happy and sad moments with you during these years. I would also like to thank your family for their warm encouragements.

In the end, I would like to thank my family and relatives for their unlimited support and love. 親愛的阿公，阿嬤，爸爸,媽媽，亞雅和瑛寶，謝謝你們這些年來的鼓勵和支持，讓我可以在國外追求自己的夢想，我愛你們。阿公，謝謝您從我小時候說故事給我聽，陪我彈鋼琴，教我說日文…雖然您在2009年離開我，但您永遠在我心中，這本論文，特別獻給您！

Chien-Ching Wu
Enschede, The Netherlands , June 2010

About the Author

Chien-Ching Wu was born on 27th July, 1981 in Kaohsiung City, Taiwan. After graduating from Kaohsiung Girls' High School in 1999, she went to study Materials Science and Engineering at National Chiao Tung University in Hsinchu, Taiwan. She obtained her bachelor degree in June 2003. In the same year, she joined the MSc program of Nanoscience provided by Delft University of Technology (TU Delft) and Leiden University in The Netherlands. Her study was funded by ASML-Netherlands Trade and Investment Office (NTIO) Joint Scholarship and TU Delft Dutch Education Learning at Top Level Abroad (DELTA) Scholarship. In August 2005, she obtained her MSc degree from TU Delft under the supervision of Prof. Thomas Schmidt at Leiden University. From May to November 2005, she did her internship in Prof. Mischa Bonn's group at FOM institute-AMOLF. Since December 2005, she started her PhD study under the supervisions of Prof. Vinod Subramaniam and Dr. Cees Otto in Biophysical Engineering Group (BPE) and Prof. David Reinhoudt, Dr. Aldrik Velders and Dr. Mercedes Crego-Calama, in Laboratory of Supramolecular Chemistry and Technology (SMCT). The results of her research are described in this thesis.